Abstract

Schoen, Michael Alexander. Experimental Investigations in 15 Centimeter Class Pulsejet Engines. Under the direction of Dr. William L. Roberts.

Testing is performed on the 15 centimeter class pulsejet engine in order to develop, study, and explore the operational characteristics. Valved and valveless operation, hydrogen and propane fuels, various fuel injection methods, and a range of geometric configurations are investigated for operational feasibility. The scaling capabilities of a valveless 15 centimeter class pulsejet of conventional design are studied by methodically varying inlet length, exit length, exit geometry, and inlet area to combustor area ratio (A_i/A_c). Engine performance is defined by measuring chamber pressure, internal gas temperatures, time-resolved thrust, operational frequency, and fuel flow rate. The scaling capability is characterized by the success of self-sustained combustion for each corresponding geometric configuration. Tail pipe length is found to be a function of valveless inlet length and may be further minimized by the addition of a diverging exit nozzle. Chemical kinetic times and A_i/A_c prove to be the two prominent controlling parameters in determining scaling behavior.

EXPERIMENTAL INVESTIGATIONS IN 15 CENTIMETER CLASS PULSEJET ENGINES

by

Michael Alexander Schoen

A thesis submitted in partial fulfillment of the
requirements for the degree of
Master of Science

Aerospace Engineering

North Carolina State University
Raleigh, NC

2005

Approved by:

_____

Dr. William L. Roberts,
Chair of Supervisory Committee

_____ _____

Dr. Andrey V. Kuznetsov,
Committee Member

Dr. Hassan A. Hassan,
Committee Member

Biography

The author was born Michael Alexander Schoen of Ann Arbor, Michigan in 1980, son of Dr. Walter and Barbara Schoen. He is the oldest son of two with one older sister. At the age of four, Schoen's family moved to Charlotte, North Carolina where his father continued to practice medicine. There, Schoen was enrolled and remained in the public education system until graduating from Providence Senior High School in 1999.

Immediately following high school, Schoen attended North Carolina State University in Raleigh, North Carolina where he received his Bachelor of Science in aerospace engineering in May 2003, graduating with high honors. Schoen entered the Masters of Science program for aerospace engineering at North Carolina State and received his degree under the direction of Dr. W. Roberts.

Acknowledgements

The author would like to acknowledge the supporting agency, Defense Advanced Research Projects Agency (DARPA), for funding all research performed in this study; his advisor, Dr. William Roberts, and defense committee, as well as Dr. Terry Scharton, for their advice and unconditional assistance; and the invaluable love and support received from all family and friends throughout the course of his trials and studies, without whose patience this work could not have been completed.

Table of Contents

List of Figures

List of Tables

1 Introduction

From June 2004 to May 2005, the Defense Advanced Research Projects Agency (DARPA) funded a developmental program to investigate the operational feasibility in down-scaling the overall size of the pulsejet engine, under DARPA grant number HR0011-04-1-0036. A vital step in the process of scaling pulsejet geometry is the functionality study of 15-centimeter class engines. No documented work on pulsejets of such size or smaller can be found in the available literature.

1.1 Background/History

After World War II, the aviation industry saw a major advancement in flight capabilities with the development and implementation of the turbine engine. With this new technology, aircraft could fly higher, faster, and farther than ever before. However, along side early turbine development was a different type of jet power, commonly known today as the pulsejet. The pulsejet promised lower thrust specific fuel consumption (tsfc), more robust operating characteristics, and, most importantly, a design that was significantly simpler mechanically than its turbine counterparts. However, interest in pulsejets subsided due to poor thrust performance versus size and horrific decibel performance. Improvements upon such limitations were never achieved owing mostly to a lack of fundamental understanding for the pulsejet's operation. This, in turn, caused the pulsejet to fade from history's timeline and the turbine engine to emerge as the dominant

propulsion option. Today, pulsejet technology shows promise as a viable source for alternative propulsion purposes, but the general lack of fundamental understanding remains a foremost inhibiter.

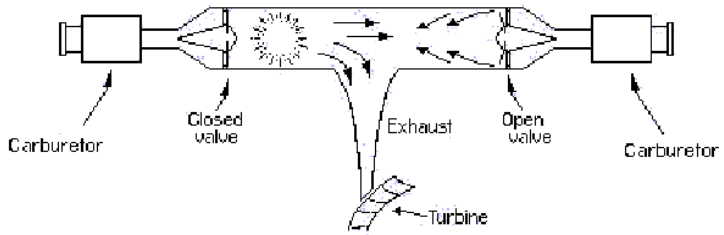

Figure 1.1-1: A schematic of the Esnaut-Peltrie push-pull combustion engine.

Pulsejets operate on a cyclical combustion event, characteristic of its geometry and fuel. The discovery of the pulsating flame, or "sensitive flame," was first noted around 1777 (Zinn, 1986). Conceptual designs of pulsating combustion devices then followed almost one and a half centuries later. It was not until the turn of the 20th century that the possibility of a cyclical combustion engine was realized and documented. Two French engineers, Esnault and Peltrie, patented a design for an engine that drove a turbine wheel (Foa, 1960; Reynst, 1961; Zinn, 1986). This engine worked based on the principle of two opposing pulsating combustion columns fitted in a single straight, tubular chamber working out of phase from one another (Figure 1.1-1) (Zinn, 1986). Shortly thereafter, another Frenchman named Georges Marconnet patented a device that was essentially a variation to the Esnault-Peltrie design (Reynst, 1961). Here, Marconnet replaced the flap

valves with what he termed an “aerodynamic valve.” A simple area constriction served a similar purpose as the mechanical valve – to let fuel and air into the combustion chamber but inhibit exhaust gasses from escaping in the opposite direction. Shown in Figure 1.1-2, Marconnet’s engine is, in principle, half of Esnault and Peltrie’s combustor column without valves.

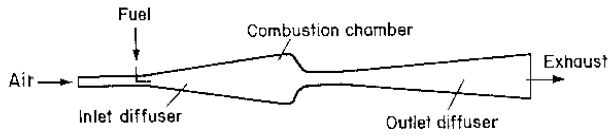

Figure 1.1-2: A schematic of the Marconnet valveless pulsejet.

Successful development of an operational pulsating combustion engine did not come about until the 1930’s when a German named Paul Schmidt (Foa, 1960; Reynst, 1961) developed and tested the Schmidt tube, or a constant area chamber with flapper valves at one end and an opening at the other, shown below in Figure 1.1-3. During World War II, Germany incorporated Schmidt’s design into the development of their V-1 missile program, or the 'Buzz Bomb,' sister project to the infamous V-2 rocket. Schmidt's design served as the powerhouse behind Germany's V-1 weapon.

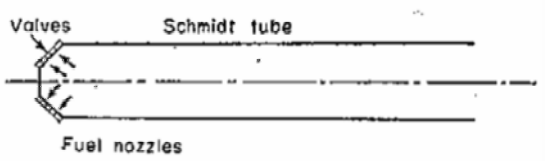

Figure 1.1-3: The Schmidt tube.

The Buzz Bomb (Figure 1.1-4) terrorized England's countryside with its enormously loud namesake buzz heard from miles away and is given credit for being the first successful pulsejet utilized for thrust capabilities (Reynst, 1961). After the war, America (among other countries) continued development of pulsejet power. Specifically, the United States worked on developing a valveless variant to pulsejet engines through several secret, military-funded programs. From the declassified documents available today (Emmerich, 1953; Lockwood, 1963; Lockwood, 1964; Logan, 1951; Logan, 1949; Logan & Finamore, 1948; Rudinger, 1951; Wilder, 1949), it is clear that an understanding of the fundamental physics responsible for the successful operation of pulsating combustion engines was never truly achieved.

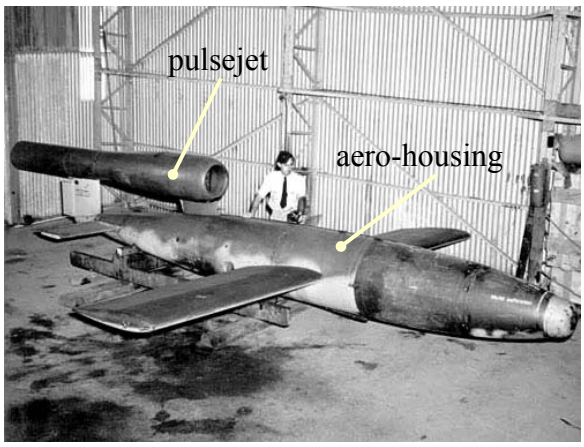

Figure 1.1-4: The V-2 'Buzz Bomb'

1.2 Related Work

Valveless pulsejets were not an exclusive American development. The French company SNECMA (today a child company to the SAFRAN technology group of Paris, France), for example, was the first to use a valveless pulsejet for commercial use in powered flight (Ogorelec, 2002). The Escopette, illustrated in Figure 1.2-1, was a valveless design employed as a backup propulsion source for the French Emouchet sailplane in the early 1950's (Ogorelec, 2002; SNECMA, 2005). Other foreign interests such as Russia, China, and Germany were involved in valveless development, as well. Still, the United States government made considerable advances in valveless pulsejet technology before eventually putting the idea to rest until recent years.

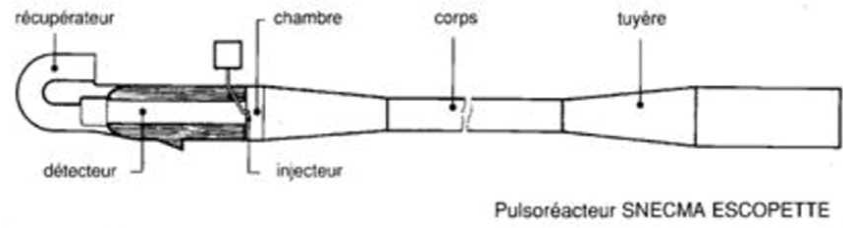

Figure 1.2-1: The French 'Escopette' valveless pulsejet.

Two prominent declassified American collaborations are noted for valveless pulsejet research in the 1950's to early 60's. Project Squid (Logan, 1951; Logan, 1949; Logan & Finamore, 1948; Rudinger, 1951; Wilder, 1949), a collaborated effort between the United States Navy and Air Force to research and develop all potential sources of jet propulsion available at that time, became greatly involved in the investigation of

valveless pulsejets. Under the initial direction of J.G. Logan at the Cornell Aeronautical Laboratory, Project Squid's valveless pulsejet work began as an investigation into 'small scale models' (Logan, 1951; Logan, 1949) for fundamental research purposes and later grew to applications in helicopter rotor tip propulsion (Emmerich, 1953). Logan performed the majority of testing on a valveless design concept conceived from a hobby-scale valved pulsejet known as the Dynajet (Logan & Finamore, 1948). Logan replaced the flapper valves by a flat plate, completely closing the jet at one end, and injected fuel and air directly into the combustion chamber. Project Squid investigated performance characteristics with hydrocarbon fuels on multiple geometric configurations of the 'Logan' pulsejet, respectively named after its chief designer (Logan, 1949; 1951). It has been suggested that the Logan jet improved rate of heat release and cycle efficiency (Reynst, 1961). However, such a design differed from pulsejets of the present work in that air was directly injected during operation rather than accommodated for self-sustainability.

The Bureau of Naval Weapons and the Advanced Research Division of Hiller Aircraft Corporation conducted a cooperative investigation of valveless pulsejet reactors for the development of lift-propulsion systems from 1961 to 1963 (Lockwood, 1963). Numerous valveless designs were developed, produced, and tested in the course of the project. The most well known of these designs was the Hiller-Lockwood pulsejet illustrated and diagramed below in Figure 1.2-2. The Hiller company was successful in several developmental breakthroughs in pulsejet research, namely decreasing combustor size with the advent of converging bulkheads at the entrance and exit of the combustor

section (Lockwood, 1963; Crow, 1976). Other accomplishments included the thrust-efficient design of the Hiller-Lockwood jet, tsfc improvements via effective thrust augmenters, and scaling studies on a range of size classes (Lockwood, 1963).

In a related concurrent program summarized in a report presented by Lockwood (1964), the Hiller Aircraft Corporation, under support from the United States Army Transportation Research Command (TRECOM), also performed work on conventional valveless designs resembling that of a Logan jet or the pulsejets utilized in the present work. Investigations into miniature valveless pulsejets led the Hiller team to develop an engine with a minimum combustion diameter of 0.75 inches, an inlet to combustor area ratio of 0.34, and an overall length of 12.0 inches (Lockwood, 1964). However, poor response led to a lack of recorded data. The Hiller reports are by far the most relevant detailed engineering work that can be applied to the direction of the following study.

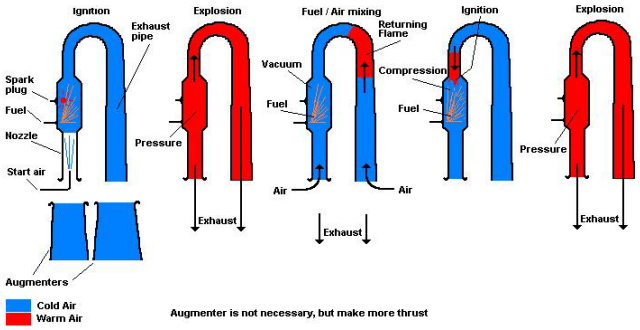

Figure 1.2-2: Schematic of the Hiller-Lockwood pulsejet.

1.3 The Pulsejet Cycle of Operation

1.3.1 Valved Cycle

Pulsated combustion can be achieved from rather simple, traditional designs. Characteristic of a valved pulsejet engine, combustion occurs with no prior pre-compression of gasses or associated moving parts. Fuel and oxidizer (air) are ingested upstream of the flapper valves. By a spark ignition event, combustion of unburned gasses sends a compression wave down the tube where the flow encounters the outside ambient air and responds with an expansion wave sent up the tube. Expansion-induced low pressure opens the flapper valves to allow an inflow of air and fuel, as well as, draw air and burned gasses from the opposite end of the tube inward toward the 'fresh' mixture. From contact with hot residual combustion products, a new ignition event is induced and the cycle repeats. Ignition is not propagated along the axis as is associated with shock ignition; rather, the ignition event originates at the walls and the flame travels radially inward towards the axis centerline (Reynst, 1961).

1.3.2 Valveless Cycle

In 1909, Marconnet developed what he termed an aerodynamic valve that replaced the flapper valves of conventional design. The objective of the aerodynamic valve was to allow the intake of air for oxidation but, at the same time, offer resistance to backflow momentum created by the combustion event. In Marconnet's pulsejet (Figure 1.1-2), the latter is achieved by a cone-shaped inlet diffuser geometry where the air intake throat diameter of the diffuser is significantly smaller than that of the combustion

chamber exit to the tail pipe. Nevertheless, a significant loss of momentum still occurs and the peak combustion pressure is reduced by the varying geometry of the inlet diffuser (Reynst, 1961).

Numerous designs (Foa, 1960; Ogorelec, 2002; Reynst, 1961; Zinn, 1986) for preventing backflow losses of the valveless pulsejet while conserving thrust and specific fuel consumption have been introduced. One such design was incorporated into the French Escopette of Figure 1.2-1. Simply an inlet pipe of small diameter ratio (to that of the combustor tail pipe exit diameter) and an abrupt area change in the opening from the inlet to the combustor section was utilized to conserve momentum thrust. The abrupt area change helped to resist backflow momentum loss out the inlet duct (Reynst, 1961).

Several flow rectifiers have also been suggested (Foa, 9160; Reynst, 1961; Zinn, 1986) that generally consist of a device placed before the intake inlet which prevents flow in one direction but allows passage of flow in the opposite. A popular design (Figure 1.3-2) was introduced by J.V. Foa (1960) where an annular, convergent inlet allows fresh air to enter but redirects out flowing gasses through side ducts. The ducts bend the flow 180^0 to avoid thrust losses. Rectifiers are often complex devices that add difficulty to production without proven benefits (Foa, 1986).

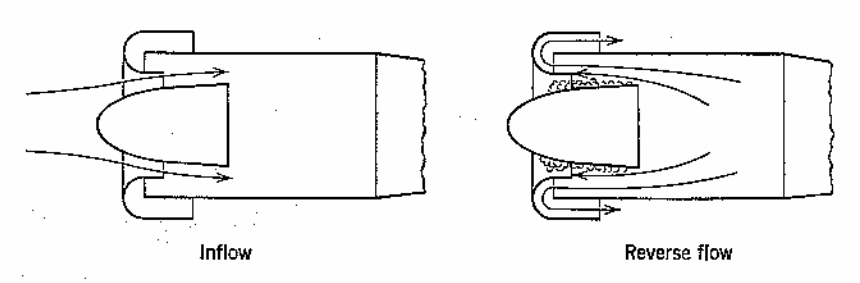

Figure 1.3-1: Flow rectifier proposed by Foa.

1.3.3 Pulsejet Cycle Theory

Several prominent figures in the history of pulsating combustion research have offered theories based upon their respective areas of specialization on the fundamental physical processes responsible for the pulsejet's cycle of operation. F. H. Reynst, best known for his 'combustion pot' discovery, devoted most of his professional career to understanding the principles behind pulsating combustion engines. Reynst believed pulsejet engines operate on an acoustic resonating principle analogous to that of a ¼ wave organ pipe. In a 1955 journal article, Reynst (1961) relates the pressures and velocities in a characteristic Schmidt tube cycle to standing wave theory for small amplitude oscillations (i.e. linear acoustics). In a tube open at one end pressures and velocities can be represented by sine waves 90 degrees out of phase from each other. As is presented by the journal author (Figure 1.3-2), experimental velocity lags pressure by a quarter period if a correction factor of Z/4 is applied to the flow velocity. Reynst rightfully attributes the necessity of such a correction factor to the fact that the pressure and velocities were measured at opposite ends of the tube, simultaneously. In doing so,

his ¼ wave hypothesis is shown to be arguably supported by experimental evidence. Regardless of his acoustic interpretations, Reynst, in several published works, expressed a keen understanding of the combustion and fluid dynamic processes involved in the intermittent cycles of a pulsejet engine (1961).

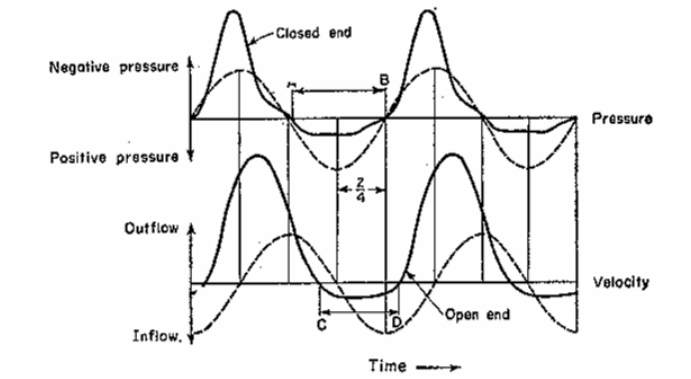

Figure 1.3-2: Diagram showing pressure and velocities in the Schmidt tube. C-D air inflow at open end; A-B valves open; Z cycle time.

In a collection of works edited by Felix Weinberg, the author Ben Zinn (1986) gives a very thorough development of pressure oscillations in a closed tube driven by linear heat addition (i.e. amplitudes of oscillation and heat addition are small). Starting from a system of wave equations, Zinn (1986) utilizes the Green's function technique to prove the validity of Rayleigh's empirical criterion for heat driven oscillations, similar to common techniques for investigating combustion noise. He derives a relationship between heat addition and pressure amplitude where a proportionality constant may be used to determine the potential for modal excitation within the tube. By extending his results for boundary effects at the walls (i.e. momentum influx and outflux), they can

then be well applied to pulsating combustor problems. As is the case, Zinn uses the practical example of the previously described Esnault-Peltrie combustor. The author presents a convincing argument based on the assumption that pressures behave like the fundamental acoustic mode for a closed tube, or $P_{E\text{-}P}(x) \sim \cos(\pi x/L)$. Zinn suggests that the Esnault-Peltrie analysis can be easily adjusted for the ¼ wave structure of a pulsejet simply by substituting the fundamental mode approximation for that of a tube open at one end and closed at the other. In theory, such a solution would determine the characteristics of the oscillations inside the engine and the range of operating conditions for which pulsating operation is possible (Zinn, 1986).

A detailed discussion on ideal pulsejet performance theory is presented by J.V. Foa (1960). An ideal pulsejet, as defined by Foa, is "a pulsejet in which ram pre-compression of the charge is fully utilized, all flow processes except combustion are isentropic, and the exhaust velocity is a square-wave function of time." It can be shown (Foa, 1960) that the cycle efficiency, as well as the air specific impulse, inevitably approaches that of the ideal ramjet as free-stream Mach number increases. In reality, pulsejet performance differs strongly from ideal theory mainly due to the loss of ram pressure compression of combustible gasses. As was discussed above, pressure inside the combustion chamber immediately before ignition is generally equivalent to atmospheric free-stream conditions.

1.4 Application Concepts

A key advantage of the pulsejet engine, to which no other mechanical thrust device compares, lies in its simplicity. Though the physical fundamentals of operation may be far from simple, the pulsejet's construction, especially that of the valveless design, is exquisitely unsophisticated. This fact alone places the pulsejet as a forerunner in the innovative field of miniature propulsion. Pulsejets have begun to receive renewed interest as a possible source of miniature and/or micro propulsion. However, a basis for powered thrust should not be considered its only application. The valveless pulsejet could be an excellent source for micro-heating. Past investments have been made toward the use of conventional-sized pulsejets in central heating systems. Cost is significantly reduced by the simplistic nature of valveless pulsejet construction. Moreover, for the purposes of battery applications where thrust is not a leading concern, the potential energy produced by the pulsejet's high thermal efficiency may be harnessed for thermoelectric power.

2 Experimental Apparatus and Setup

The thrust of these experiments was to develop, study, and explore pulsejets of the 15 centimeter class, or whose size correspond to roughly one third of pulsejet sizes used by today's hobby enthusiasts. Each type of pulsejet developed was modified several times in the span of experimentation in order to satisfy shifting experimental goals and techniques. Propane and hydrogen were employed as potential fuel variants with atmospheric or standard grade compressed air as an oxidizer. Propane was chosen because it is a readily available hydrocarbon fuel as per the customer requirements. Hydrogen was chosen because it offers a higher rate of reaction than most hydrocarbon fuels which was an inherent requirement for successful operation. A pulsejet was considered to have achieved successful operation if it breathed independently.

2.1 Pulsejets

2.1.1 15cm Construction

Initial testing was performed using a pulsejet whose dimensions were a direct 3:10 scale down of the Bailey Machine Services (BMS) hobby-scale pulsejet, Figure 2.1-1**,** hereafter referred to as 'the 15cm' pulsejet. The main pulsejet body comprising the combustion chamber, transition section, and tailpipe were reamed from stainless steel.

The head component and locking ring used in valved assessments of the 15cm were composed entirely of aluminum.

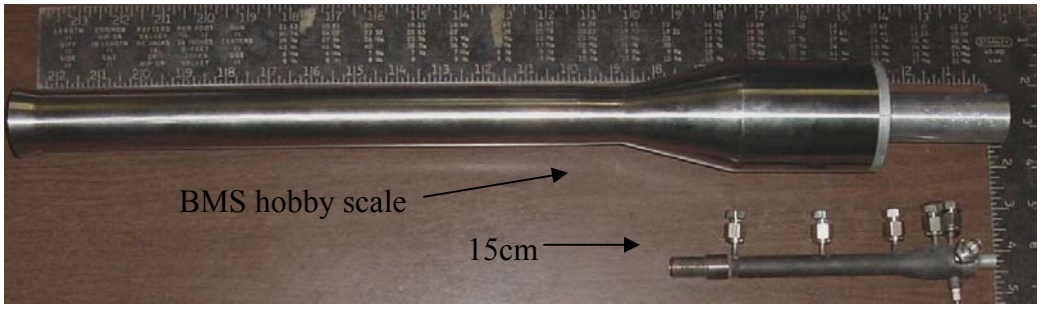

Figure 2.1-1: Pulsejet size scale.

A few minor changes were made in the scaled construction of the 15cm as compared to the hobby-scale. Those being (1) the venturi located at the intake manifold of the pulsejet head was removed and replaced by a constant area duct. Because only gaseous fuels would be employed for the 15cm, there was no need for the associated venturi effects. And, for that matter, the fuel injector/atomizer system was disregarded in construction, as well. (2) The cooling fins surrounding the intake venturi (refer to Figure 2.1-2) were reduced in number and do not correspond in thickness to the scale down factor. This was made necessary due to limitations in the material. (3) The thread type and count used to attach the head component to the jet body do not follow the scale factor, as well. Because it was yet uncertain as to the peak pressures expected from combustion, a 32 thread pitch was incorporated to increase thread count and assure stability. It was also for this reason that (4) a small block of additional material was

added to a section of the combustion chamber wall. This allowed for the placement of a setscrew in order to further secure the position of the inlet head. The material would later be used to tap a hole for a fuel injector as the set screw was determined unnecessary. The reed valves (Figure 2.1-2) used for the 15cm operation were wire electric discharge machined from blue tempered spring steel. Their general dimensions observe the scale down factor; however, (5) the relative distance between each pedal at their base had to be increased for manufacturing purposes.

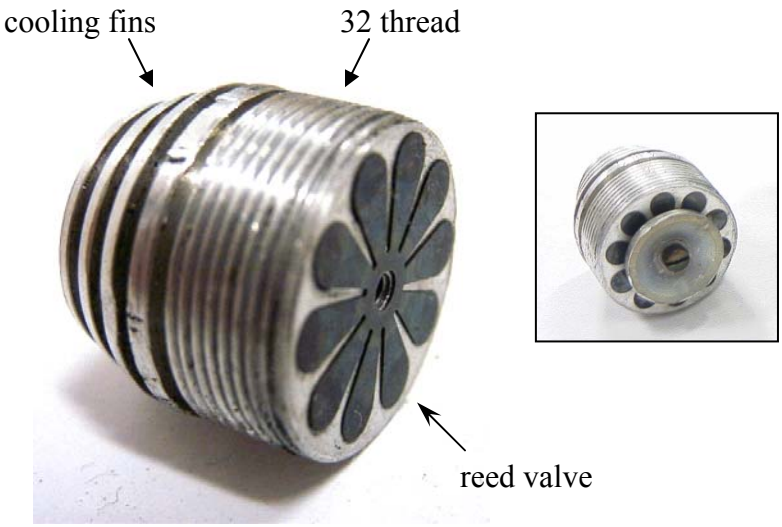

Figure 2.1-2: 15cm valved intake head.

2.1.2 Modified Pulsejet Construction

To study reverse inlet operation, whereabouts thrust is conserved by directing inlet and exit momentum in the same direction, a new jet construction was developed. Careful consideration was taken in designing the additional jet to accommodate an ease of instrumentation. Also, it was important to allow for quick and simple modifications in

reverse inlet configurations. As Figure 2.1-3a illustrates, a steel 'combustion cylinder' component was developed that not only allowed the use of existing extensions as standard tail pipes, but permitted the attachment of conventional inlets for respective testing. A hole, equal in diameter to the combustion chamber, was placed in the front face of the combustion cylinder. To seal this hole for reverse inlet operation, a steel plug similar to that created for the 15cm was screwed into the hole using a 32 thread pitch.

For ease of manufacturing, the outer diameter of the combustion cylinder was kept constant while varying the inner diameters according to desired pulsejet dimensions (Figure 2.1-3b). In doing so, wall thicknesses also remained at a sufficient width to facilitate the instrumentation of spark plugs, fuel injectors, pressure ports, thermocouples, etc.

The combustion cylinder was specifically design for the implementation of multiple reverse inlets. Holes for inlets could be easily drilled into the rear flat face, surrounding the tail pipe (Figure 2.1-3c), in any configuration desired. The inlets were drilled so that they intersected the incline of the transition walls and remained parallel to the tail pipe. Adding inlets or modifying existing inlets was then just a matter of drilling more holes. The new construction proved simpler in manufacturing, instrumentation, and use than the 15cm pulsejet. It was therefore used in both the scalability experiments of conventional configurations and the testing of reverse inlet capabilities.

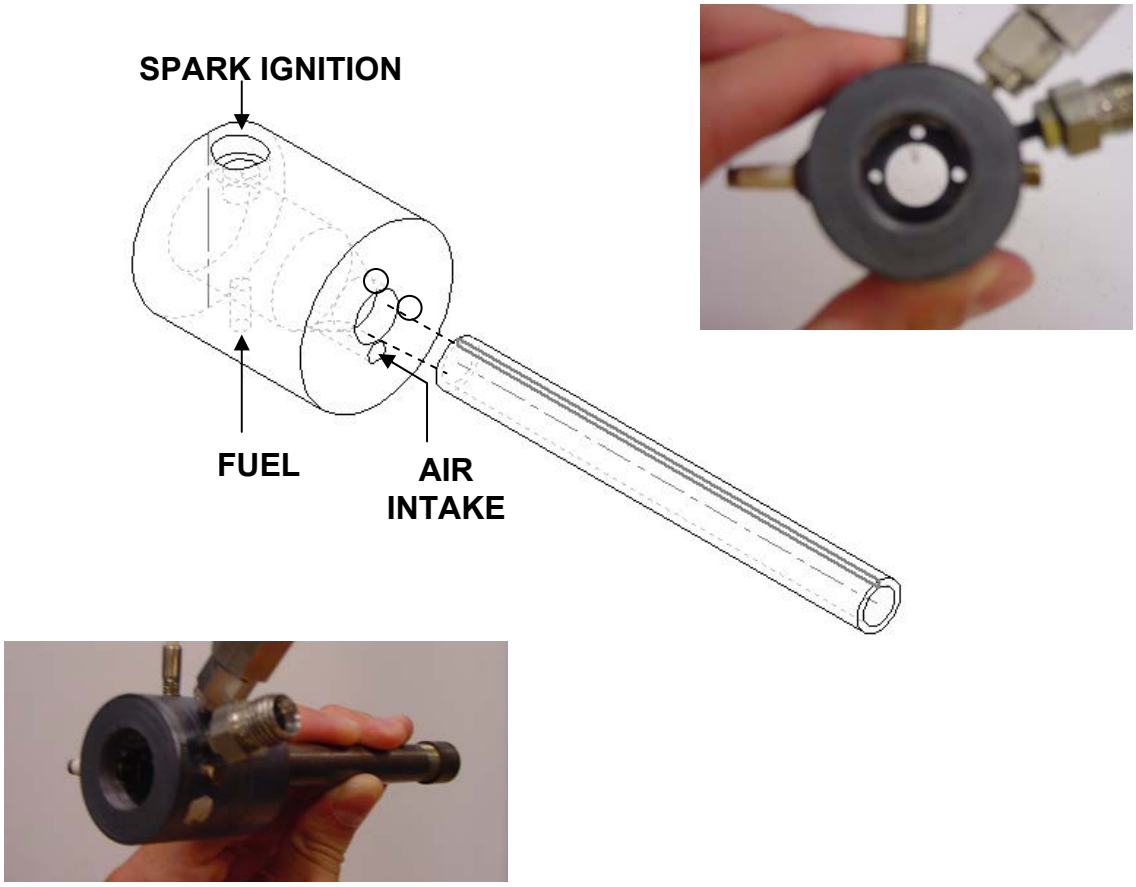

Figure 2.1-3: **(a) Bottom, combustion cylinder and tail pipe extension, (b) middle, combustion cylinder wall contour and hole placement, (c) top, view of inlets from front face of combustion chamber.**

2.2 Ignition

Unlike the BMS pulsejet, the 15cm was not initially ignited via a spark plug. Instead, a hotwire ignition source was implemented immediately downstream of the reed valves. As Figure 2.2-1(a) illustrates, 30 gauge NiCr wire was placed in a manner as to promote contact with fresh fuel/air mixture entering the combustion chamber. The wire was isolated from the jet walls by ceramic tubing and heated with an electric current

controlled by a variable voltage supplier. The ceramic tubing was inserted through a hole drilled into the small block of addition material on the wall of the combustion chamber (originally used for the head-stabilizing setscrew) and held in place by JB Weld high-temperature epoxy. Problems occurred where flow velocities at a local point over the wire were small, and the localized temperature of the wire at that point was allowed to reach a critical level associated with burn out. To avoid the problem of burn-out, the wire diameter was maximized to 22 gauge. Unfortunately, however, burn-out persisted. Due to the tedious process of refitting the 15cm with a new ignition wire after every burn-out event, a 7mm x 1.0 hole was tapped to accommodate a miniature spark plug. The location of the hole is illustrated by Figure 2.2-1b, set 90º in the radial plane from the direct fuel injector. Greater success in ignition was found with the spark plug than with the previous wire ignition system.

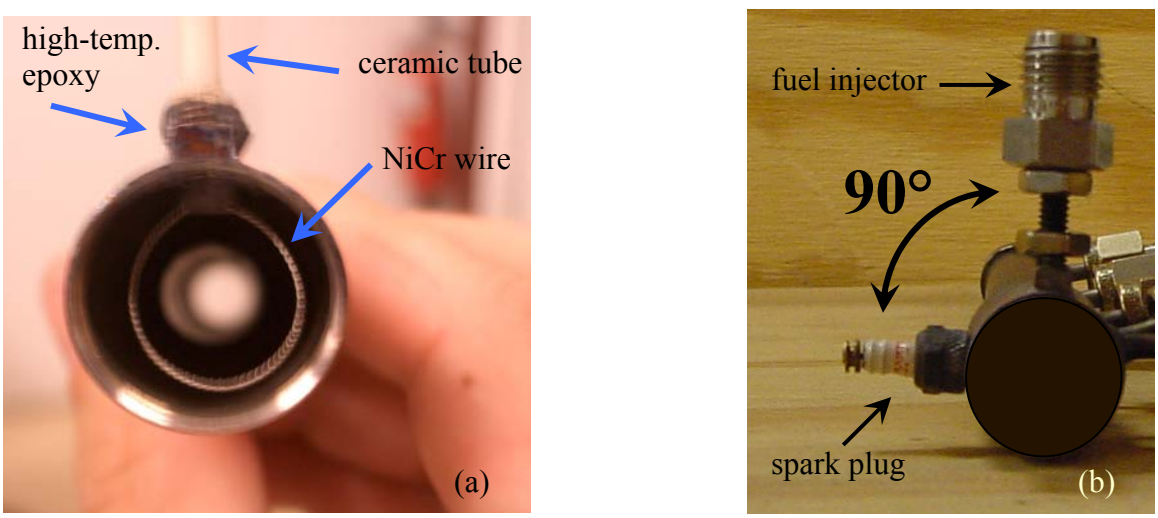

Figure 2.2-1: 15 cm ignition placement of (a) NiCr wire, (b) spark plug.

2.3 Valveless Inlet Geometry

At a point in experimentation, the valved pulsejet head was replaced with a valveless configuration to study the operational feasibility of alternative inlet designs. Several variations of the valveless design were manufactured and tested (Figure 2.3-1). Multiple inlet area to exit area ratios were chosen. Preliminary ratios were selected based on successful examples of full-scale pulsejets found in previous works (Lockwood, 1964; Logan, 1951). Each inlet was tested at multiple lengths, and will be discussed in the following chapters. Initially, the valveless heads were made from aluminum. However, when the aluminum threads began to melt due to the high temperatures observed at the combustion chamber, all valveless heads were replaced by stainless steel duplicates.

Figure 2.3-1: Valveless inlets.

The effects of varying inlet location for valveless operation were studied, as well. Two 0.5" x 0.25" metal blocks were welded to the 15cm to support inlet extensions at different positions about the combustion chamber. Specifically, as shown in Figure 2.3-2, an inlet was placed perpendicular to the longitudinal jet axis, aligned circumferentially with the direct fuel injector. Also shown in Figure 2.3-2, an additional inlet port was situated perpendicular to the transition section such that the incoming charge was directed towards the center of the combustion chamber, impinging upon the injected fuel flow. It was felt that by maximizing mixing, successful operation may be more likely to occur. To isolate the operation of specific inlets, several plugs were made to seal undesired inlet holes. Each additional inlet port was tapped in order to facilitate inlet components and, thus, solid steel threaded rods could be used as inlet plugs (Figure 2.3-2). At the threshold of the combustion chamber, a larger plug replaced the pulsejet head junction.

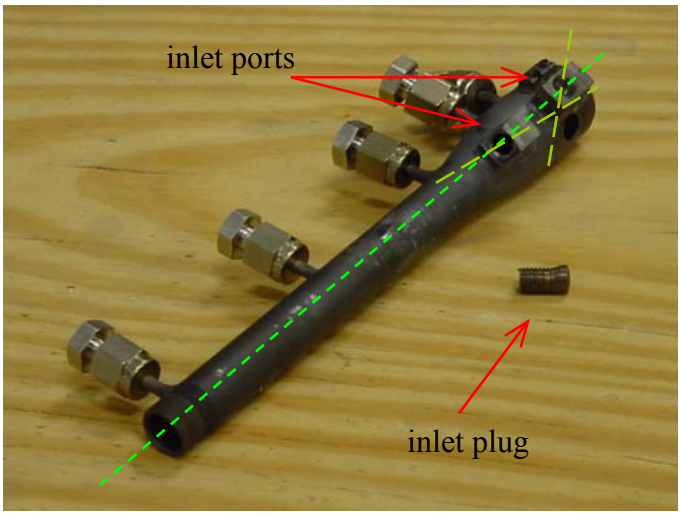

Figure 2.3-2: Additional inlet orientations.

2.4 Exit Geometry

To accommodate a quick and easy process of changing the pulsejet length configurations and exit geometries, 1/2 inch-32 threads were machined into the end of the tail pipe. Several coupling collars were produced in order to attach differing exit shapes and length extensions (Figure 2.4-1). Extensions were created at three different lengths – 1, ½, and ¼ times the original length of the 15cm tail pipe (4.17", 2.09", and 1.04", respectively). Two types of diverging segments were created to study the effects of varying wave transmission within the pulsejet to the surrounding atmosphere, as seen in Figure 2.4-1.

Figure 2.4-1: Length extension shapes and coupling collars.

2.5 Fuel Injection

Fuel injection methods saw a gradual development, as well. Fuel was first injected upstream of the reed valves through a 1/16" stainless steel tubing inserted through the constant area inlet, as shown (Figure 2.5-1a). The fuel was added via four small holes drilled circumferentially about the tube, allowing the fuel to be introduced perpendicular to the direction of the flow. Such an angle of injection allowed for maximum mixing while minimizing momentum disruption of the mean flow. Fuel was also introduced as a premixed fuel/air charge upstream of the valved inlet via a T-junction between the fuel and air lines. Following the junction was a short piece of ¼" metal tubing in case of flashback. Fuel injection for the valveless configurations followed similar methods. 1/16" stainless steel tubing was placed slightly upstream of the combustion chamber threshold along the inlet's longitudinal axis. The tubing was bent in such a way to allow it to be placed through a hole in the walls of the inlet (see Figure 2.5-1b). Fuel was then introduced 90º or 45º incident to the direction of mean flow through four circumferential holes in the steel tubing.

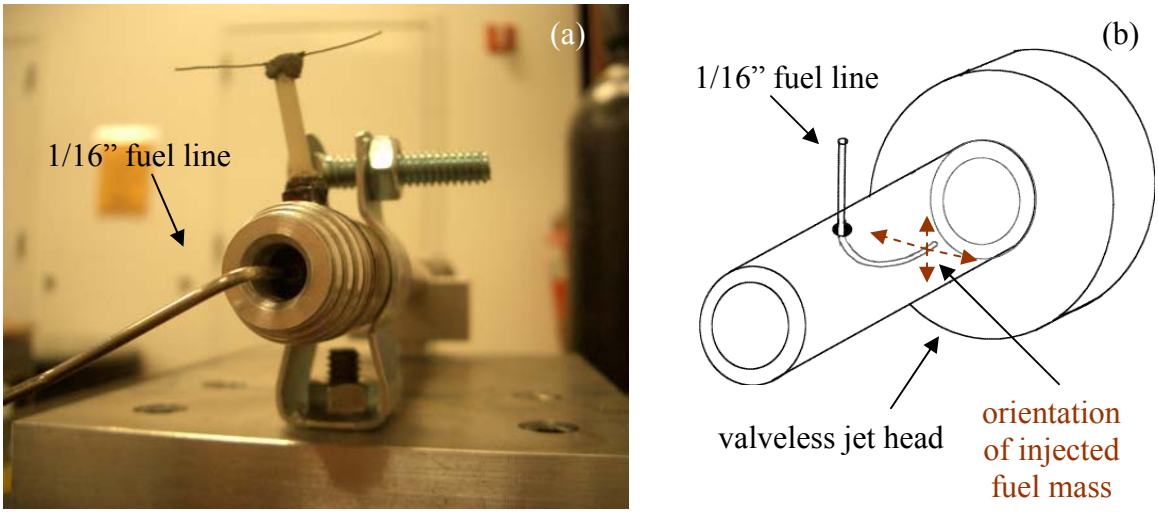

Figure 2.5-1: (a) Stainless steel fuel line through valved head, (b) valveless upstream fuel injection.

Direct injection of fuel into the combustion chamber was accomplished by retrofitting the aforementioned ceramic tubing hole, used for the insulation of ignition wire, to accommodate a simple fuel injector (Figure 2.5-2). A short 8-32 setscrew, bored through the center, was coupled with a modified ¼” tubing cap (for connection with a ¼” fuel line) and placed in the retrofitted hole of the combustion chamber wall. This enabled the injection of fuel directly into the combustor section of the 15cm without any obvious consideration for mixing. However, improved mixing most likely occurred due to the shear forces within the turbulent boundary layer of the combustion chamber walls.

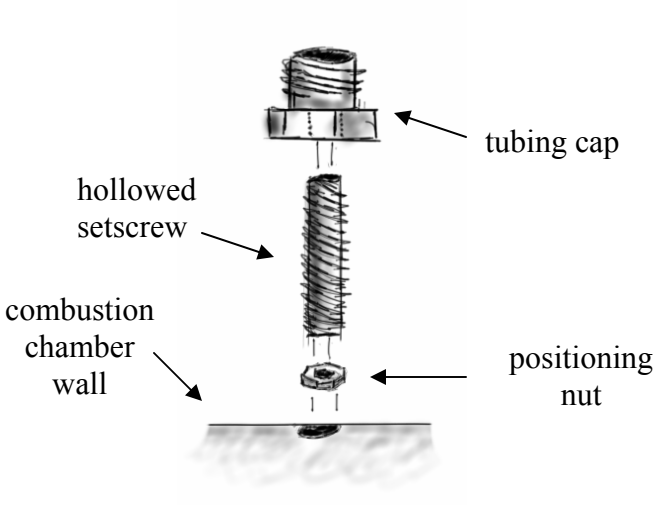

Figure 2.5-2: Direct fuel injector.

2.6 Instrumentation

2.6.1 Pressure Ports

The 15cm was instrumented with five pressure ports located at different distances along the axis of the pulsejet. The ports were placed 0.39, 0.79, 1.75, 3.46, and 5.51 inches from the combustion chamber threshold. These locations correspond to immediately after the location of direct fuel injection, just before the transition section, just after the transition section, halfway down the exhaust tube, and just before the exit plane, respectively. The ports were attached to the 15cm by drilling 1/8" holes at their respective positions and welding 1/8" stainless steel tubing segments, each 0.75 inch in length, to all five holes. A pressure transducer could then be placed at each port by

coupling the DPX-to-¼”-NPT transducer component to 1/8” compression fittings via Swagelok stainless steel reducing unions.

2.6.2 Thrust Stand and Testing Rig

The experimental setup for testing all pulsejets is shown in Figure 2.6-1. A low-friction linear bearing assembly used for thrust measurements was mounted to a 27.5” x 19.75” x 0.625” steel plate (detailed by Figure 2.6-2). An aluminum plate device, however, secured the pulsejet to the linear bearing assembly and differed according to the specific pulsejet under testing. For the 15cm, a miniature steel pipe clasp held the tail pipe between a small aluminum block which screwed into the aluminum plate via four screws. For the combustion cylinder setup, the miniature steel clamp was replaced by another aluminum block that clamped down on the tail pipe using two screws on either side. The aluminum plate was attached to a black anodized aluminum shuttle which rested on the rods of the linear bearing assembly. An Omega No. 14 rotometer and a Hastings Instruments Model 40 flow meter measured fuel flow rates.

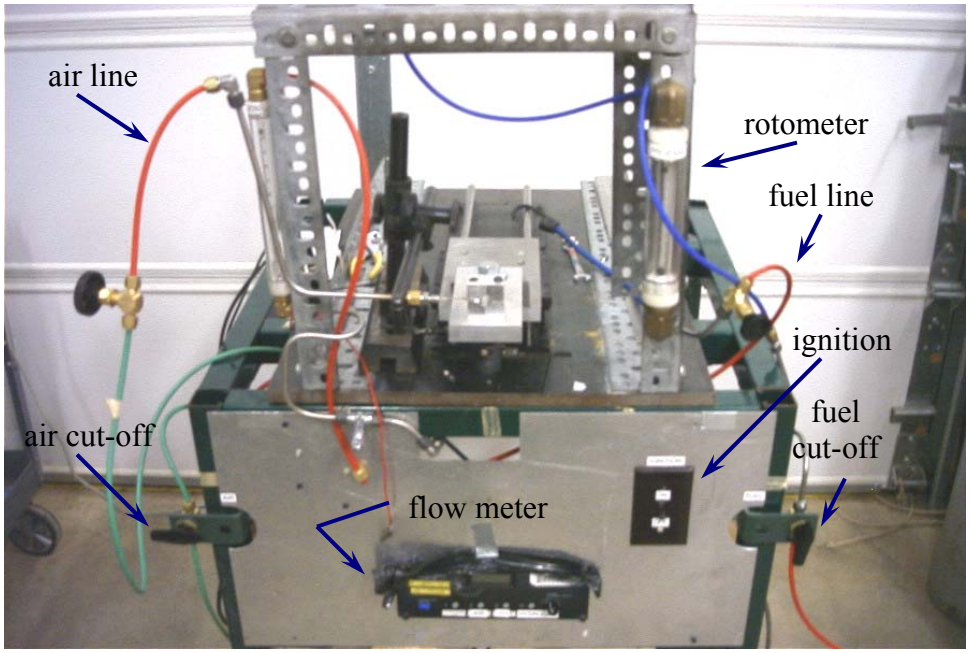

Figure 2.6-1: Instrumentation and experimental setup.

Time resolved thrust data was measured via an Entran piezoelectric load cell in combination with a Kistler Type 5004 dual mode charge amplifier. The thrust stand configuration was incorporated directly into the pulsejet testing rig. The load cell was exposed to shear loads in the direction of positive and negative thrust. The required preload was achieved by compressing the load cell between two aluminum plates via a ½ inch bolt, as shown in Figure 14. The top-lying aluminum plate held the pulsejet while the underlying plate was secured to the anodized aluminum shuttle. A magnetically shielded BNC cable was incorporated to prevent interference in the data signal. Instantaneous static pressure measurements were taken using an Omega DPX 101-250 high speed quartz crystal pressure transducer coupled to an Omega ACC-PS1 power supply box. All pressure and thrust data were recorded on an Agilent two-channel

oscilloscope. Average temperature measurements were collected using custom Type B thermocouples and a standard Omega DP460 thermocouple readout.

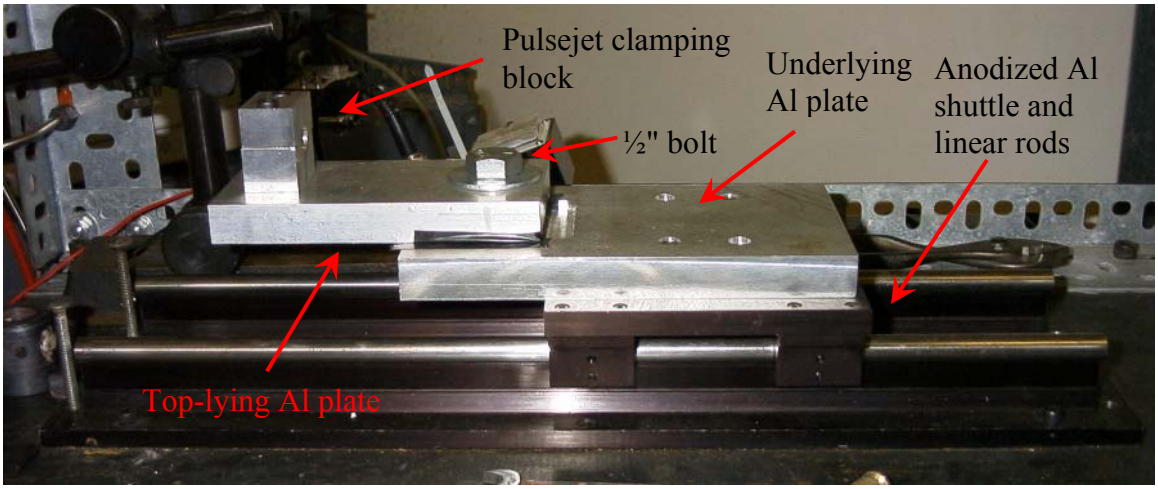

Figure 2.6-2: Thrust stand setup and low-friction linear bearing assembly.

3 Valveless Pulsejet Performance Measurements

3.1 Scale Effects

Scalability characteristics of the 15 centimeter class pulsejet were investigated by varying inlet length, inlet inner diameter, tail pipe length, and tail pipe exit geometry. For each case, the inlet to combustion chamber area ratio was held constant while varying inlet and tail pipe lengths. For each inlet length, runs were performed at several exhaust lengths using identical incremental steps for each case. To begin an inlet study, the tail pipe length was set at roughly 15 inches and the engine was tested for self-sustaining combustion. This baseline length was chosen based upon the empirical assumption that, at that tail pipe length, all inlet configurations would resonate. The tail pipe length was then stepped down twice in approximately 4-inch increments contingent upon success at each length previous. If the pulsejet continued to achieve self-sustaining combustion, the exhaust length was stepped down once more by about 2 inches, resulting in a final tail pipe length of 4 inches.

At each exhaust length, two different exit plane geometries were studied. Temperature, pressure, and thrust were simultaneously observed for each jet configuration. For every run, a conservative fuel flow rate was chosen based upon the steady response of the pulsejet engine. Finally, maximum fuel flow rates were tested at both the full jet length and the shortest length attainable. A summary of results for all cases explored is listed in Table 3.1-1 below.

Pressure ports were located at the combustor chamber and immediately downstream of the transition section, as illustrated in Figure 3.1-1. Port 1 designates the pressure port placed 0.39 inches from the front face of the combustion cylinder in the same plane as the fuel injector and spark plug but 90 degrees offset, circumferentially. Port 2 designates the pressure port 0.39 inches downstream of port 1, placed roughly in the mid-plane of the combustion chamber. Port 3 refers to the pressure port located immediately downstream of the transition section, 0.18 inches from the rear face of the combustion cylinder.

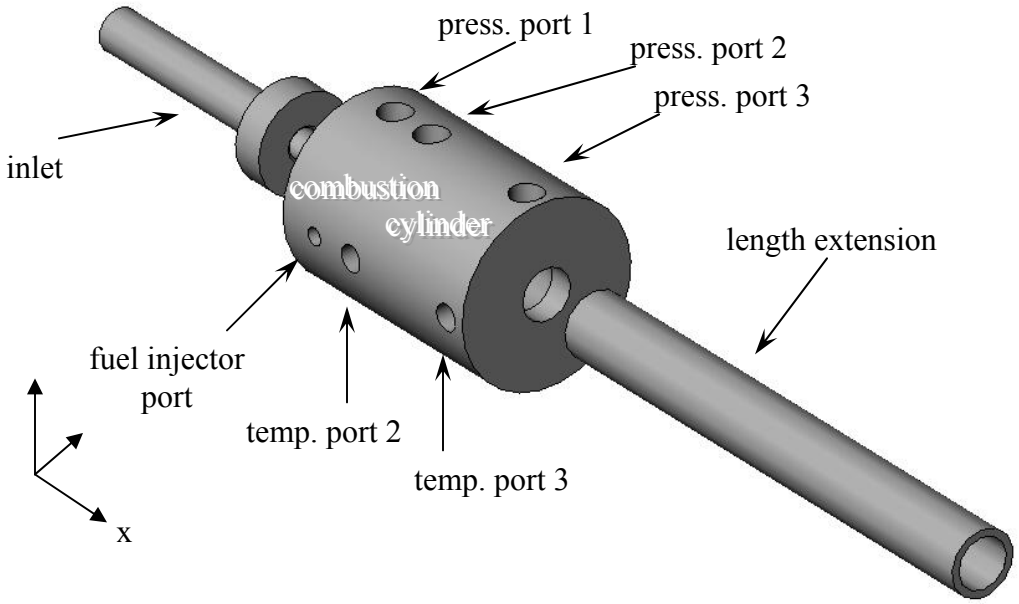

Figure 3.1-1: Schematic of data port placement for scalability experimentation.

Two separate temperature ports were drilled in the combustion cylinder (Figure 3.1-1). Temperature port 2 was located at the same axial (x) position as pressure port 2,

in line with the fuel injector. Temperature port 3 was in the same location as pressure port 3. Each temperature port accommodated a Type B (Pt 6% Rh vs. Pt 30% Rh) thermocouple by allowing a sheath, housing a 1/8 inch ceramic tube containing the thermocouple wires, to be screwed securely in to place. The ceramic tubing was fastened to the stainless steel sheath with red RTV silicone. All unused ports were plugged with appropriate hex-head stainless steel screws. Figure 3.1-2 offers a detailed view of the instrumentation assembly for the combustion cylinder.

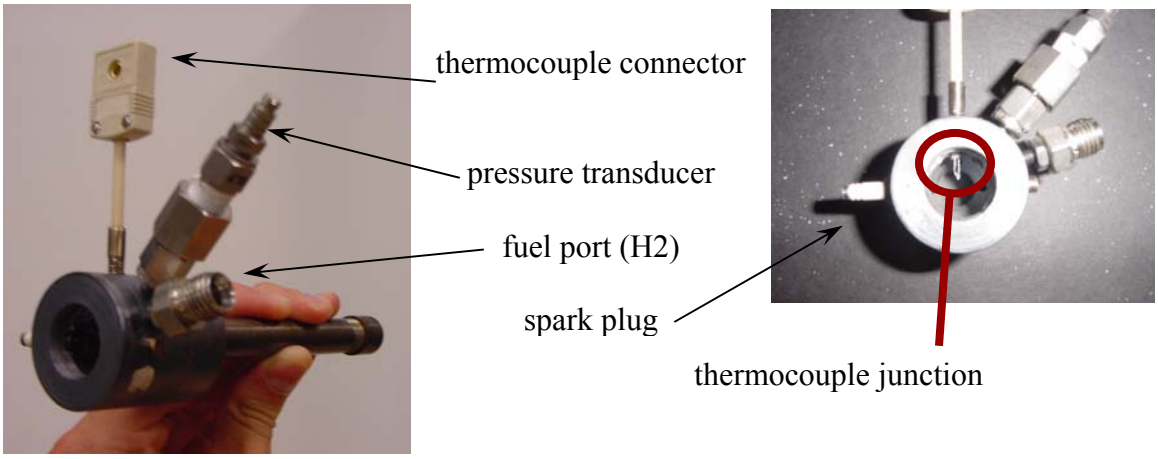

Figure 3.1-2: Instrumentation for scalability study.

Case	Area Ratio (A_i/A_c)	Inlet length L_i (in.)	Tail pipe lengths (in.) at which self-sustained combustion was achieved		Nozzle
			w/o nozzle	*w/ nozzle*	
1.1	0.130	2.0	N/A	20.875, 18.75, 16.625, 14.375, 12.25	B
1.2	0.130	1.5	18.0, 11.5	20.375, 18.25, 16.0, 13.875, 11.75, 9.75	B
1.3	0.130	1.0	17.5, 15.375, 13.25, 11.125	17.75, 15.625, 13.5, 11.25, 9.125	B
1.4	0.130	0.5	16.875, 14.75, 12.625, 10.5, 8.375, 6.25	17.125, 15.0, 12.875, 10.75, 8.625	B
2.1	0.086	2.0	16.375, 14.25	18.75, 16.625, 14.5, 12.375	B
2.2	0.086	1.5	18.0, 13.75, 9.375	18.25, 13.875, 9.625, 7.75	A/B
2.3	0.086	1.0	17.375, 13.0, 8.875	17.875, 13.5, 9.375, 7.125	A
2.4	0.086	0.5	16.875, 12.5, 8.375, 6.125	17.375, 13.0, 8.875, 6.625	A
3.1	0.040	2.0	18.5, 14.25	19.0, 14.75, 12.625	A
3.2	0.040	1.5	18.0, 13.625, 11.625	18.5, 14.125, 10.0	A
3.3	0.040	1.0	17.438, 13.125, 8.875	17.938, 13.625, 9.375, 7.25	A
3.4	0.040	0.5	16.875, 12.625, 8.375, 6.25	17.375, 13.125, 8.875, 6.75	A

Table 3.1-1: Scalability case summary.

3.1.1 Case 1

Case 1 examines a 0.130 cross-sectional inlet area to combustion chamber area ratio. Figure 3.1-3 shows pressures (ports 1 and 2), operating frequencies, and average temperatures (port 3) for an inlet length of two inches. Each plot corresponds to a different exit length, each with a diverging nozzle B exit geometry (refer to Figure 2.4-1). The nozzle geometry is noted for each length configuration on the respective plot by the letter which appears in parentheses immediately following the overall length in inches,

located at the top of each graph. Those with no letter following the length marker denote a constant area exit geometry.

3.1.1.1 2.0-Inch Inlet

For the initial inlet configuration, resonance with the conventional constant area exit geometry was not achieved at any length tested. All plots of Figure 3.1-3 show peak pressures not exceeding five psi. Frequencies at pressure ports 2 and 3 are identical for each length observed. Self-sustaining combustion was only attainable at 18.75, 16.625, and 14.375 inches. However, to obtain resonance at lengths below 16.625 inches, relatively high fuel flow rates were required on the order of two to three times that of longer jet lengths. Maximum fuel flow rates were tested at the longest and shortest tail pipe lengths observed to be sustainable for significant periods of time. Results are plotted in Figure 3.1-4, where pressure fluctuations at port 2 are plotted along with simultaneous thrust. Average temperature, operating frequency, and fuel flow rates are noted, as well. The maximum thrust values obtained remained on the order of one pound. At 14.375 inches, the thrust appears to follow a discernable trend whose frequency appears to match well with the jet's operational frequency. Maximum and minimum pressures correspond with maximum and minimum thrust. Yet, the thrust appears to lag pressure by a very small fraction of time.

For thrust runs taken at this configuration and all runs following, temperature measurements were taken at port 2. From comparison with port 3 measurements, it was determined that average temperatures did not vary significantly between ports.

3.1.1.2 1.5-Inch Inlet

The inlet length was then reduced 0.5 inch to 1.5 inches while keeping the area ratio constant at 0.130. Tests were repeated at the same jet lengths with and without the nozzle B attachment. The order of absolute pressure did not change (Figure 3.1-5), but combustion was sustainable at shorter lengths, as well as with a constant area exit geometry. At lengths below 13 inches, however, the jet was predisposed to cut-off as the engine heated up (approximately 10-15 seconds after ignition was achieved). Shorter lengths had success with a nozzle B jet configuration but were unsuccessful with only a conventional exit geometry.

Maximum fuel flow tests shown in Figure 3.1-6 were performed at tail pipe lengths of 15 inches and 6.5 inches. Higher fuel flow rates were achievable at shorter lengths, yet absolute pressures were comparable at around 2 psi for both lengths. Again, a discernable thrust pattern was only ascertained at minimal lengths. However, the pressure then lagged the thrust suggesting that the phase shift between the two is different than was seen at 14.375 inches with an inlet length of 2.0 inches.

3.1.1.3 1.0-Inch Inlet

Inlet length was reduced to 1.0 inch and plotted data can be found in Figure 3.1-7. Chamber pressure generally remained in the ±3.0 psi range throughout all jet length increments. Absolute thrust, however, fluctuated somewhat considerably between exit geometries. Maxima and minima values are greater for runs performed with the nozzle B in place. Furthermore, such values remained fairly constant from length to length for the respective exit geometry. Excluding, that is, the 9.125-inch nozzle B configuration where

maximum thrust values increased two fold and remained disproportional to minima values.

The same disproportionate characteristic is observed (see Figure 3.1-8) in the maximum fuel flow test for the identical 9.125-inch configuration. Once again, a clear pattern is witnessed in the thrust data for the short lengths as opposed to the apparently random behavior of longer configurations. Maximizing the fuel flow rate for the 17.5-inch nozzle B pulsejet produced maximum pressure rises almost twice that of more conservative fuel flow rates.

Significant heating incurred by the pressure transducer caused noticeable drift in pressure data, resulting in an offset from origin in a couple of plots. This effect is most noticeable in the pressure data for the 9.125-inch nozzle B configuration at both conservative and maximum fuel flow rates. Heat induced offset of pressure data was unfortunately a problem periodically throughout testing.

3.1.1.4 0.5-Inch Inlet

Figure 3.1-9 shows the pressure and thrust transition from the full length of 17.125 inches to the shortest tail pipe increment, 6.25 inches, for an inlet length of 0.5 inch and an inlet area ratio of 0.130. At this inlet length, patterns in the thrust data become discernable even at the longest jet lengths tested. Pressure minimums stayed under -2.0 psi while maxima do not exceed 4.0 psi. The maximum fuel flow plots of Figure 3.1-10, however, reveal even larger positive pressure rises. Most plots, like that of the 17.125-inch plot of Figure 3.1-10, exhibit greater positive pressure peaks than

negative peaks. This suggests that pressure rise in the combustion chamber due to combustion is not completely returned by opposing refraction waves.

Interesting to note, however, is the apparent progression in pressure waveform behavior as jet length is decreased. Illustrated by Figure 3.1-11 (viewed from left to right), the minor twin peaks seen in the pressure wave of the longer jet configurations appear to weaken and merge into a single peak. The major peaks than lessen in strength as the pressure wave takes on the shape of the shortest jet configuration, where no minor or major events are evident.

Figure 3.1-3:

Pulsejet scalability performance for an inlet length of 2.0 inches and a 0.130 area ratio.

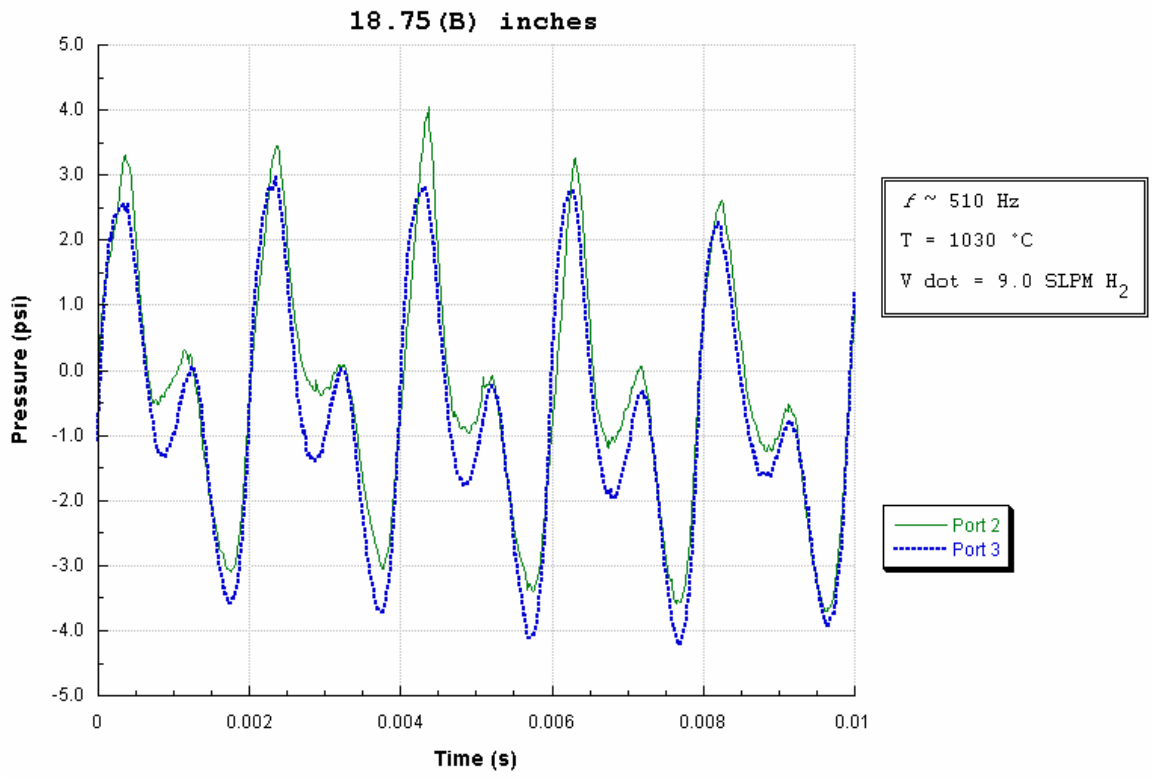
18.75 (B) inches
Pressure (psi)
Time (s)
5.0
4.0
3.0
2.0
1.0
0.0
-1.0
-2.0
-3.0
-4.0
-5.0
0
0.002
0.004
0.006
0.008
0.01
f ~ 510 Hz
T = 1030 °C
V dot = 9.0 SLPM H2
Port 2
Port 3

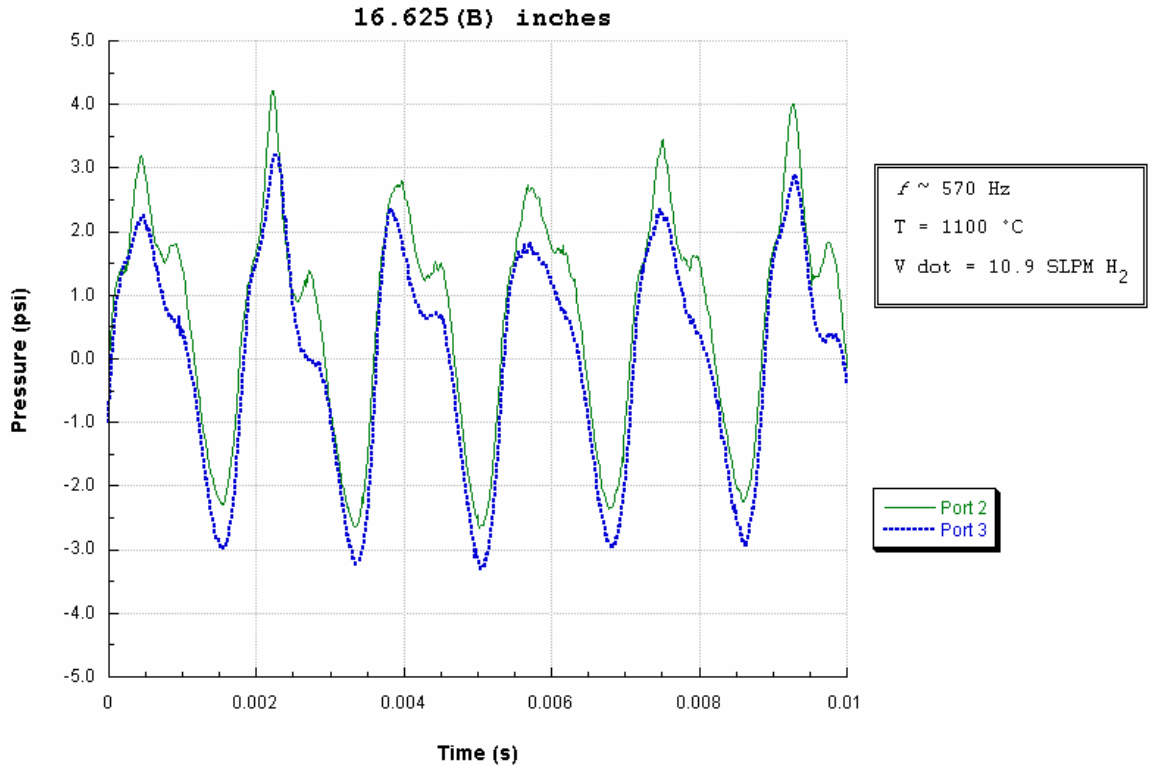
16.625 (B) inches
Pressure (psi)
Time (s)
5.0
4.0
3.0
2.0
1.0
0.0
-1.0
-2.0
-3.0
-4.0
-5.0
0
0.002
0.004
0.006
0.008
0.01
f ~ 570 Hz
T = 1100 °C
V dot = 10.9 SLPM H2
Port 2
Port 3

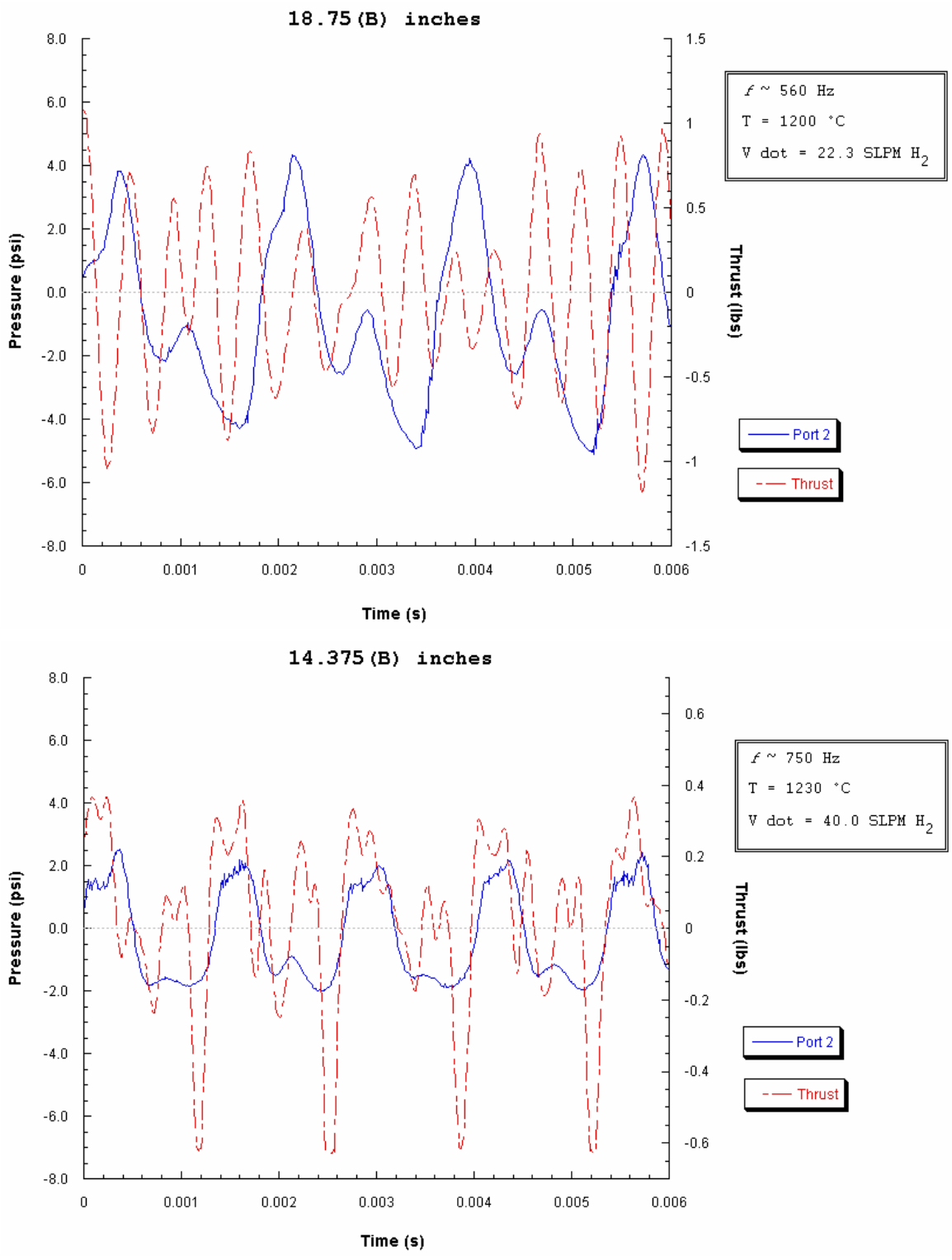

Figure 3.1-4: Maximum $\dot{V}_{H_2}$ at maximum and minimum scalability lengths for an inlet length of 2.0 inches and a 0.130 area ratio.

Figure 3.1-5:

Pulsejet scalability performance for an inlet length of 1.5 inches and a 0.130 area ratio.

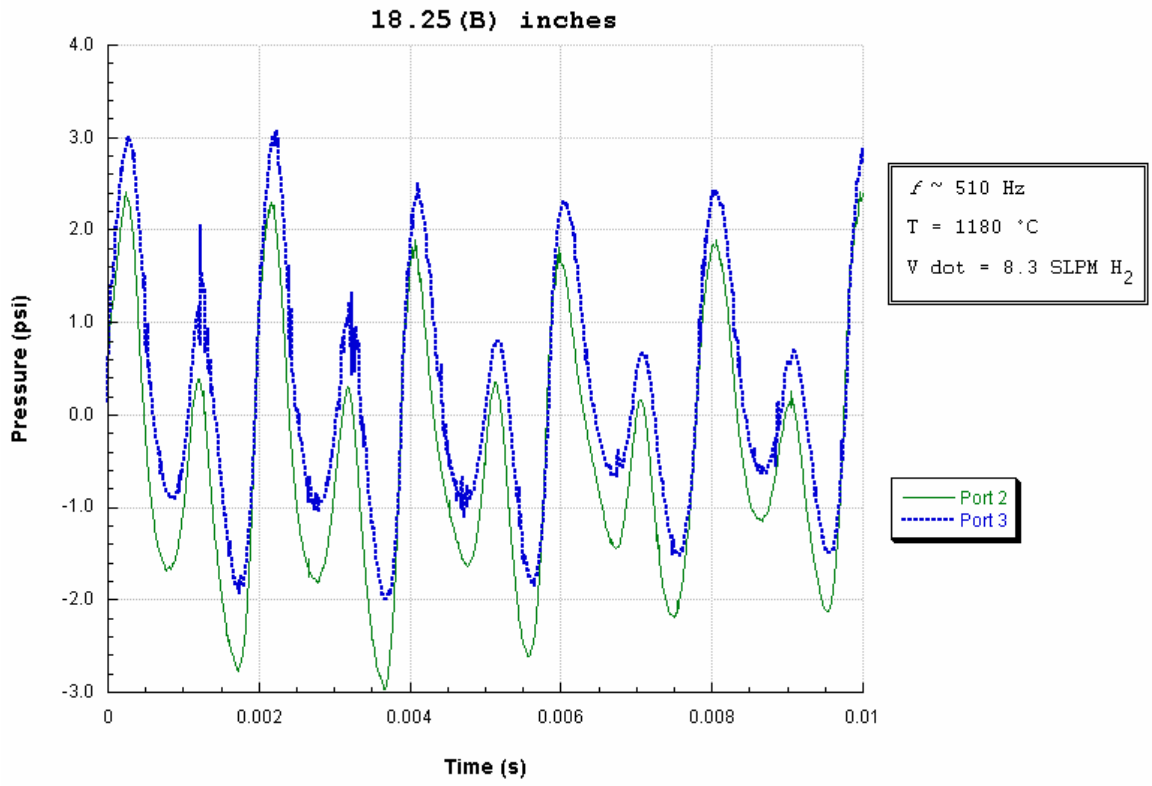
18.25 (B) inches
Pressure (psi)
Time (s)
4.0
3.0
2.0
1.0
0.0
-1.0
-2.0
-3.0
0
0.002
0.004
0.006
0.008
0.01
f ~ 510 Hz
T = 1180 °C
V dot = 8.3 SLPM H2
Port 2
Port 3

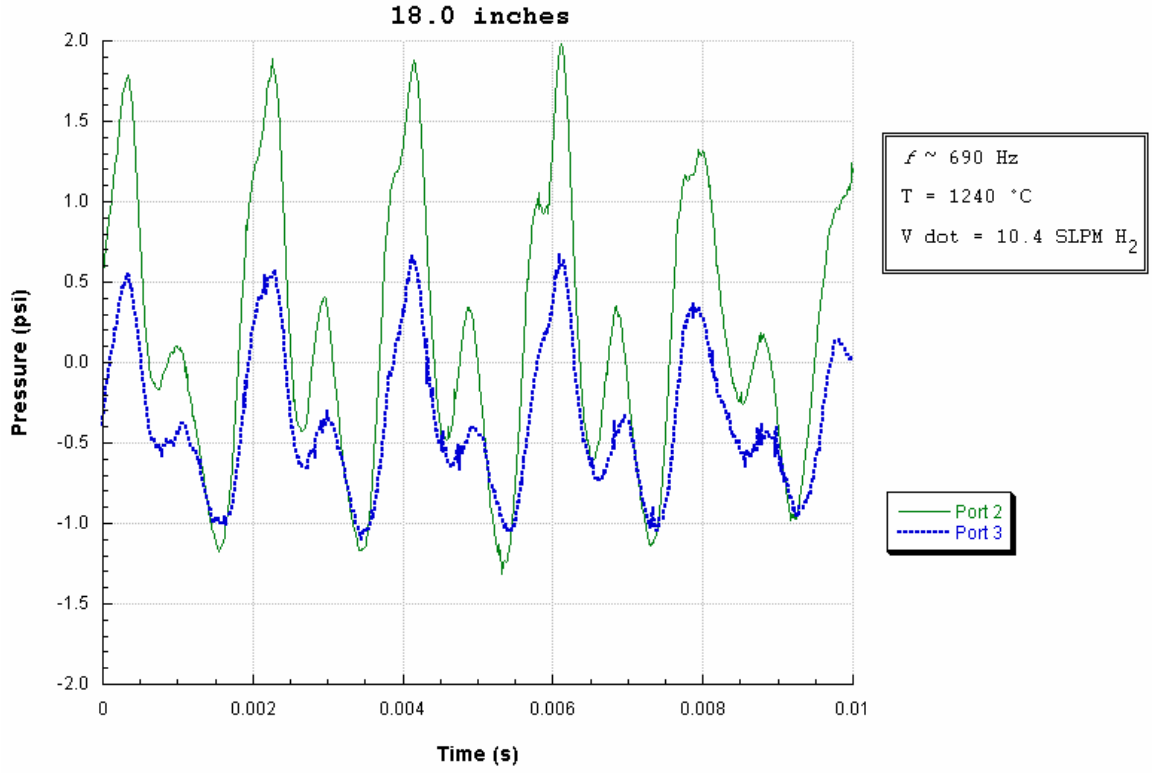
18.0 inches
Pressure (psi)
Time (s)
2.0
1.5
1.0
0.5
0.0
-0.5
-1.0
-1.5
-2.0
0
0.002
0.004
0.006
0.008
0.01
f ~ 690 Hz
T = 1240 °C
V dot = 10.4 SLPM H2
Port 2
Port 3

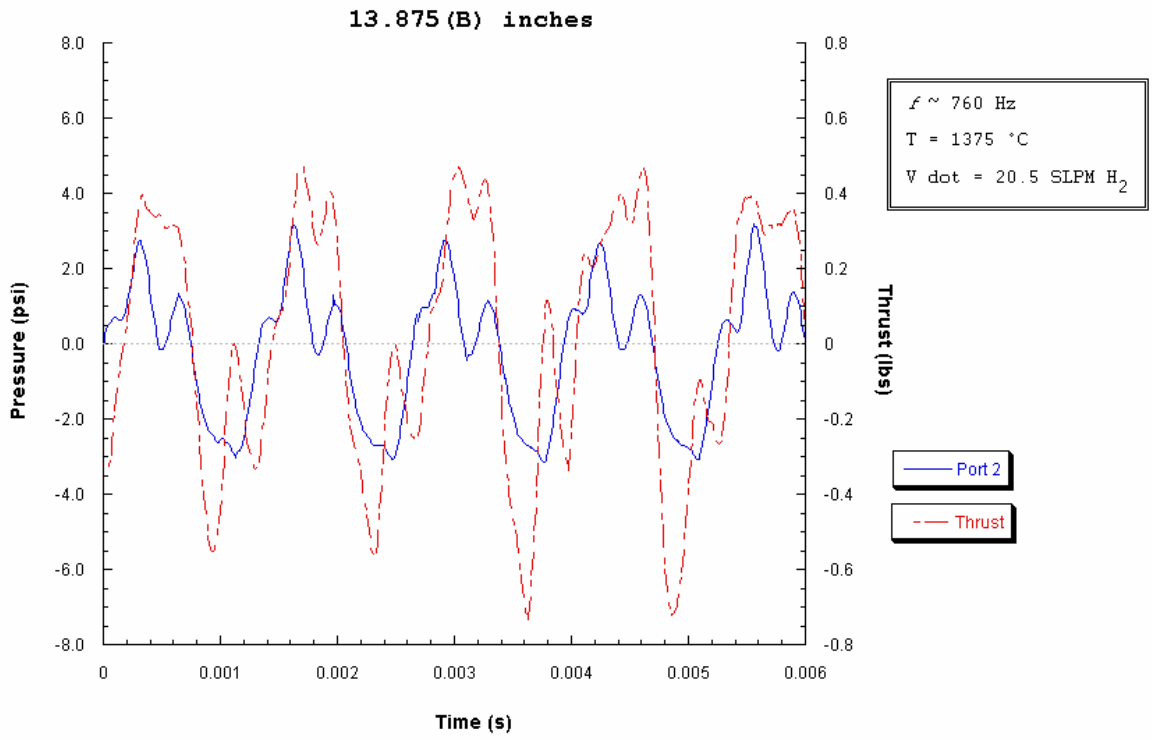
13.875 (B) inches
f ~ 760 Hz
T = 1375 °C
V dot = 20.5 SLPM H2
Pressure (psi)
Thrust (lbs)
Time (s)
Port 2
Thrust
8.0
6.0
4.0
2.0
0.0
-2.0
-4.0
-6.0
-8.0
0.8
0.6
0.4
0.2
0
-0.2
-0.4
-0.6
-0.8
0
0.001
0.002
0.003
0.004
0.005
0.006

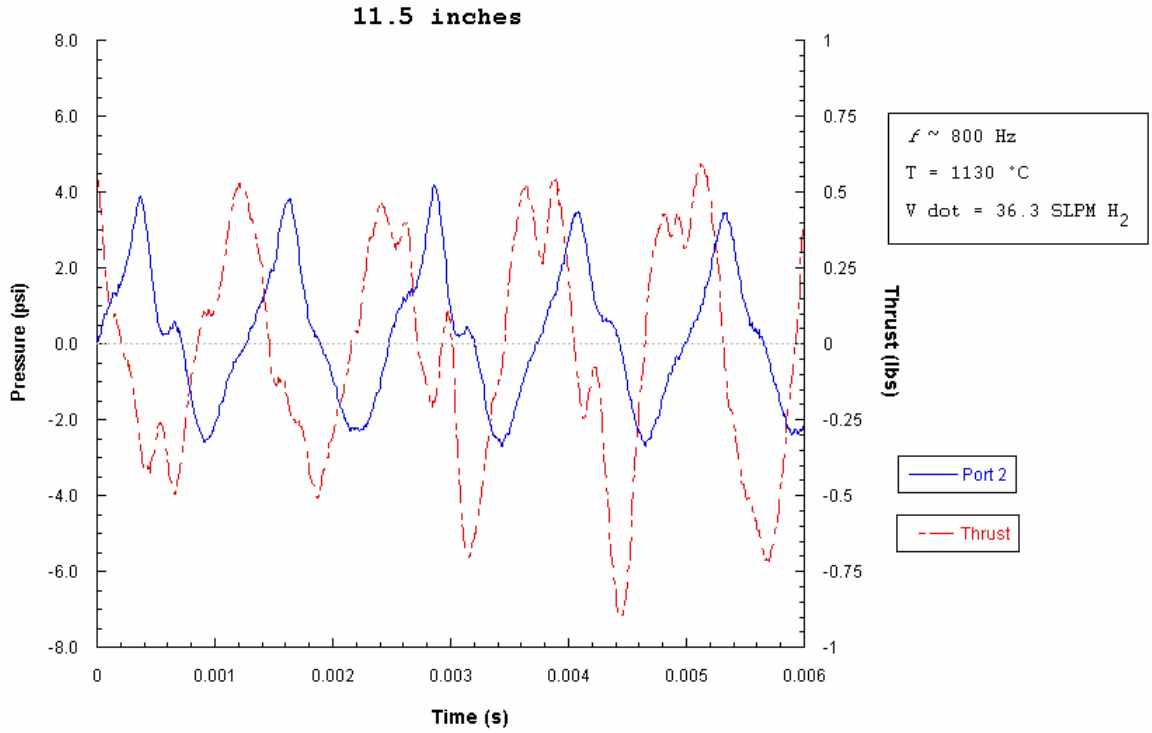
11.5 inches
f ~ 800 Hz
T = 1130 °C
V dot = 36.3 SLPM H2
Pressure (psi)
Thrust (lbs)
Time (s)
Port 2
Thrust
8.0
6.0
4.0
2.0
0.0
-2.0
-4.0
-6.0
-8.0
1
0.75
0.5
0.25
0
-0.25
-0.5
-0.75
-1
0
0.001
0.002
0.003
0.004
0.005
0.006

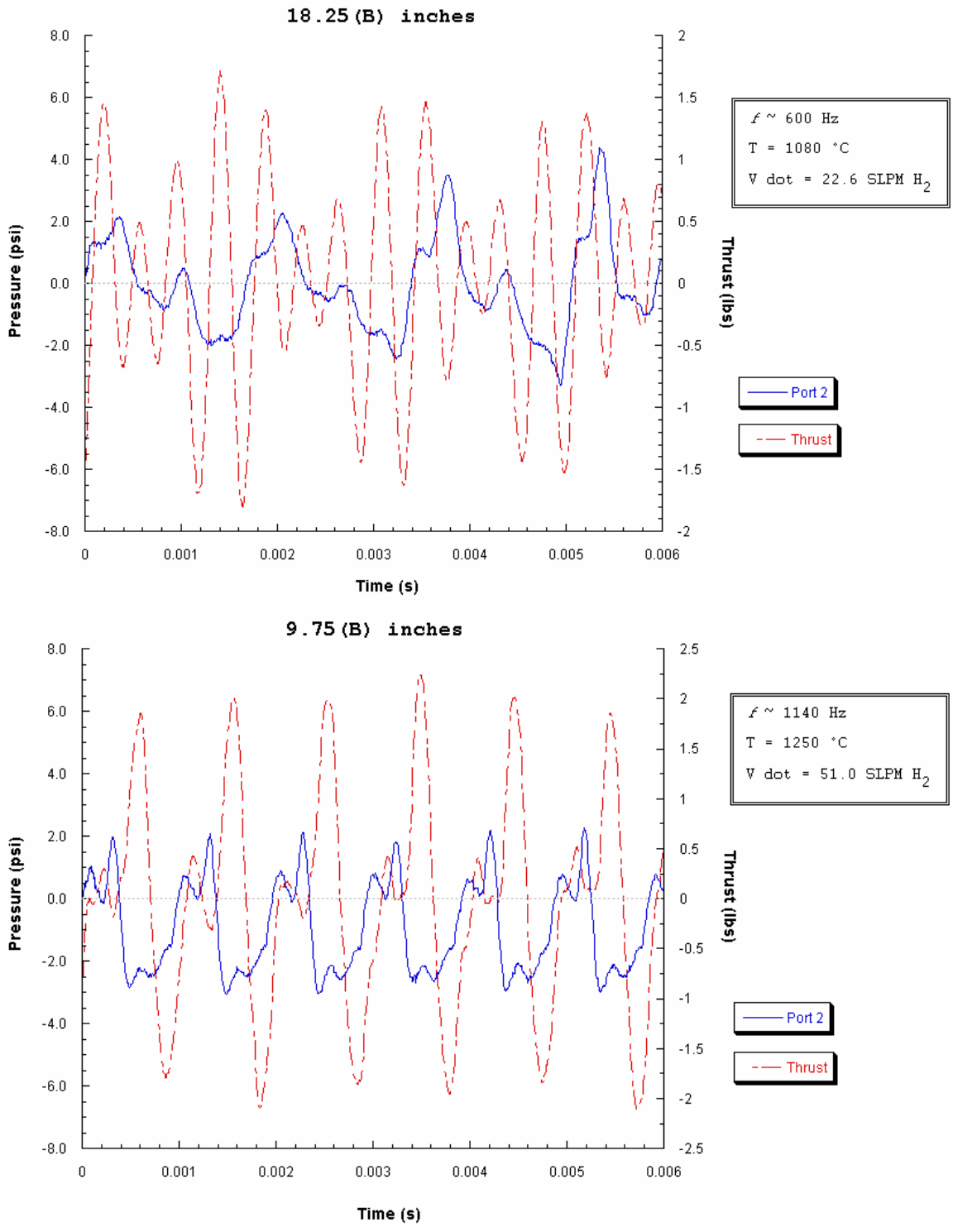

Figure 3.1-6: Maximum $\dot{V}_{H_2}$ at maximum and minimum scalability lengths for an inlet length of 1.5 inches and a 0.130 area ratio.

Figure 3.1-7:

Pulsejet scalability performance for an inlet length of 1.0 inches and a 0.130 area ratio.

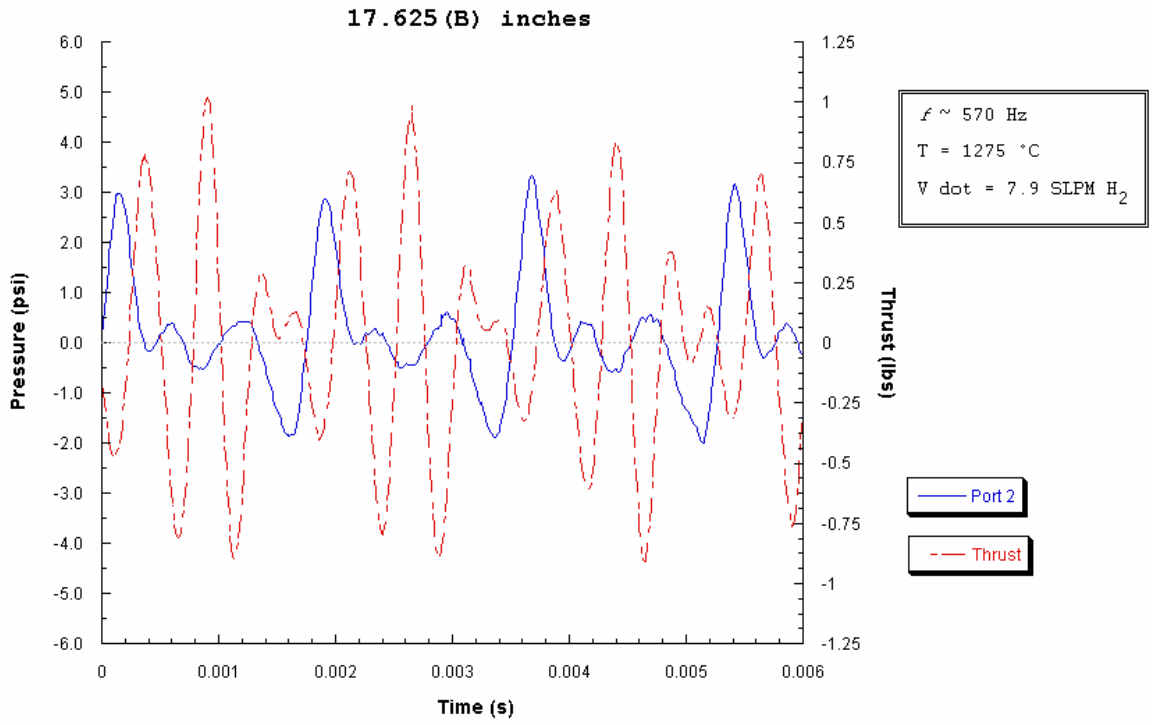
17.625 (B) inches
Pressure (psi)
Thrust (lbs)
Time (s)
f ~ 570 Hz
T = 1275 °C
V dot = 7.9 SLPM H2
Port 2
Thrust

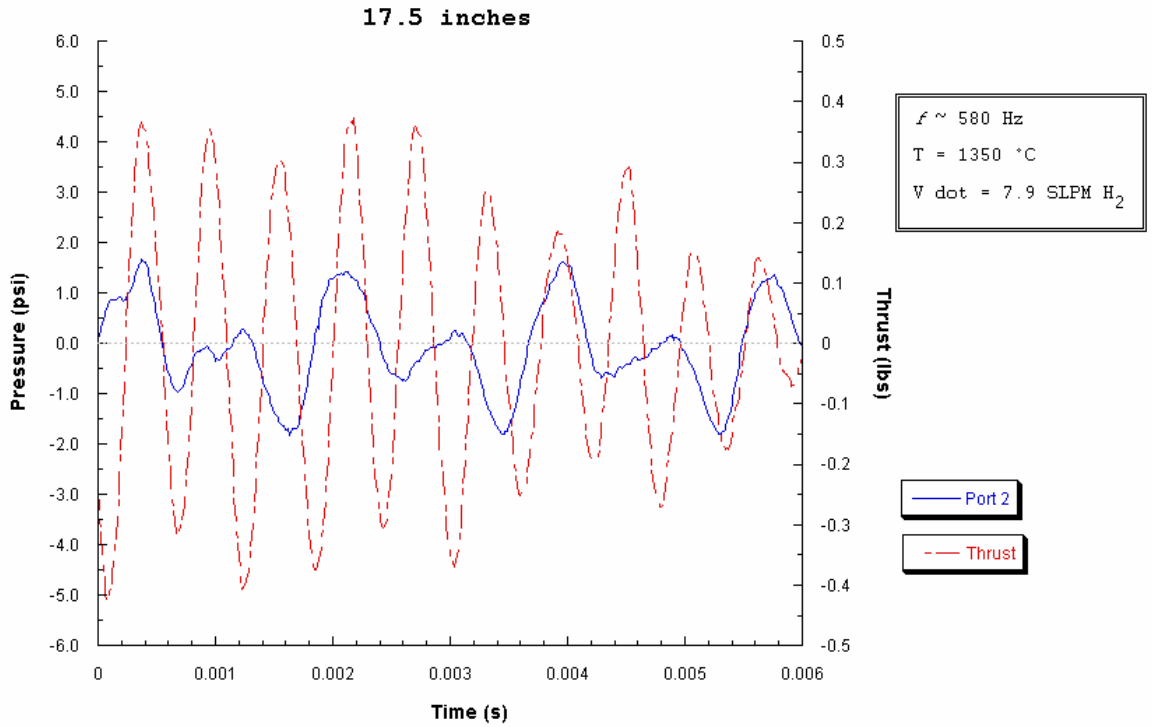
17.5 inches
Pressure (psi)
Thrust (lbs)
Time (s)
f ~ 580 Hz
T = 1350 °C
V dot = 7.9 SLPM H2
Port 2
Thrust

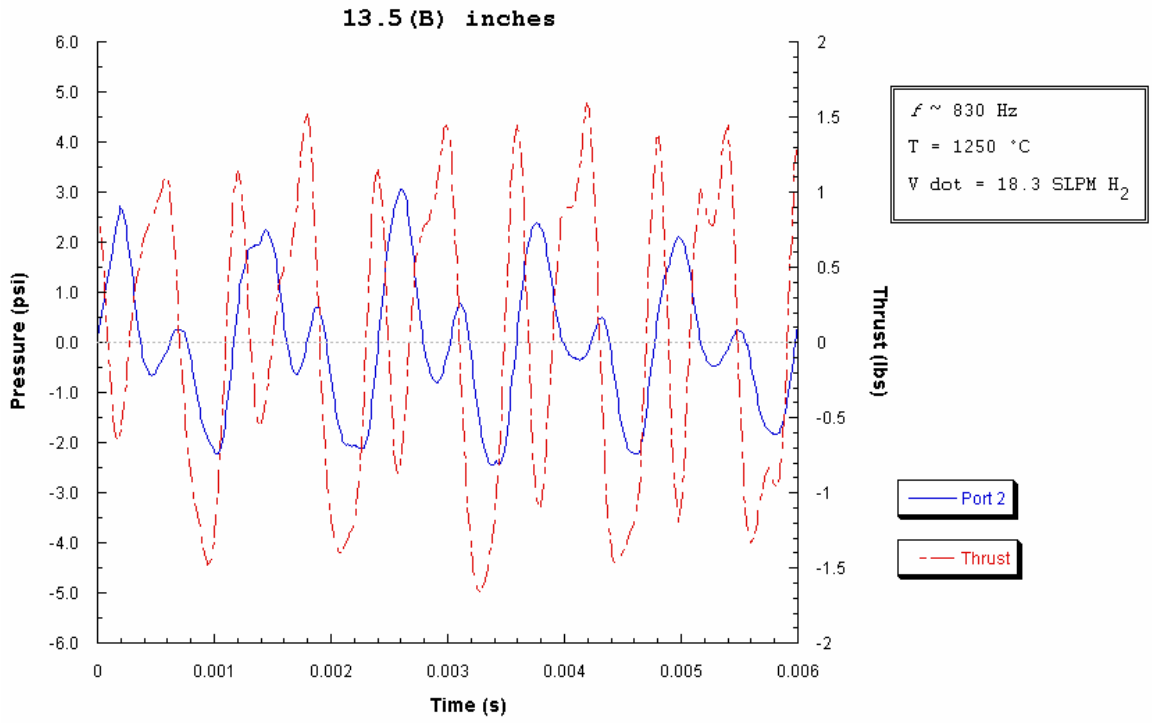
13.5 (B) inches
Pressure (psi)
Thrust (lbs)
Time (s)
f ~ 830 Hz
T = 1250 °C
V dot = 18.3 SLPM H2
Port 2
Thrust

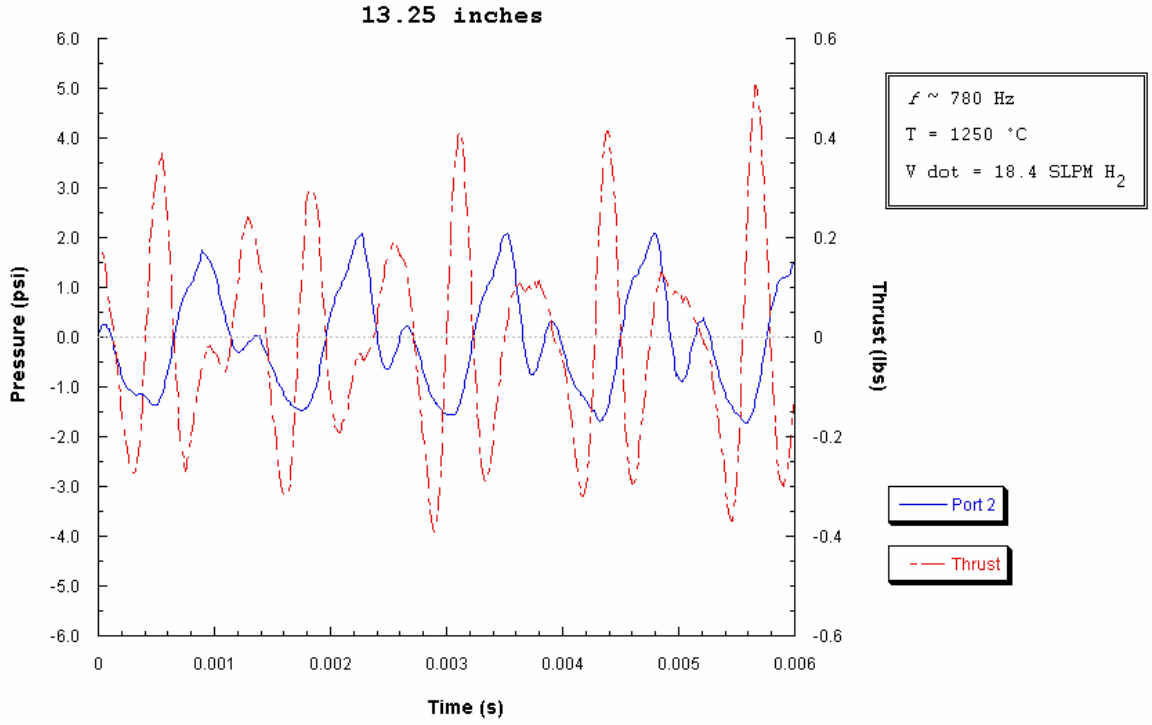
13.25 inches
Pressure (psi)
Thrust (lbs)
Time (s)
f ~ 780 Hz
T = 1250 °C
V dot = 18.4 SLPM H2
Port 2
Thrust

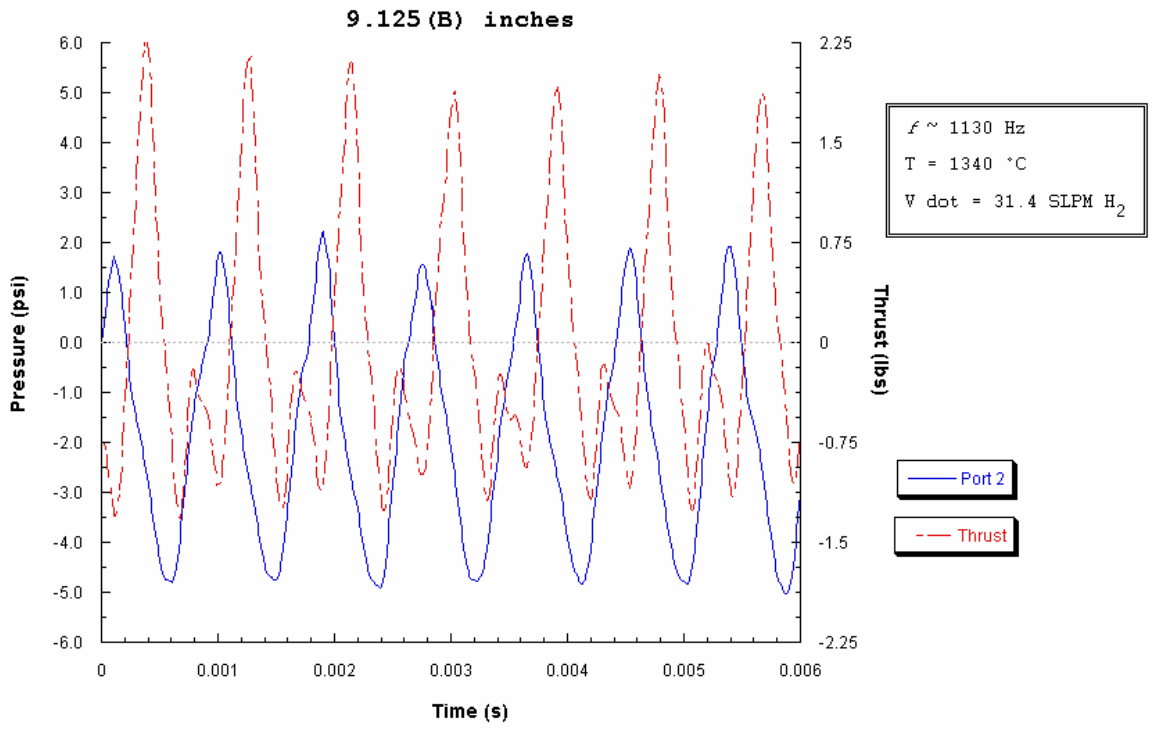
9.125 (B) inches
Pressure (psi)
Thrust (lbs)
Time (s)
f ~ 1130 Hz
T = 1340 °C
V dot = 31.4 SLPM H2
Port 2
Thrust

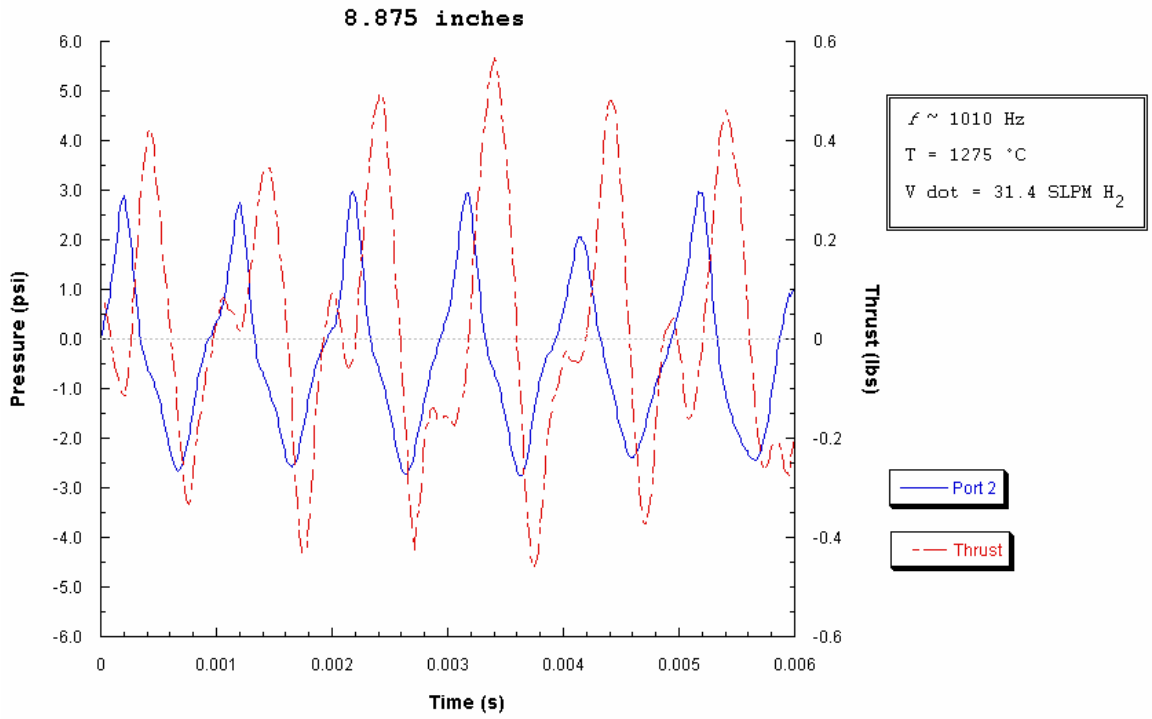
8.875 inches
Pressure (psi)
Thrust (lbs)
Time (s)
f ~ 1010 Hz
T = 1275 °C
V dot = 31.4 SLPM H2
Port 2
Thrust

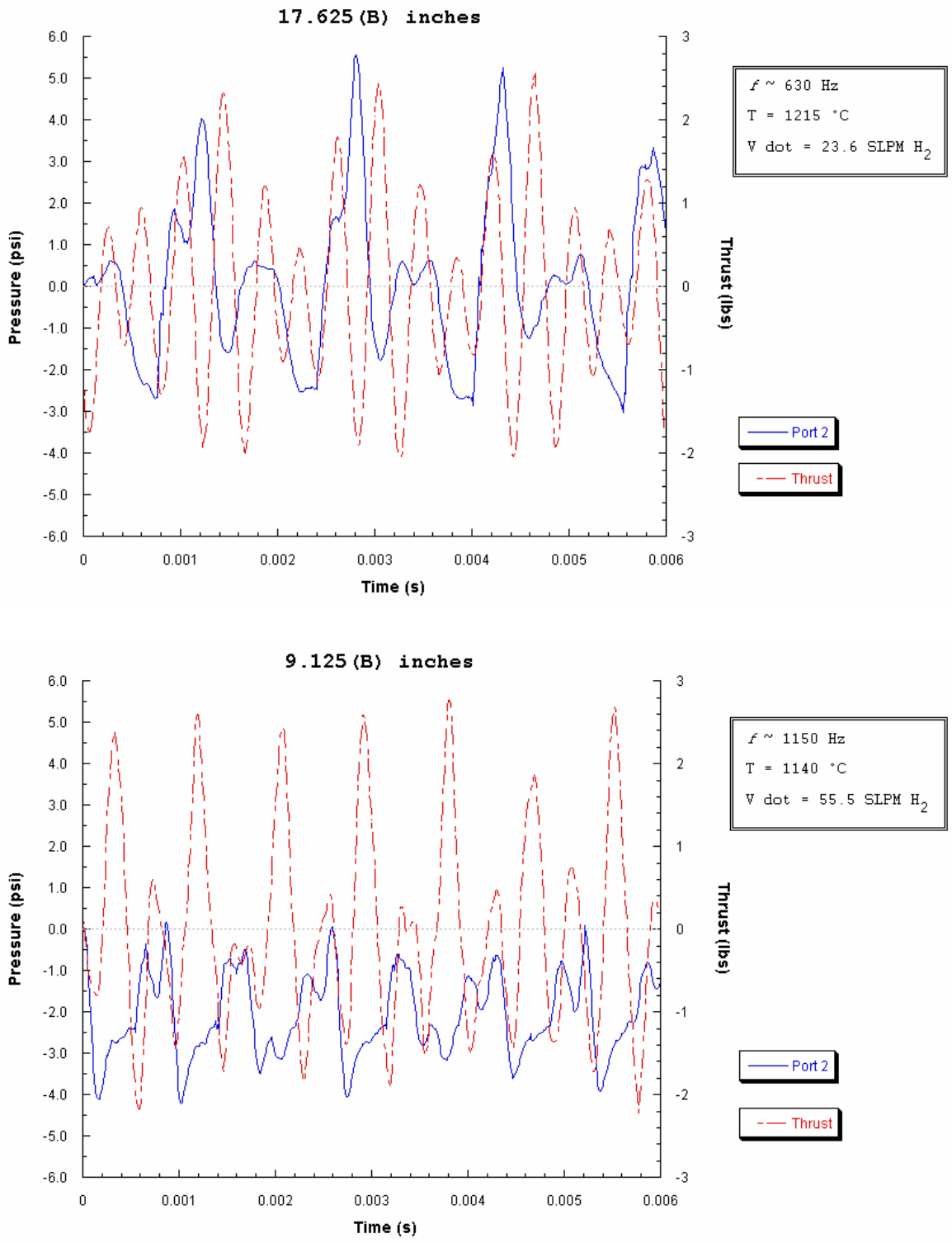

Figure 3.1-8: Maximum $\dot{V}_{H_2}$ at maximum and minimum scalability lengths for an inlet length of 1.0 inches and a 0.130 area ratio.

Figure 3.1-9:

Pulsejet scalability performance for an inlet length of 0.5 inches and a 0.130 area ratio.

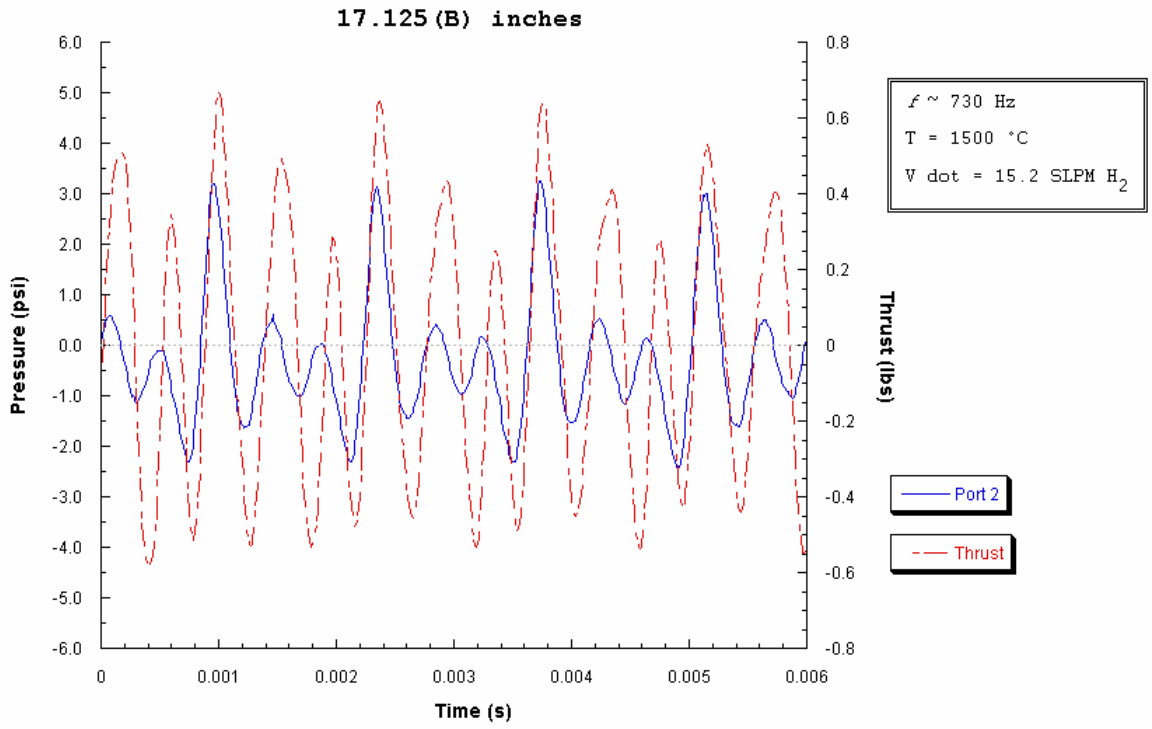
17.125 (B) inches
Pressure (psi)
Thrust (lbs)
Time (s)
f ~ 730 Hz
T = 1500 °C
V dot = 15.2 SLPM H2
Port 2
Thrust

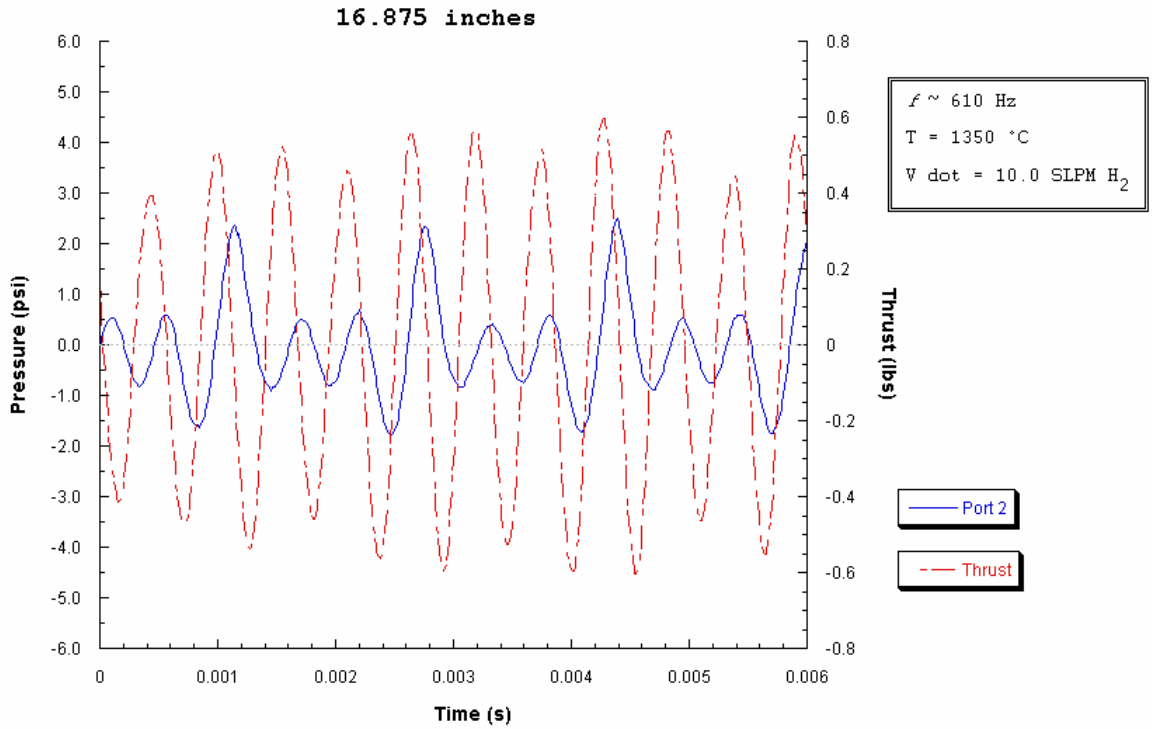
16.875 inches
Pressure (psi)
Thrust (lbs)
Time (s)
f ~ 610 Hz
T = 1350 °C
V dot = 10.0 SLPM H2
Port 2
Thrust

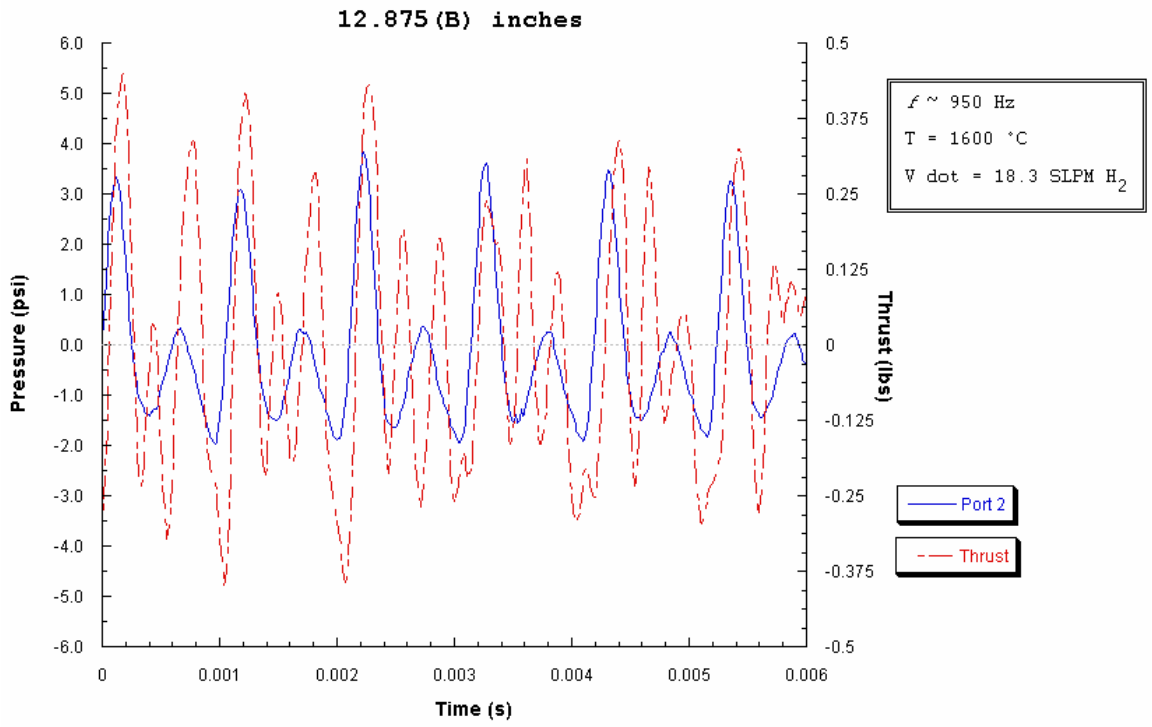
12.875 (B) inches
f ~ 950 Hz
T = 1600 °C
V dot = 18.3 SLPM H2
Pressure (psi)
Thrust (lbs)
Time (s)
Port 2
Thrust

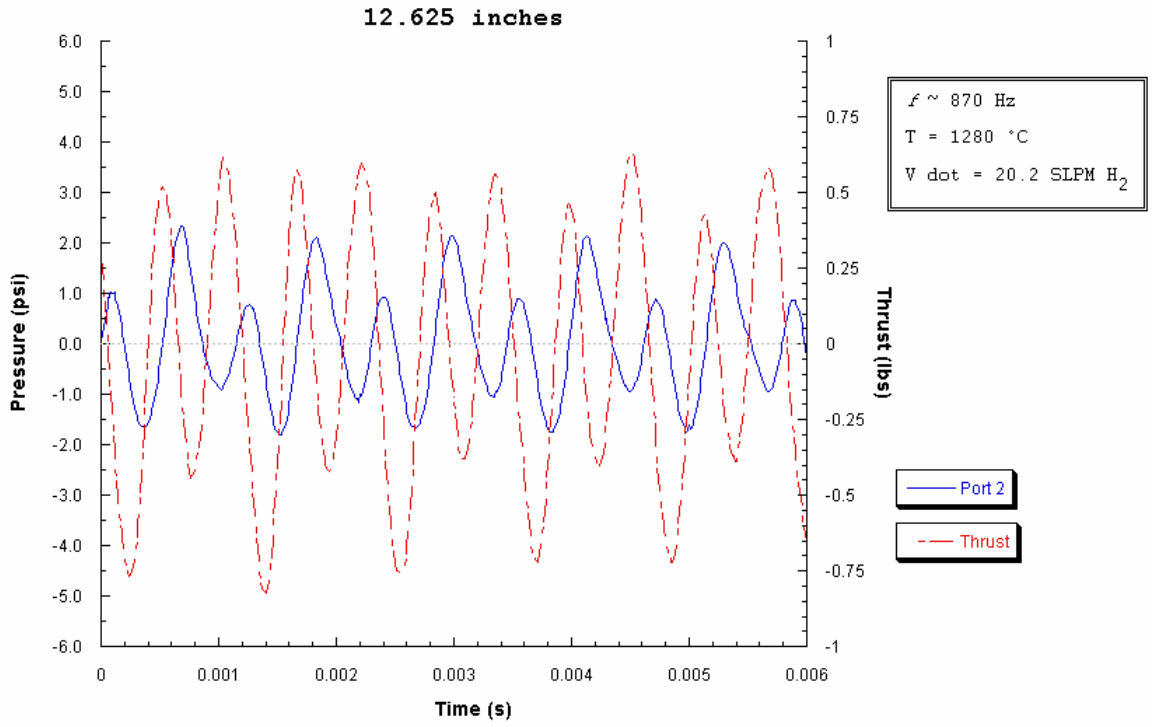
12.625 inches
f ~ 870 Hz
T = 1280 °C
V dot = 20.2 SLPM H2
Pressure (psi)
Thrust (lbs)
Time (s)
Port 2
Thrust

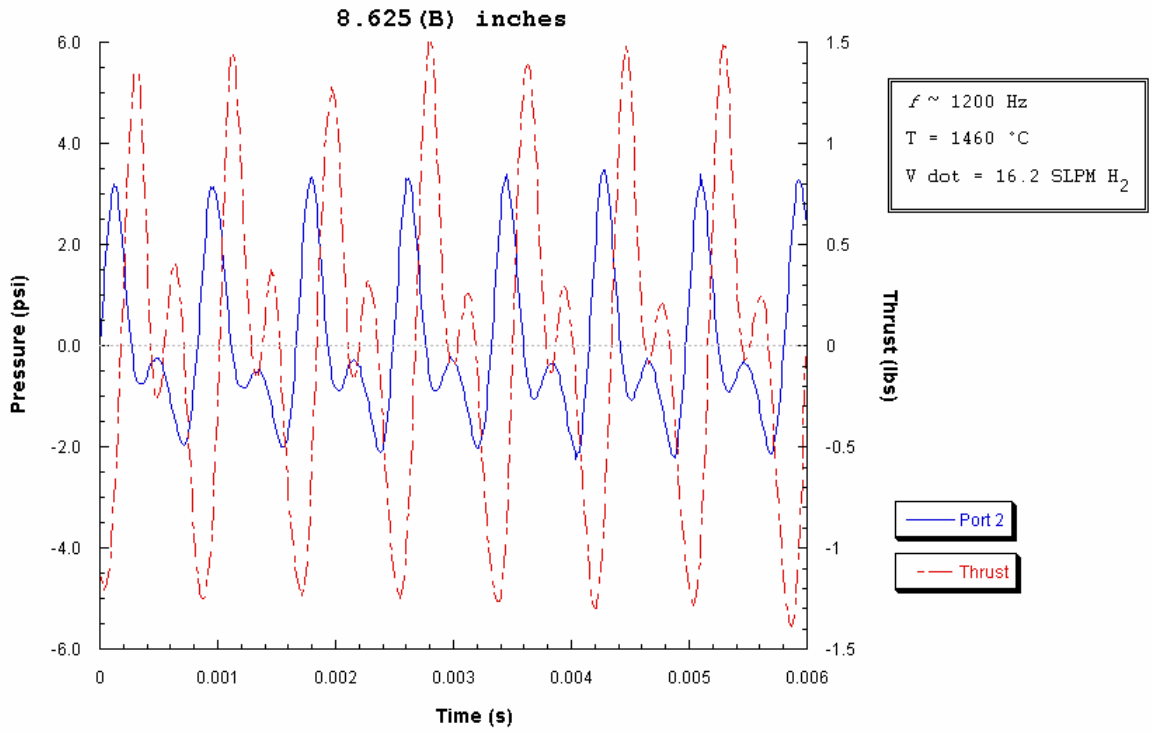
8.625 (B) inches
f ~ 1200 Hz
T = 1460 °C
V dot = 16.2 SLPM H2
Pressure (psi)
Thrust (lbs)
Time (s)
Port 2
Thrust
6.0
4.0
2.0
0.0
-2.0
-4.0
-6.0
1.5
1
0.5
0
-0.5
-1
-1.5
0
0.001
0.002
0.003
0.004
0.005
0.006

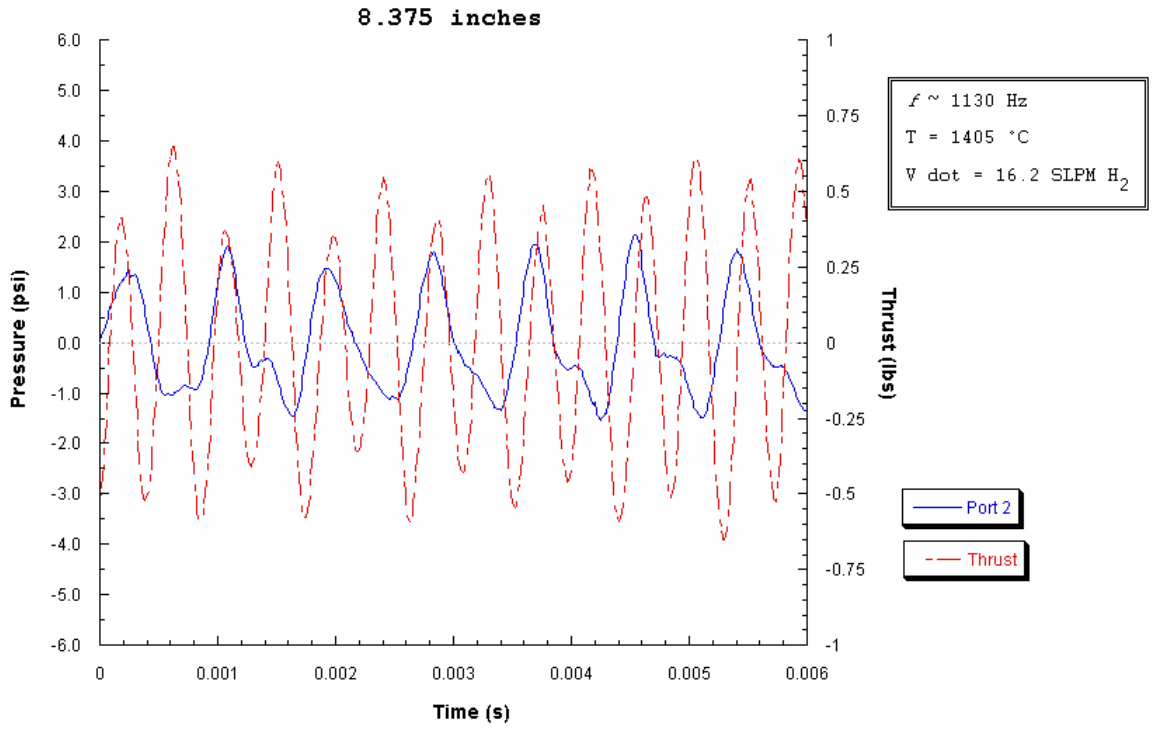
8.375 inches
f ~ 1130 Hz
T = 1405 °C
V dot = 16.2 SLPM H2
Pressure (psi)
Thrust (lbs)
Time (s)
Port 2
Thrust
6.0
5.0
4.0
3.0
2.0
1.0
0.0
-1.0
-2.0
-3.0
-4.0
-5.0
-6.0
1
0.75
0.5
0.25
0
-0.25
-0.5
-0.75
-1
0
0.001
0.002
0.003
0.004
0.005
0.006

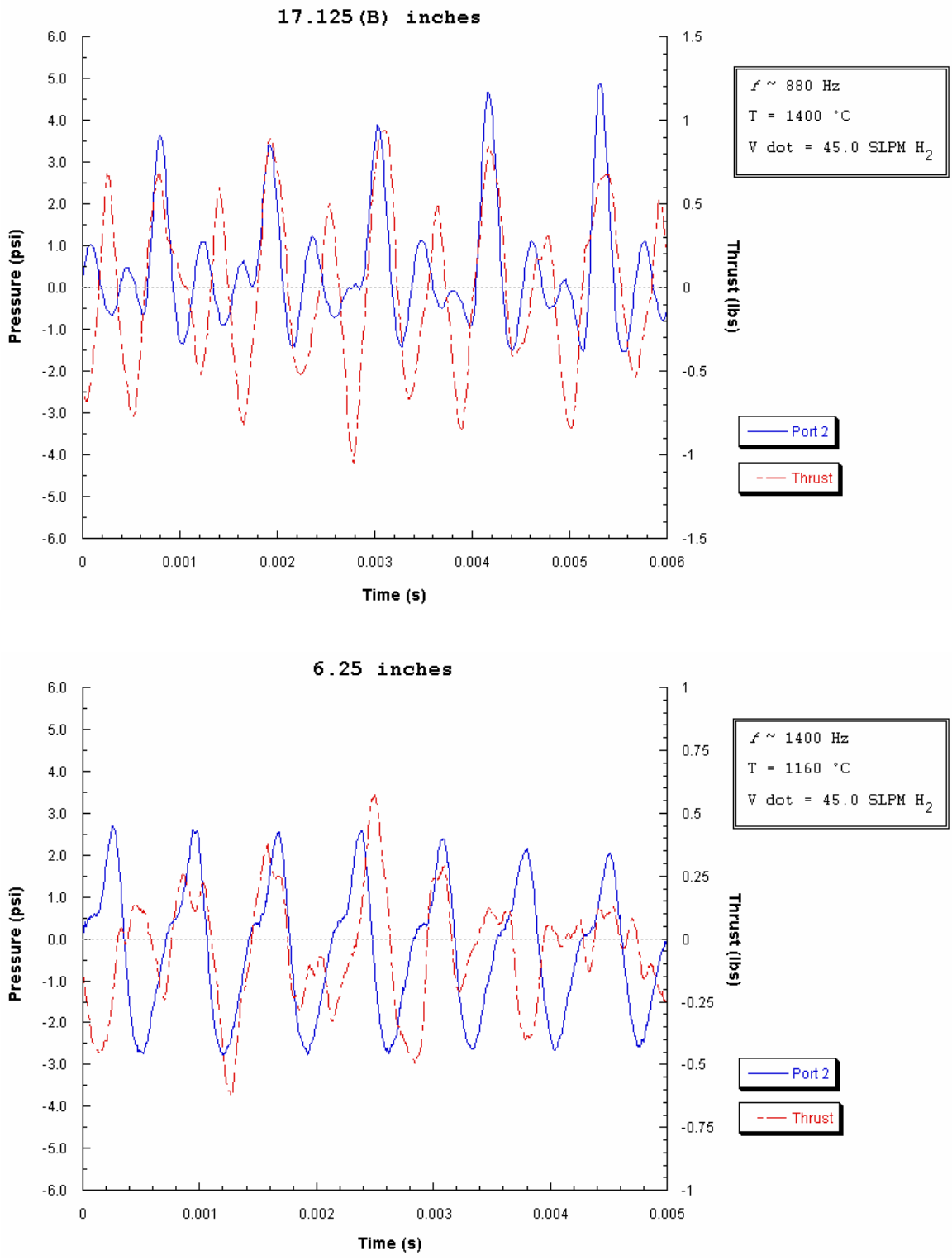

Figure 3.1-10: Maximum $\dot{V}_{H_2}$ at maximum and minimum scalability lengths for an inlet length of 0.5 inches and a 0.130 area ratio.

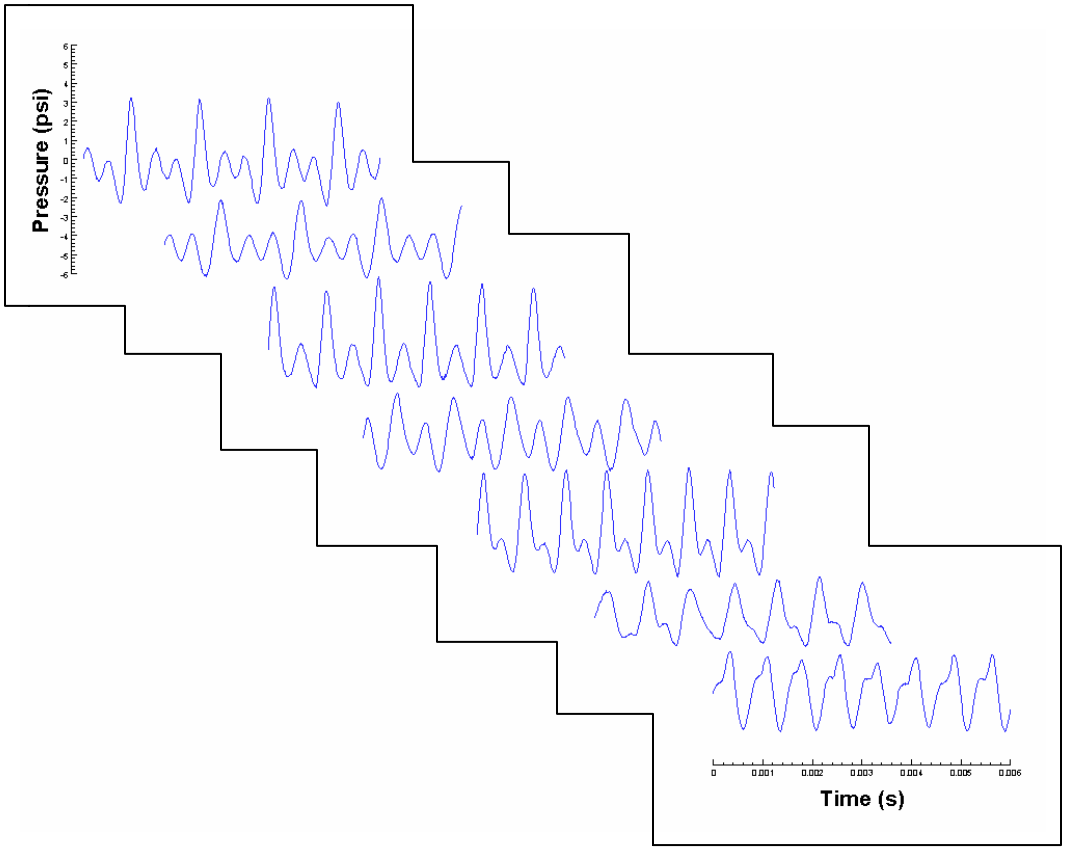

Figure 3.1-11: Pressure waveform transformation with change in overall length for a pulsejet with an inlet area ratio of 0.13 and an inlet length of 0.5 inch.

3.1.2 Case 2

3.1.2.1 2.0-Inch Inlet

Case 2 utilizes a 0.086 inlet area to combustor area ratio and follows the trends of pressure and thrust from a 2.0-inch inlet down to a 0.5-inch inlet by 0.5-inch increments (similar to Case 1). The shortest overall length operable at an inlet length of 2.0 inches was 12.375 inches including the nozzle B exhaust extension. To achieve resonance at this length, the nozzle configuration was necessary. This is a common trend found at all inlet configurations thus far. Attaching a diverging geometry to the pulsejet allows successful runs at a broader range of lengths. In set-ups discussed later, a different diverging exit geometry will be studied.

According to Figure 3.1-12, a greater range of pressures is achievable with the smaller 0.086 area ratio as opposed to the 0.130 ratio of Case 1. Chamber pressure is seen to exceed positive 8.0 psi. This is to be expected as more resistance to backflow through a smaller inlet is naturally perceived to conserve chamber pressure rise per combustion event. Then again, thrust values do not seem to be affected in such a similar manner. In fact, little fluctuation in peak thrust has been seen throughout experimentation as of yet. Maximum fuel flow results (Figure 3.1-13) show a significant increase in absolute thrust values at the shortest jet length for only a small increase in peak pressure.

3.1.2.2 1.5-Inch Inlet

Reducing the inlet length to 1.5 inches allowed self-sustaining combustion at shorter lengths compared to an inlet length of 2.0 inches at a 0.086 ratio. Here, resonance at an overall length of 7.75 inches was achieved by implementing the nozzle A exit geometry (refer to Figure 2.4-1). As previously mentioned, nozzle A was substituted for nozzle B to further study the effects of varying exit geometries. As was noticed with a nozzle B extension, replacing the conventional constant area tail pipe termination with a (in this case, abrupt) diverging configuration created greater resilience in the pulsejet to sustain combustion at shorter lengths. The shortest length depicted in Figure 3.1-14 was not achievable without a diverging nozzle.

The unusually large absolute thrust values obtained at a jet length of 9.375 inches were only sustainable for several seconds, and the pulsejet could not be restarted after non-induced termination. In acquiring the results of the maximum fuel flow test for the 18.125-inch configuration, it was determined that larger fuel flow rates were possible with nozzle B than with nozzle A at that particular length. Results of fuel flow rate studies at both 18.125 and 9.875-inch increments are plotted in Figure 3.1-15.

3.1.2.3 1.0-Inch Inlet

Figure 3.1-16 shows pressure and thrust data for a 1.0-inch inlet length. Most pressure waveforms plotted are coarse and take poor shape. Accompanied thrust results are mostly random in appearance, and clear form is lacking, as well. Desirable data sets were attained in the 8 and 9-inch regimes. Pressure fluctuations remained in the ±2.5 psi

range for most jet lengths, and absolute thrust values did not exceed 0.6 lbs – quite low as compared to thrust results discussed thus far.

Maximum fuel flow plots of Figure 3.1-17 continue the trend of undesirable data structure for the 1.0-inch inlet configuration. Thrust values, however, recovered significant strength as fuel flow rates were increased. Absolute thrust values more than tripled for a less than proportional increase in fuel flow rates for both the long and short examples.

3.1.2.4 0.5-Inch Inlet

Peak thrust values continued to decline as inlet length was reduced to 0.5 inch. All exhaust length increments and nozzle geometry configurations tested were satisfied for this inlet length and area ratio. In other words, the full range of pulsejet lengths studied in this experiment attained self-sustaining resonance at this inlet configuration. On average, this inlet configuration resulted in maximum thrust values of about a quarter of a pound. Still, all plots in Figure 3.1-18 show peak pressure values remaining in the 2.0-2.5 psi region (consistent with results for Case 2). Thrust behavior follows the familiar progression in waveform shape as jet length is shortened, except for the case of the 13-inch nozzle A configuration. In the corresponding plot, thrust and chamber pressure exhibit behaviors that seem to contradict previous results for this intermediate length increment. Both waveforms possess a sine wave structure commonly found at shorter lengths, and frequency is significantly greater than that of shorter increments. These results could not be repeated in testing. Resonance apparently assumed a higher atypical mode during operation.

There was also a notably different response in thrust performance with or without a nozzle extension at a jet length of roughly 6.0 inches. While pressures were slightly greater with the nozzle A attachment, thrust was almost four times higher in peak value without the diverging exit geometry. Furthermore, a steady sine wave thrust pattern contrasted an apparently random behavior of the 6.625-inch nozzle A configuration. Important to note, this significant increase in thrust magnitude without a nozzle extension is contradictory to trends of previous configurations.

As the fuel flow rate was increased to its allowable limit, the clean sine waveform previously observed in the 6.125-inch configuration was obscured. Maxima and minima thrust values of Figure 3.1-19 expectedly increased while little change is seen in chamber pressure values.

Figure 3.1-12:

Pulsejet scalability performance for an inlet length of 2.0 inches and a 0.086 area ratio.

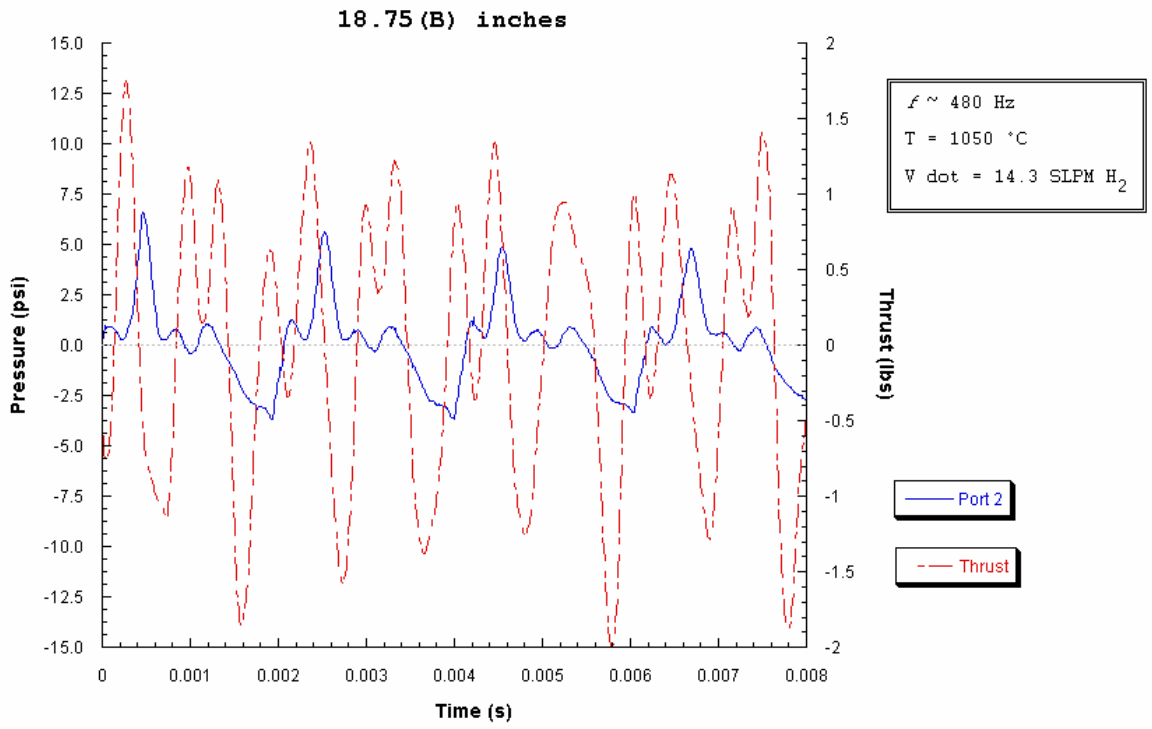
18.75 (B) inches
Pressure (psi)
Thrust (lbs)
Time (s)
f ~ 480 Hz
T = 1050 °C
V dot = 14.3 SLPM H2
Port 2
Thrust

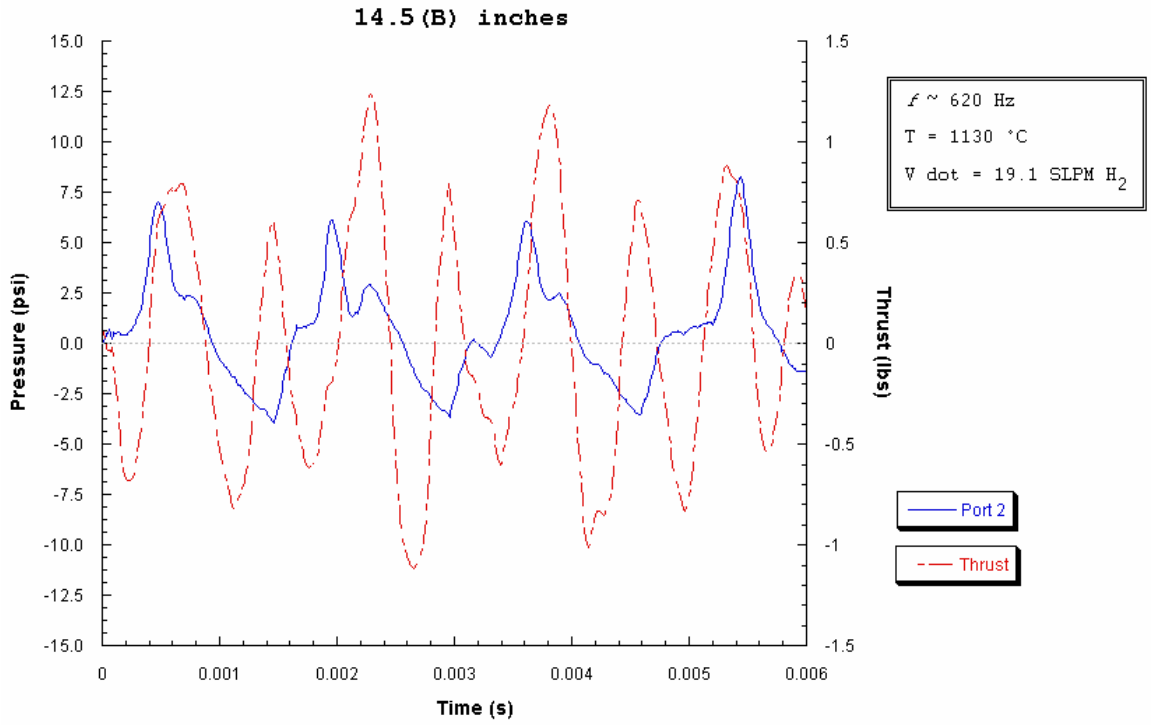
14.5 (B) inches
Pressure (psi)
Thrust (lbs)
Time (s)
f ~ 620 Hz
T = 1130 °C
V dot = 19.1 SLPM H2
Port 2
Thrust

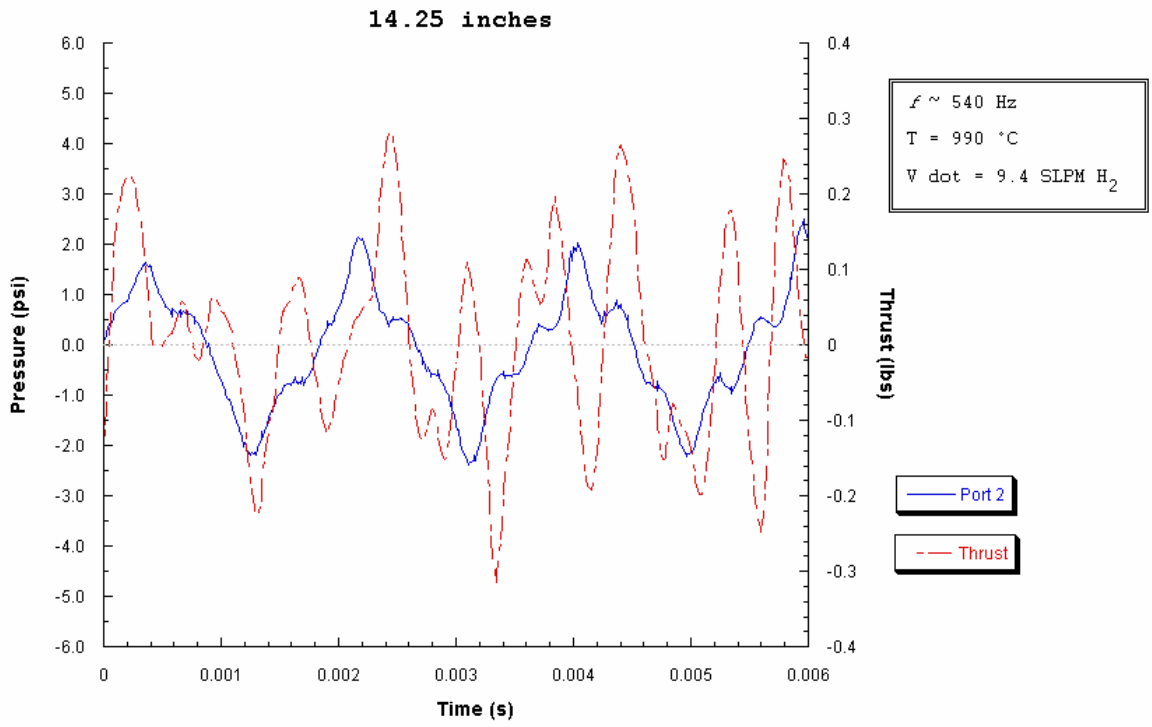
14.25 inches
f ~ 540 Hz
T = 990 °C
V dot = 9.4 SLPM H2
Pressure (psi)
Thrust (lbs)
Time (s)
Port 2
Thrust

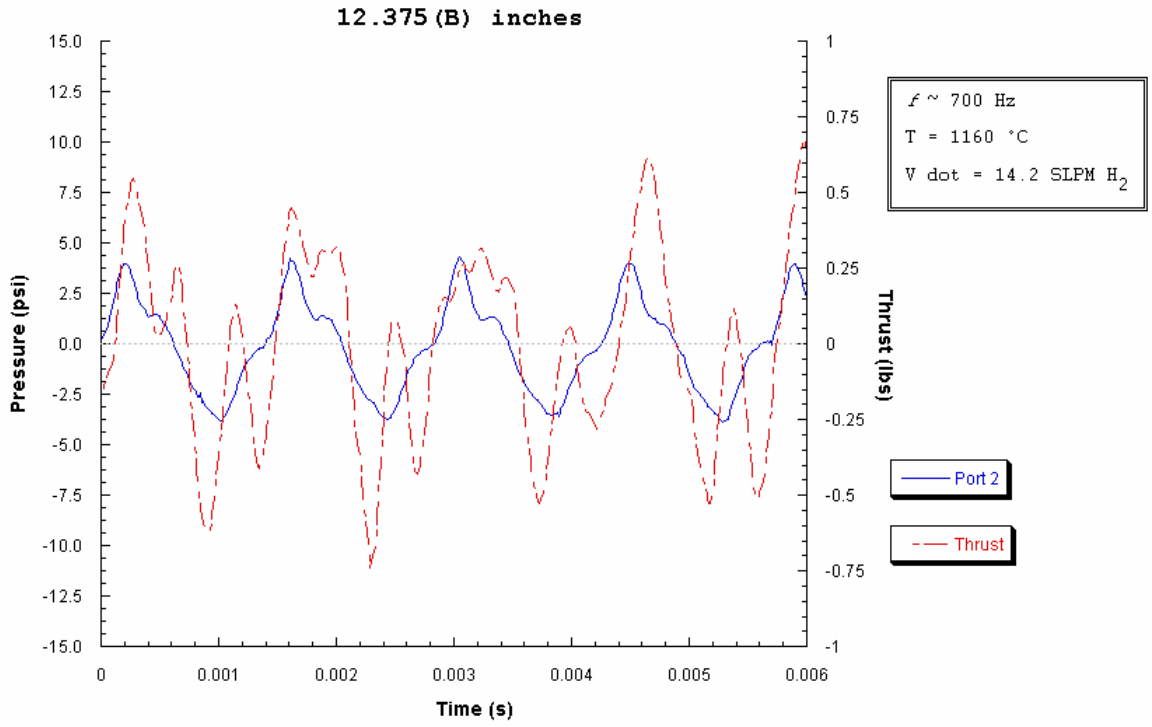
12.375 (B) inches
f ~ 700 Hz
T = 1160 °C
V dot = 14.2 SLPM H2
Pressure (psi)
Thrust (lbs)
Time (s)
Port 2
Thrust

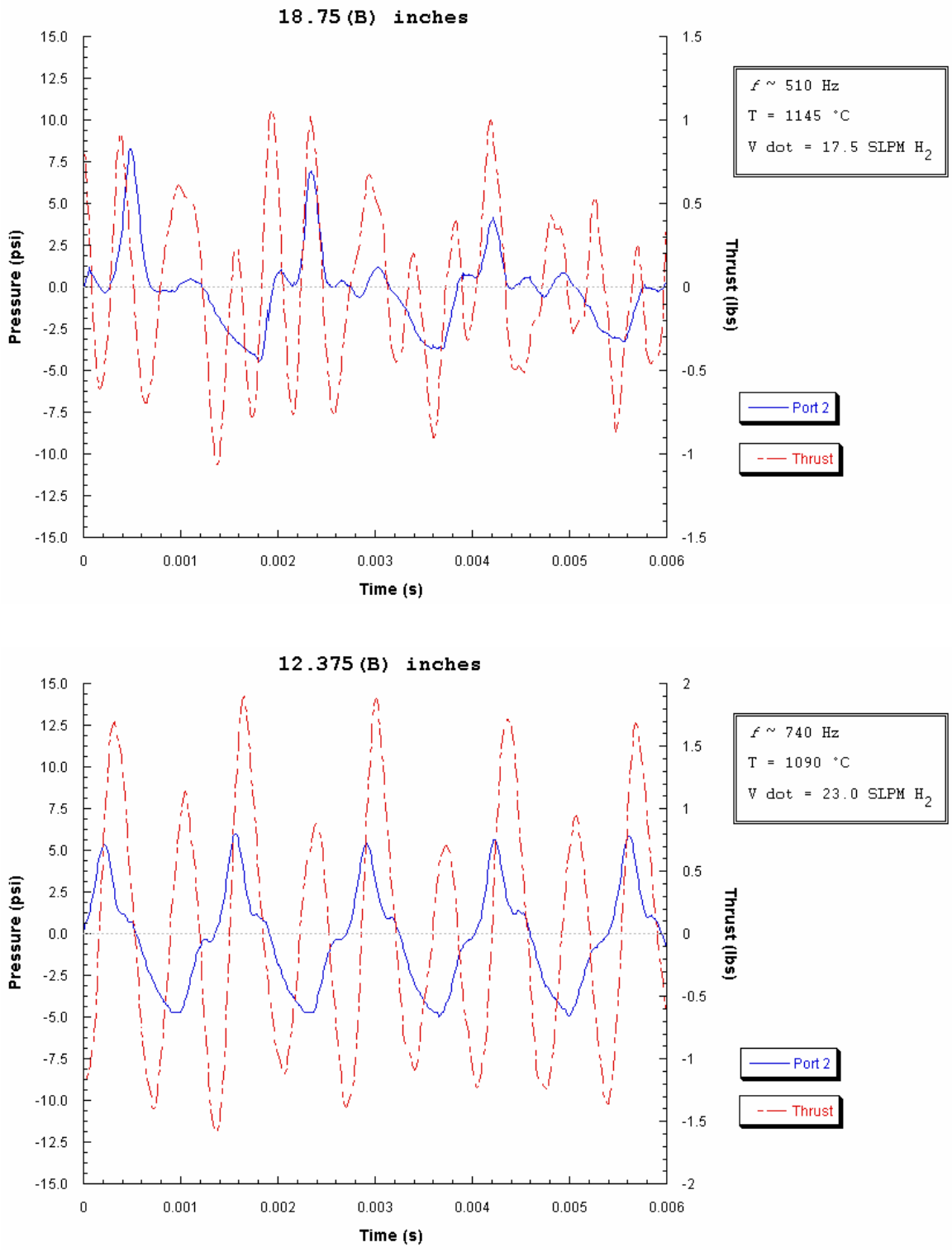

Figure 3.1-13: Maximum $\dot{V}_{H_2}$ at maximum and minimum scalability lengths for an inlet length of 2.0 inches and a 0.086 area ratio.

Figure 3.1-14:

Pulsejet scalability performance for an inlet length of 1.5 inches and a 0.086 area ratio.

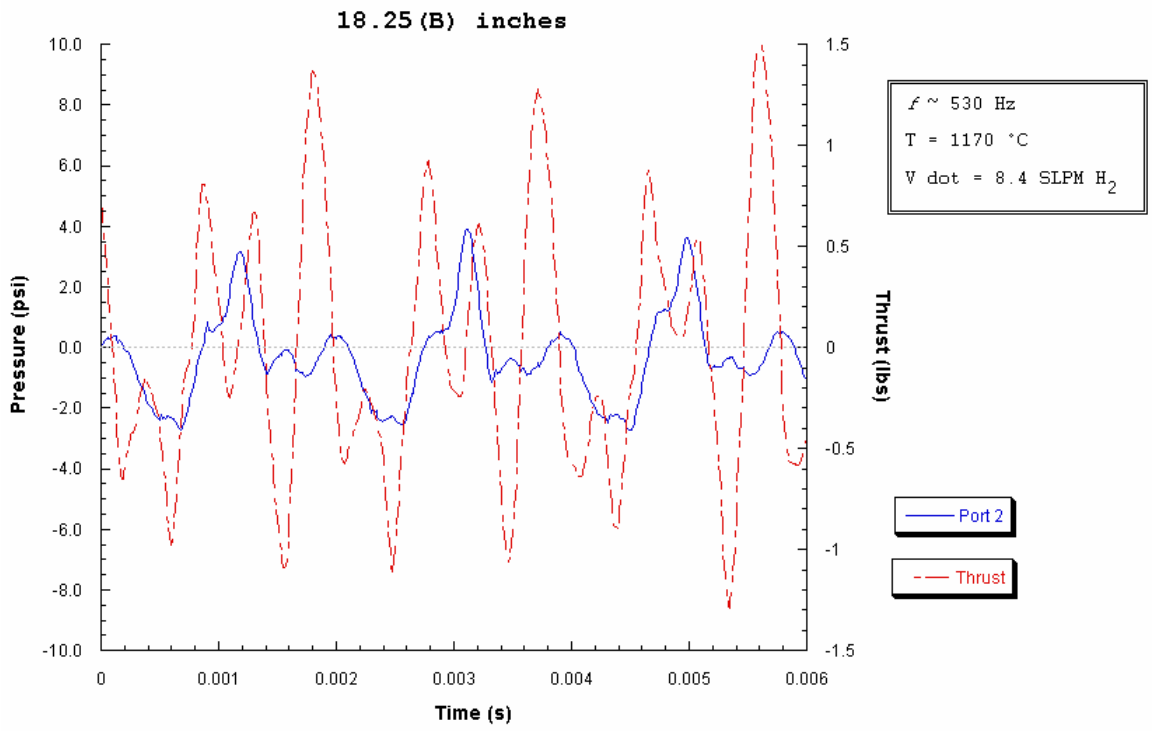
18.25 (B) inches
f ~ 530 Hz
T = 1170 °C
V dot = 8.4 SLPM H2
Pressure (psi)
Thrust (lbs)
Time (s)
Port 2
Thrust

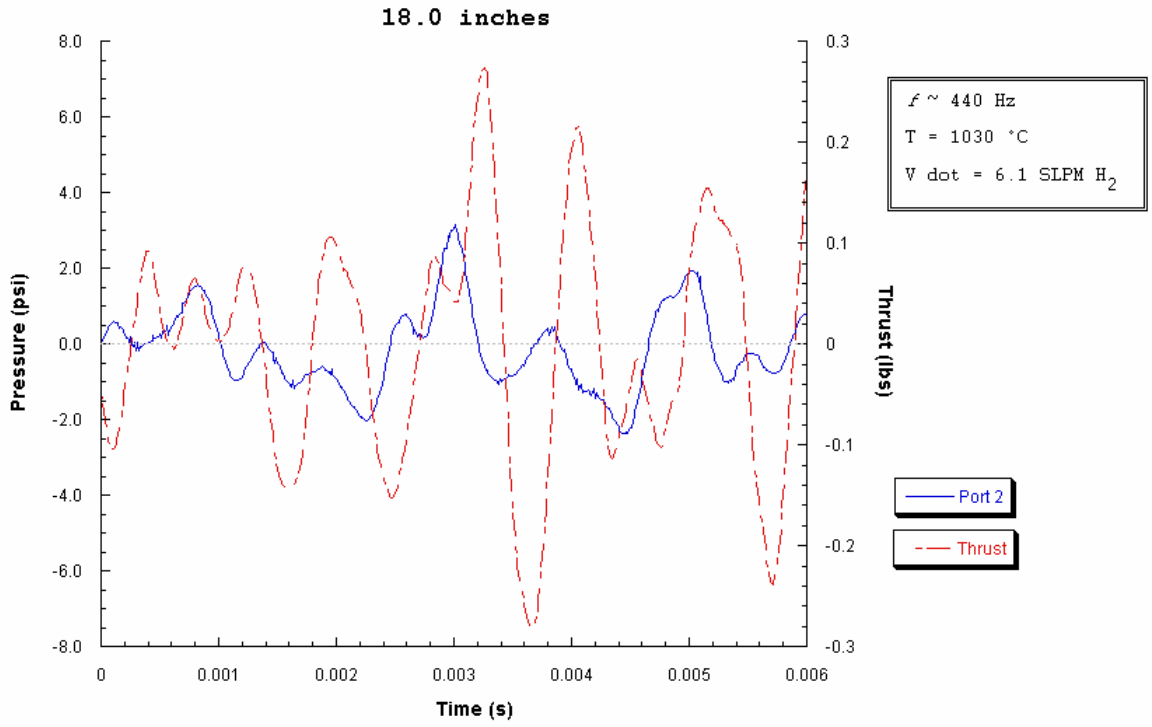
18.0 inches
f ~ 440 Hz
T = 1030 °C
V dot = 6.1 SLPM H2
Pressure (psi)
Thrust (lbs)
Time (s)
Port 2
Thrust

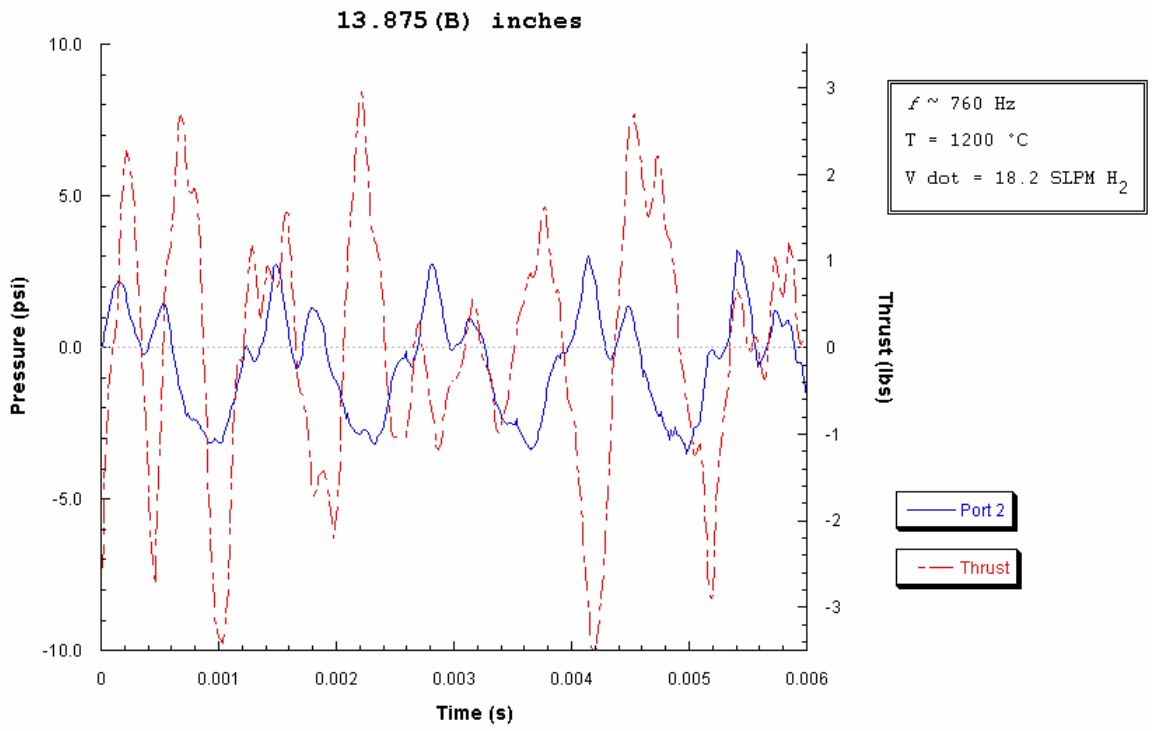
13.875 (B) inches
f ~ 760 Hz
T = 1200 °C
V dot = 18.2 SLPM H2
Pressure (psi)
Thrust (lbs)
Time (s)
Port 2
Thrust

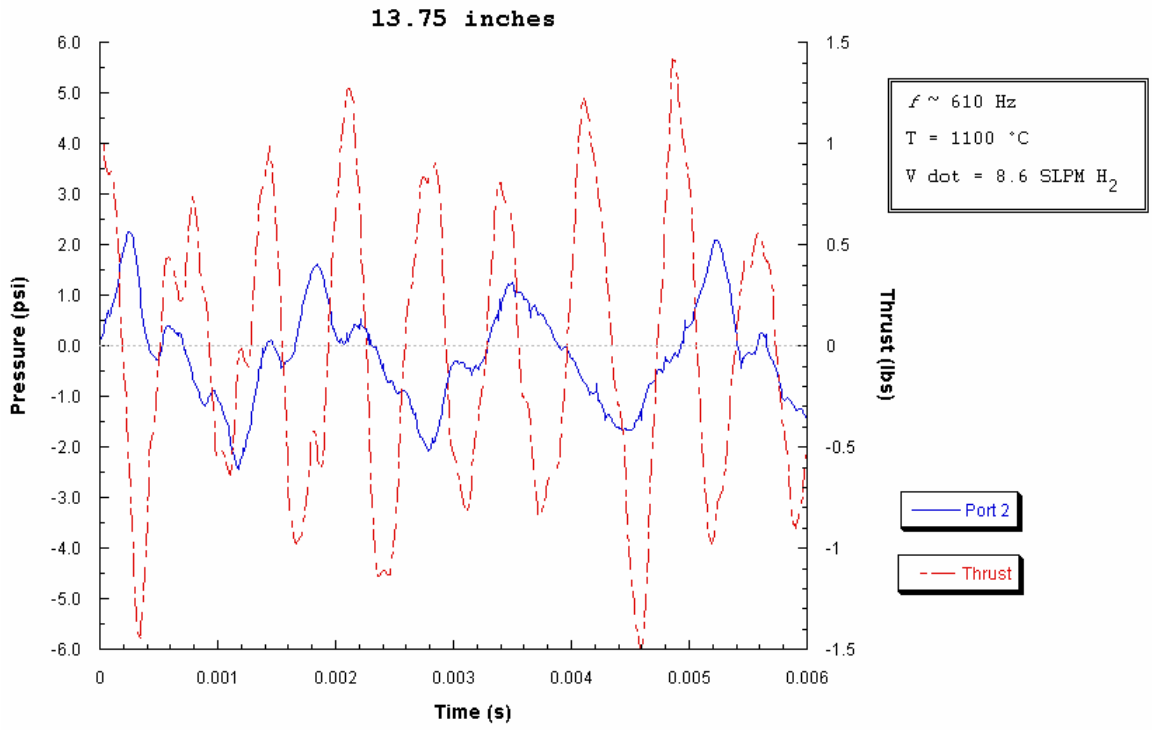
13.75 inches
f ~ 610 Hz
T = 1100 °C
V dot = 8.6 SLPM H2
Pressure (psi)
Thrust (lbs)
Time (s)
Port 2
Thrust

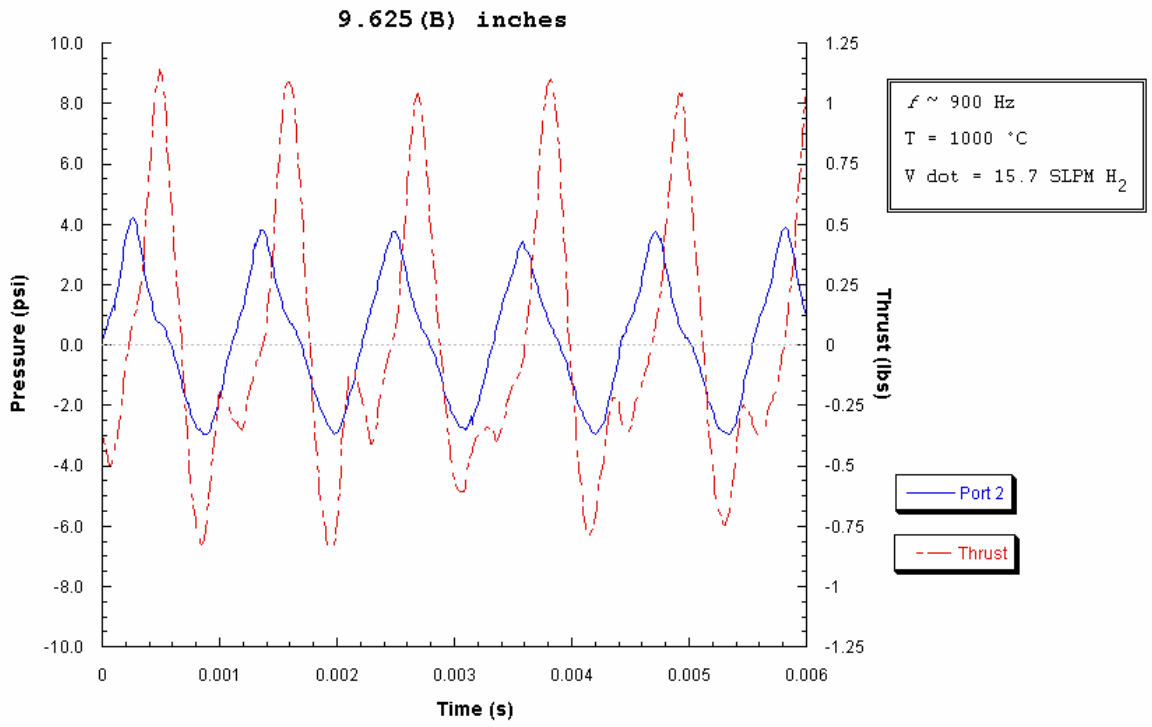
9.625 (B) inches
f ~ 900 Hz
T = 1000 °C
V dot = 15.7 SLPM H2
Pressure (psi)
Thrust (lbs)
Time (s)
Port 2
Thrust

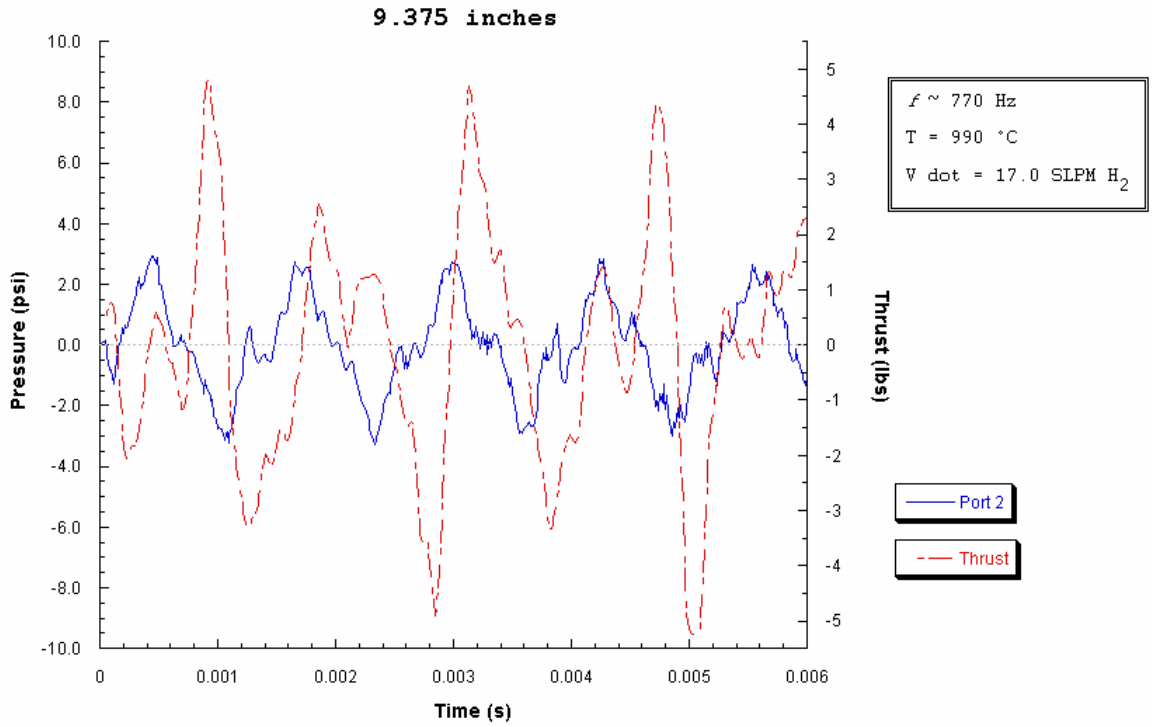
9.375 inches
f ~ 770 Hz
T = 990 °C
V dot = 17.0 SLPM H2
Pressure (psi)
Thrust (lbs)
Time (s)
Port 2
Thrust

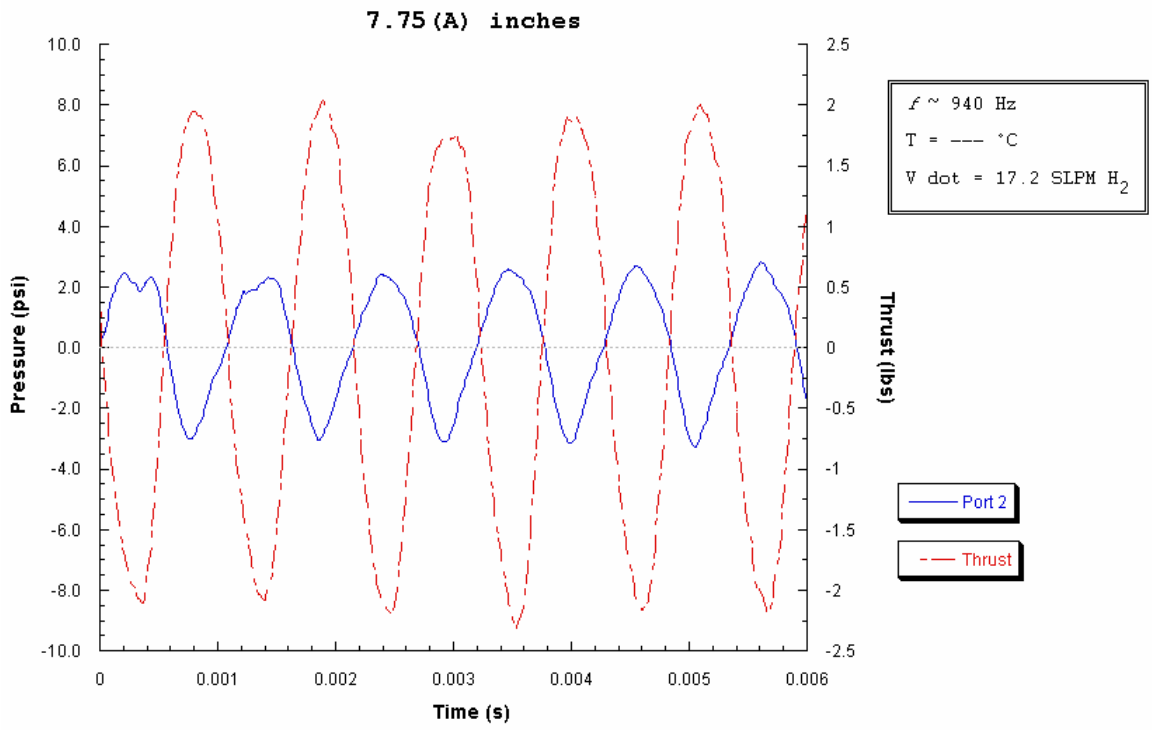
7.75 (A) inches
f ~ 940 Hz
T = --- °C
V dot = 17.2 SLPM H2
Pressure (psi)
Thrust (lbs)
Time (s)
10.0
8.0
6.0
4.0
2.0
0.0
-2.0
-4.0
-6.0
-8.0
-10.0
2.5
2
1.5
1
0.5
0
-0.5
-1
-1.5
-2
-2.5
0
0.001
0.002
0.003
0.004
0.005
0.006
Port 2
Thrust

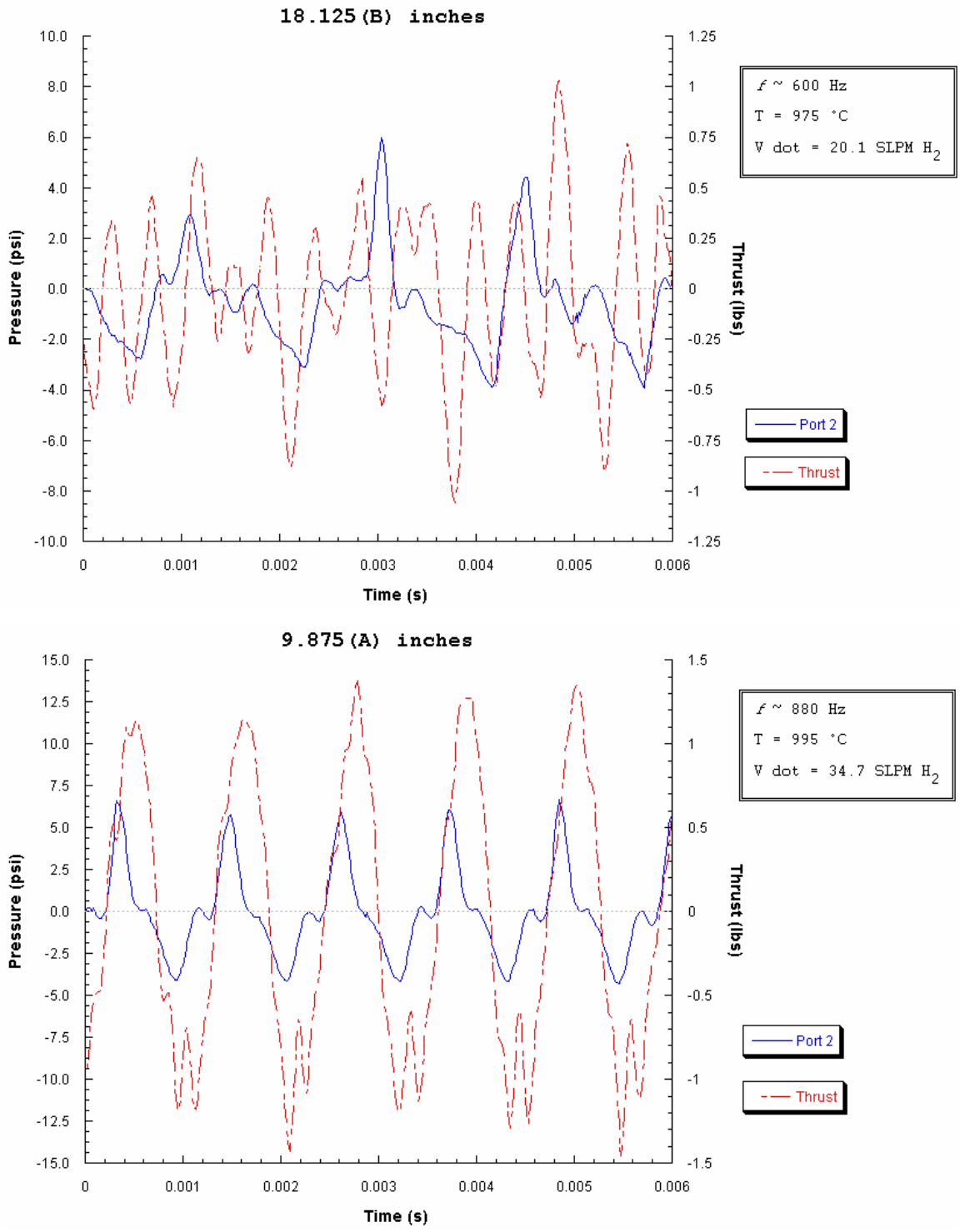

Figure 3.1-15: Maximum $\dot{V}_{H_2}$ at maximum and minimum scalability lengths for an inlet length of 1.5 inches and a 0.086 area ratio.

Figure 3.1-16:

Pulsejet scalability performance for an inlet length of 1.0 inches and a 0.086 area ratio.

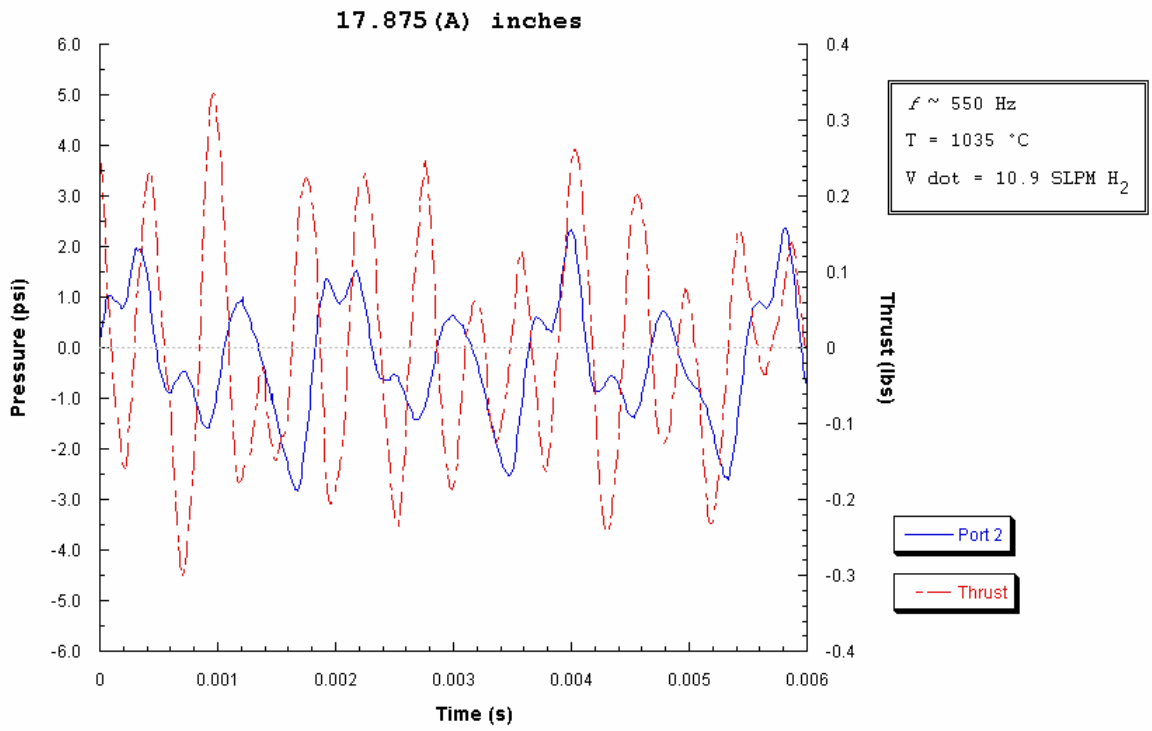
17.875 (A) inches
Pressure (psi)
Thrust (lbs)
Time (s)
f ~ 550 Hz
T = 1035 °C
V dot = 10.9 SLPM H2
Port 2
Thrust

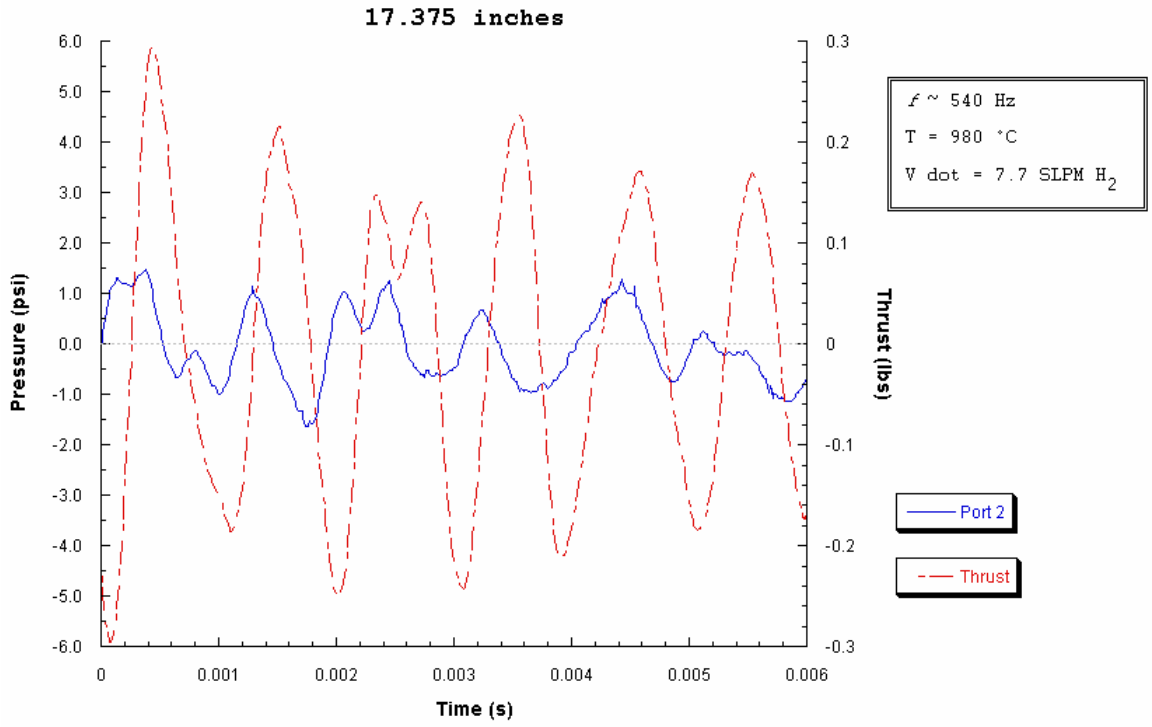
17.375 inches
Pressure (psi)
Thrust (lbs)
Time (s)
f ~ 540 Hz
T = 980 °C
V dot = 7.7 SLPM H2
Port 2
Thrust

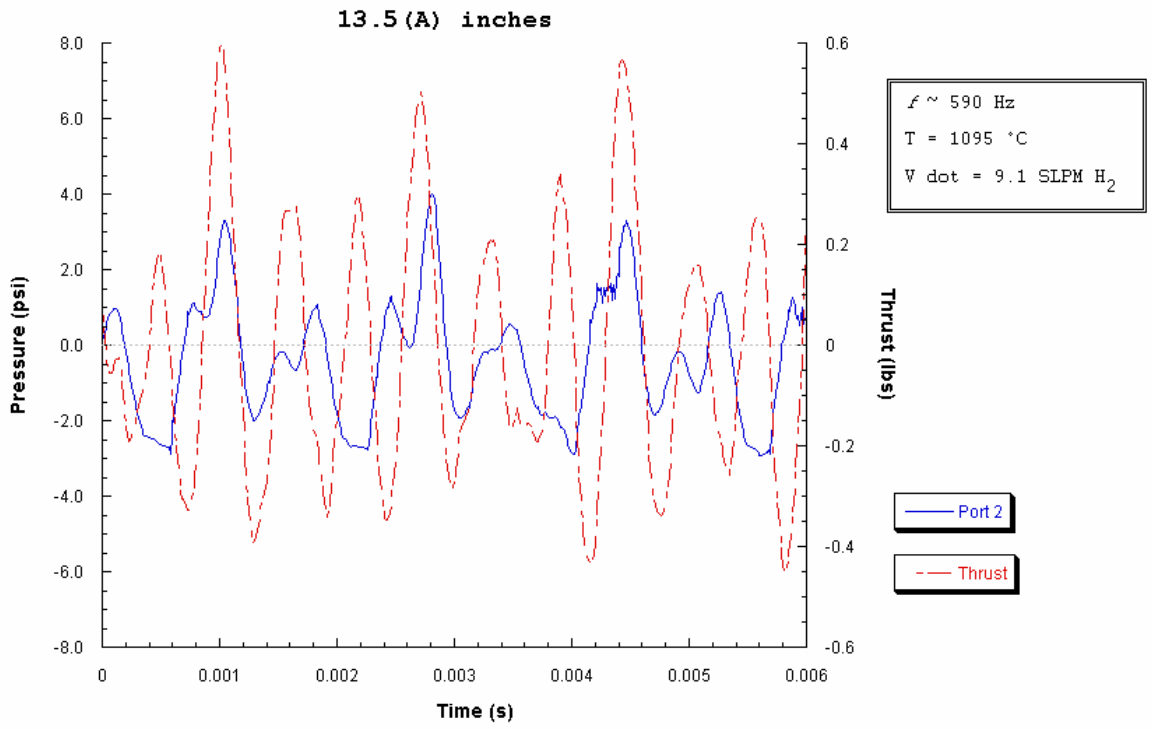
13.5 (A) inches
f ~ 590 Hz
T = 1095 °C
V dot = 9.1 SLPM H2
Pressure (psi)
Thrust (lbs)
Time (s)
Port 2
Thrust
8.0
6.0
4.0
2.0
0.0
-2.0
-4.0
-6.0
-8.0
0.6
0.4
0.2
0
-0.2
-0.4
-0.6
0
0.001
0.002
0.003
0.004
0.005
0.006

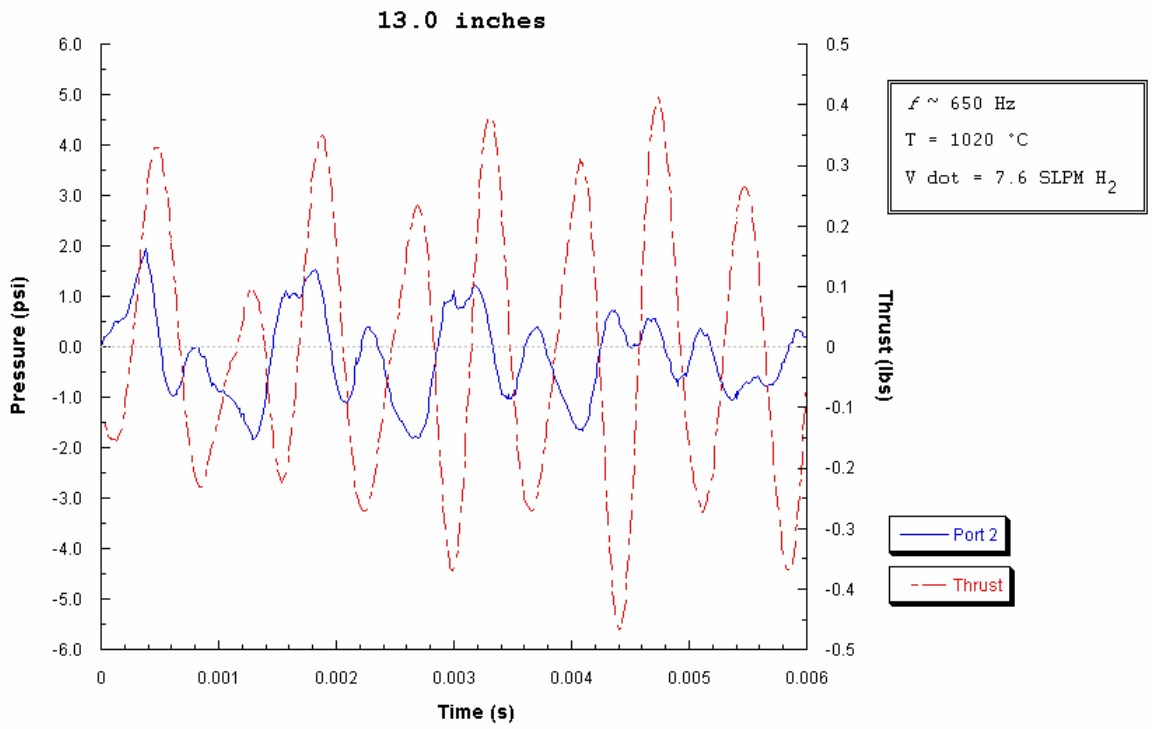
13.0 inches
f ~ 650 Hz
T = 1020 °C
V dot = 7.6 SLPM H2
Pressure (psi)
Thrust (lbs)
Time (s)
Port 2
Thrust
6.0
5.0
4.0
3.0
2.0
1.0
0.0
-1.0
-2.0
-3.0
-4.0
-5.0
-6.0
0.5
0.4
0.3
0.2
0.1
0
-0.1
-0.2
-0.3
-0.4
-0.5
0
0.001
0.002
0.003
0.004
0.005
0.006

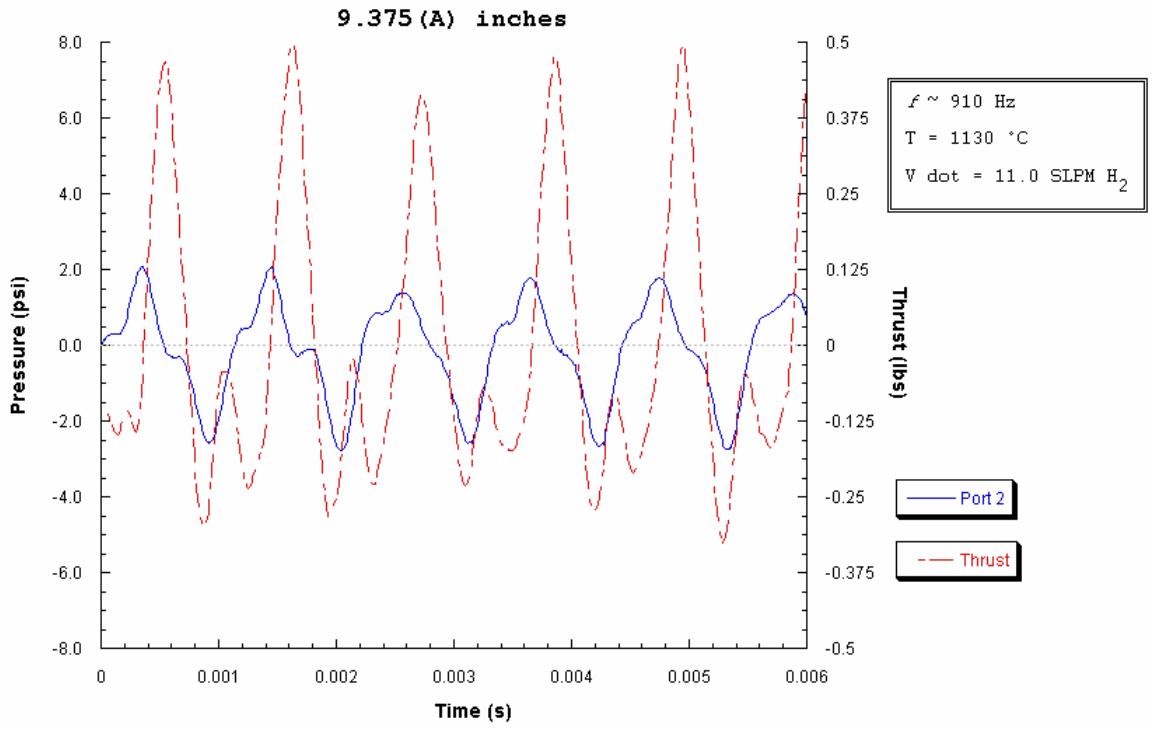
9.375 (A) inches
Pressure (psi)
Thrust (lbs)
Time (s)
f ~ 910 Hz
T = 1130 °C
V dot = 11.0 SLPM H2
Port 2
Thrust

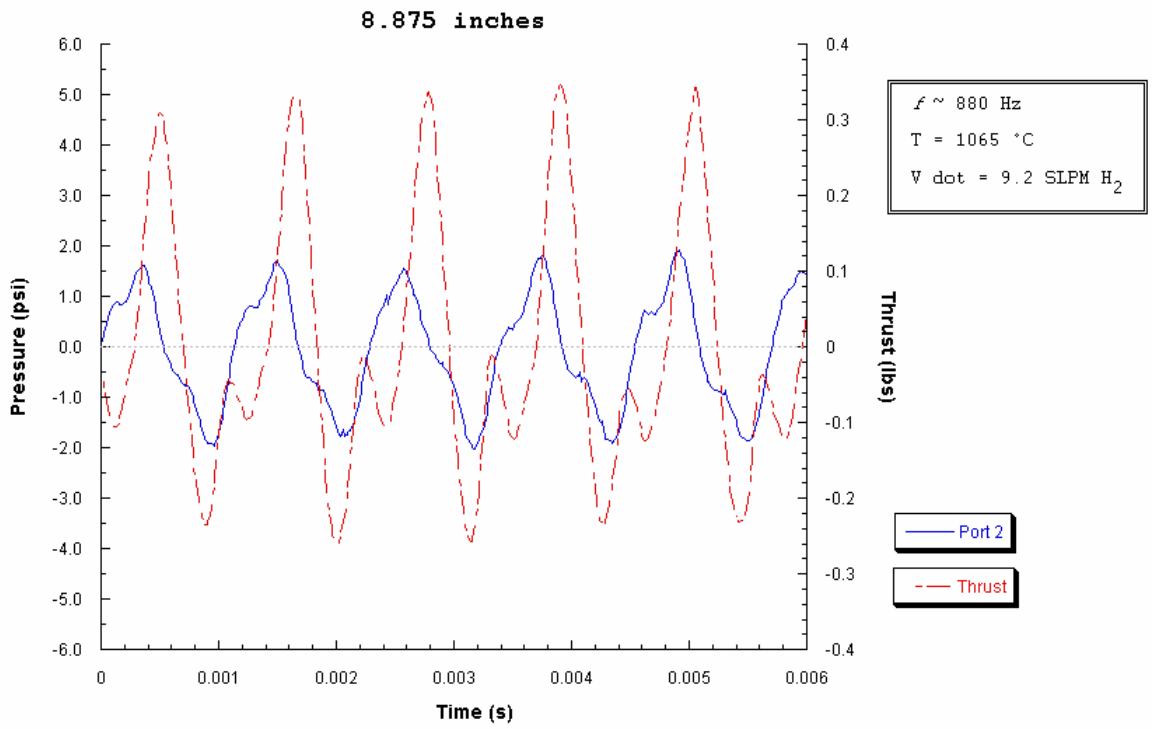
8.875 inches
Pressure (psi)
Thrust (lbs)
Time (s)
f ~ 880 Hz
T = 1065 °C
V dot = 9.2 SLPM H2
Port 2
Thrust

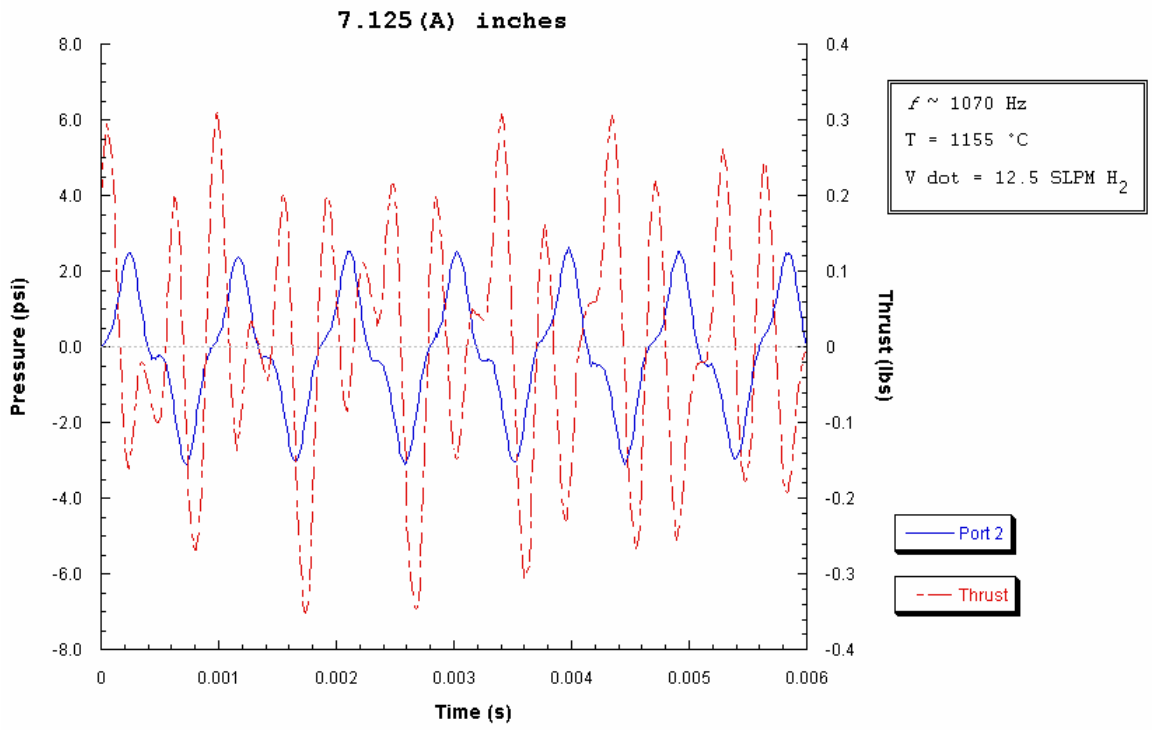
7.125 (A) inches
Pressure (psi)
Thrust (lbs)
Time (s)
8.0
6.0
4.0
2.0
0.0
-2.0
-4.0
-6.0
-8.0
0.4
0.3
0.2
0.1
0
-0.1
-0.2
-0.3
-0.4
0
0.001
0.002
0.003
0.004
0.005
0.006
f ~ 1070 Hz
T = 1155 °C
V dot = 12.5 SLPM H2
Port 2
Thrust

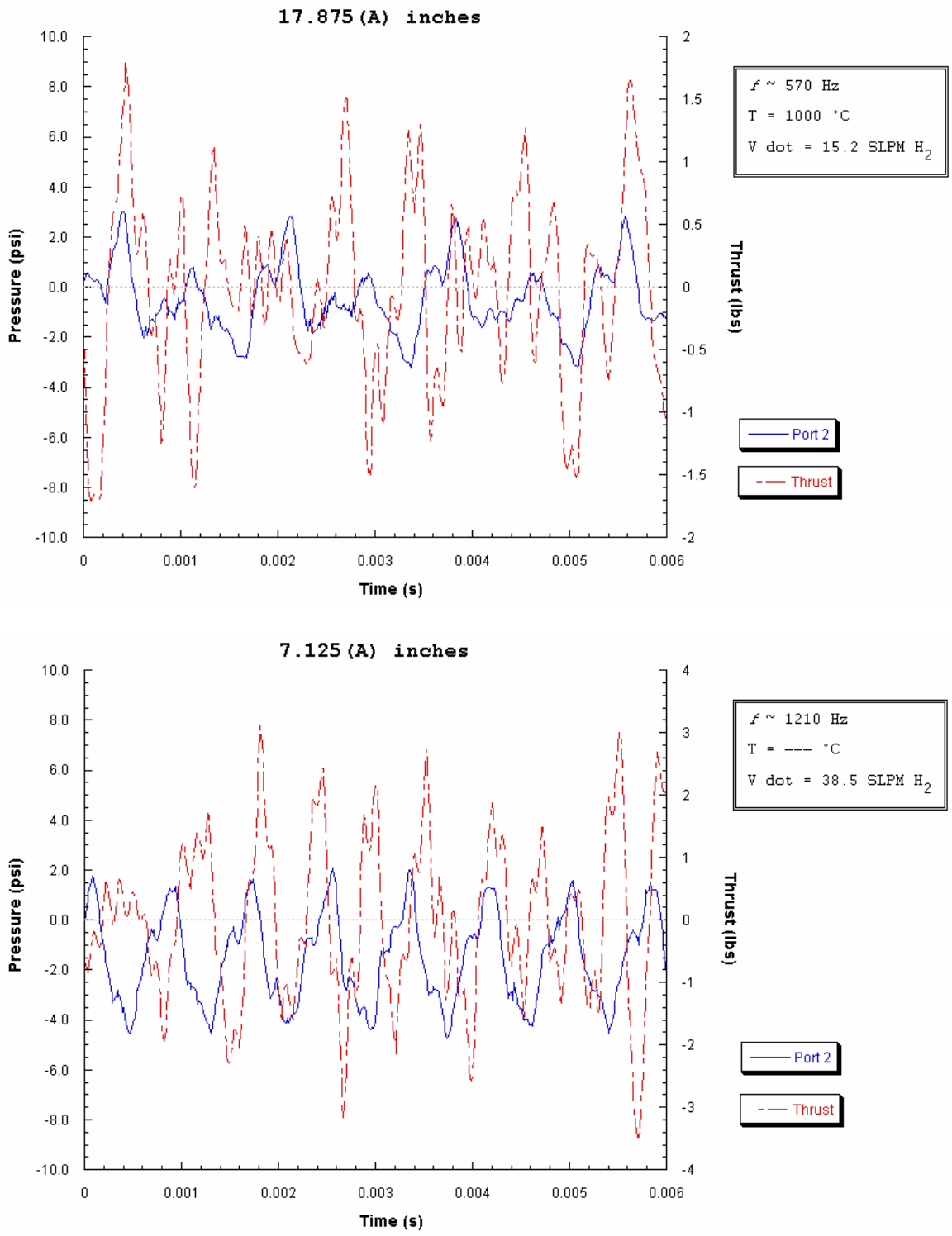

Figure 3.1-17: Maximum $\dot{V}_{H_2}$ at maximum and minimum scalability lengths for an inlet length of 1.0 inches and a 0.086 area ratio.

Figure 3.1-18:

Pulsejet scalability performance for an inlet length of 0.5 inches and a 0.086 area ratio.

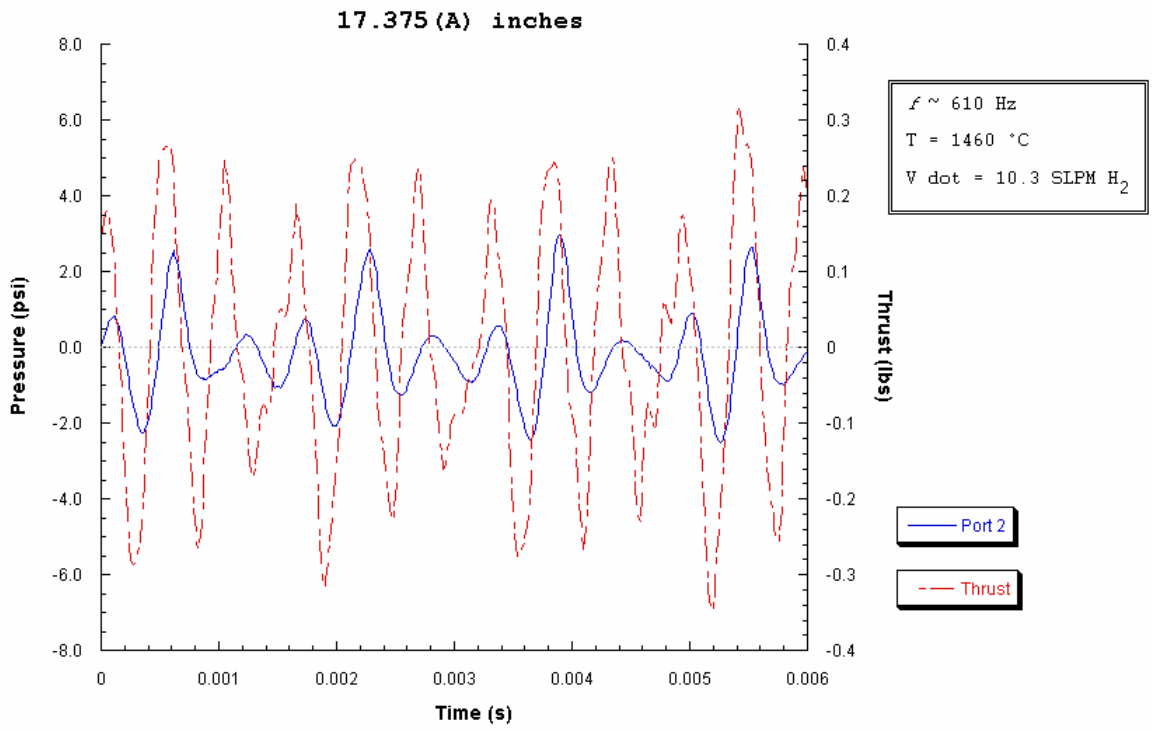
17.375 (A) inches
f ~ 610 Hz
T = 1460 °C
V dot = 10.3 SLPM H2
Pressure (psi)
Thrust (lbs)
Time (s)
Port 2
Thrust

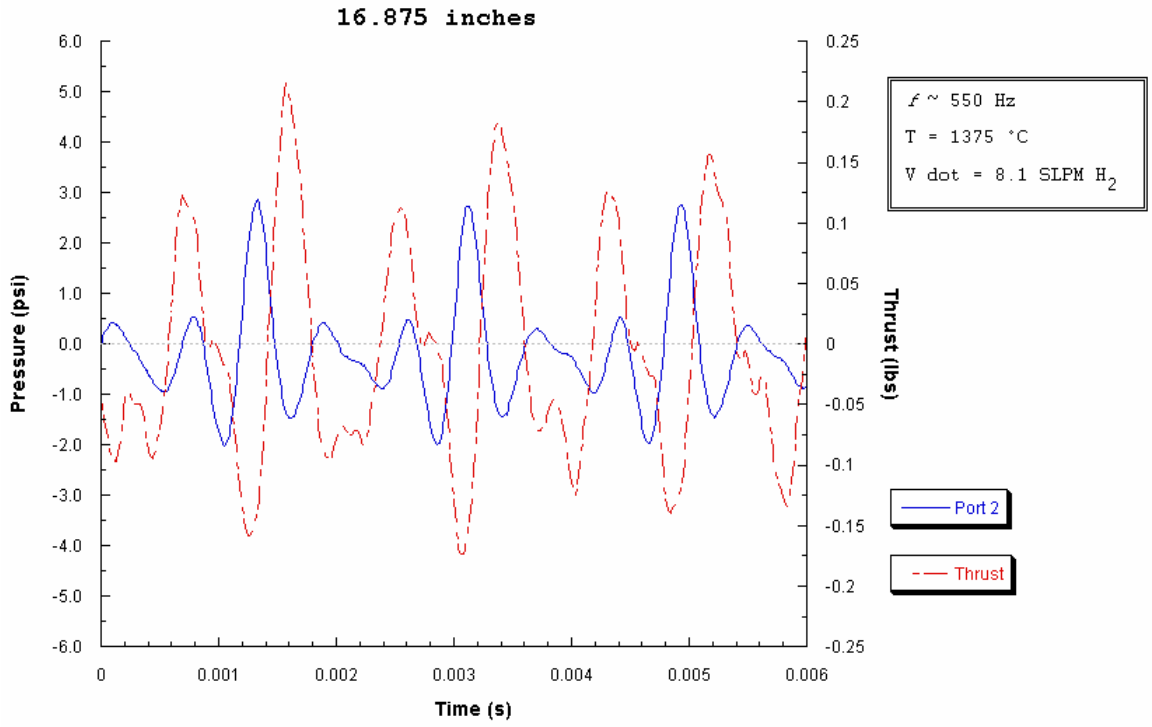
16.875 inches
f ~ 550 Hz
T = 1375 °C
V dot = 8.1 SLPM H2
Pressure (psi)
Thrust (lbs)
Time (s)
Port 2
Thrust

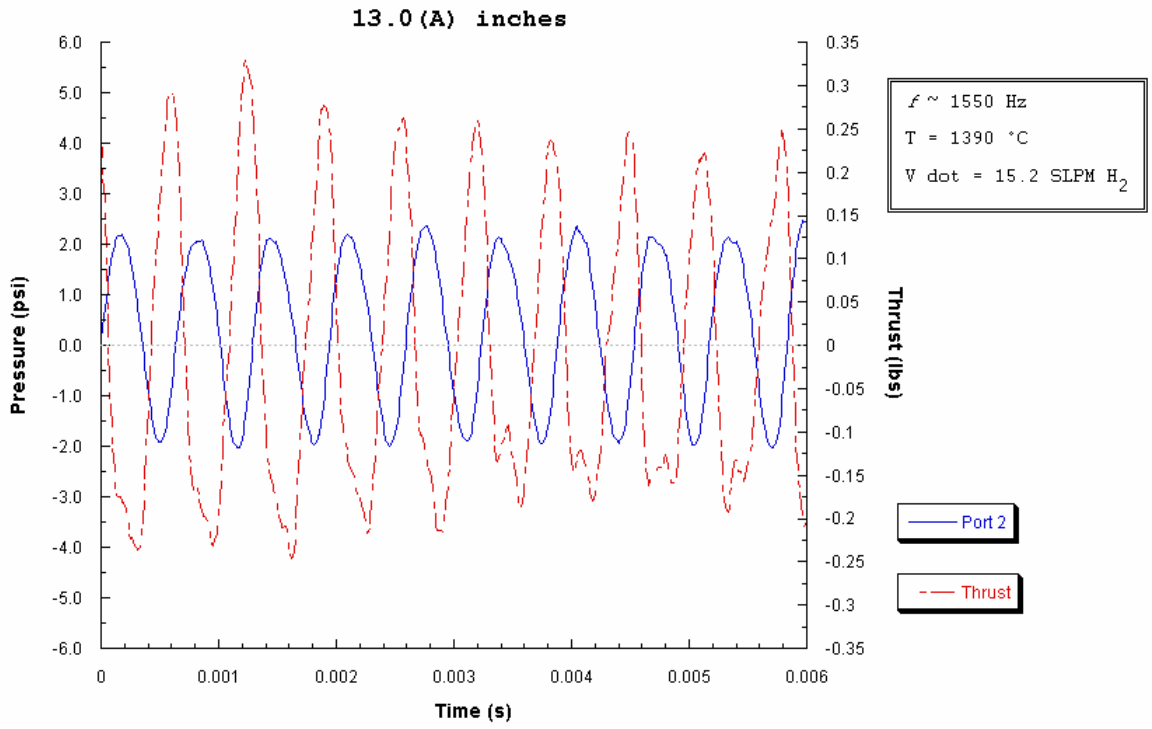
13.0 (A) inches
f ~ 1550 Hz
T = 1390 °C
V dot = 15.2 SLPM H2
Pressure (psi)
Thrust (lbs)
Time (s)
Port 2
Thrust

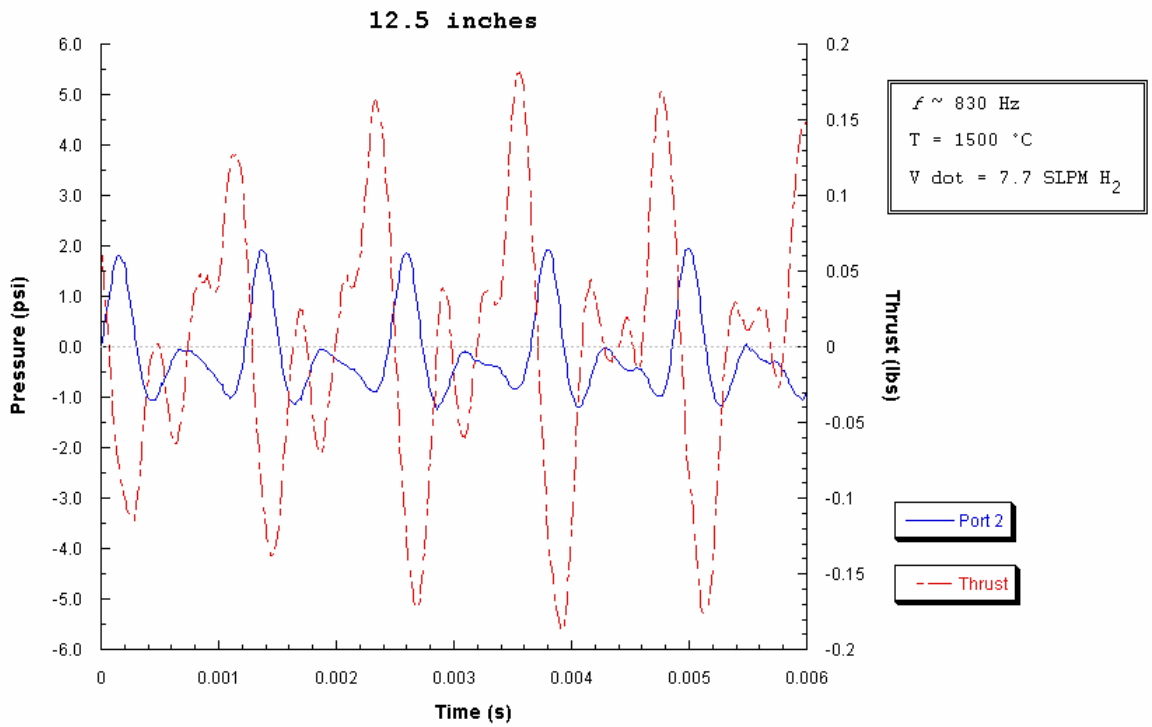
12.5 inches
f ~ 830 Hz
T = 1500 °C
V dot = 7.7 SLPM H2
Pressure (psi)
Thrust (lbs)
Time (s)
Port 2
Thrust

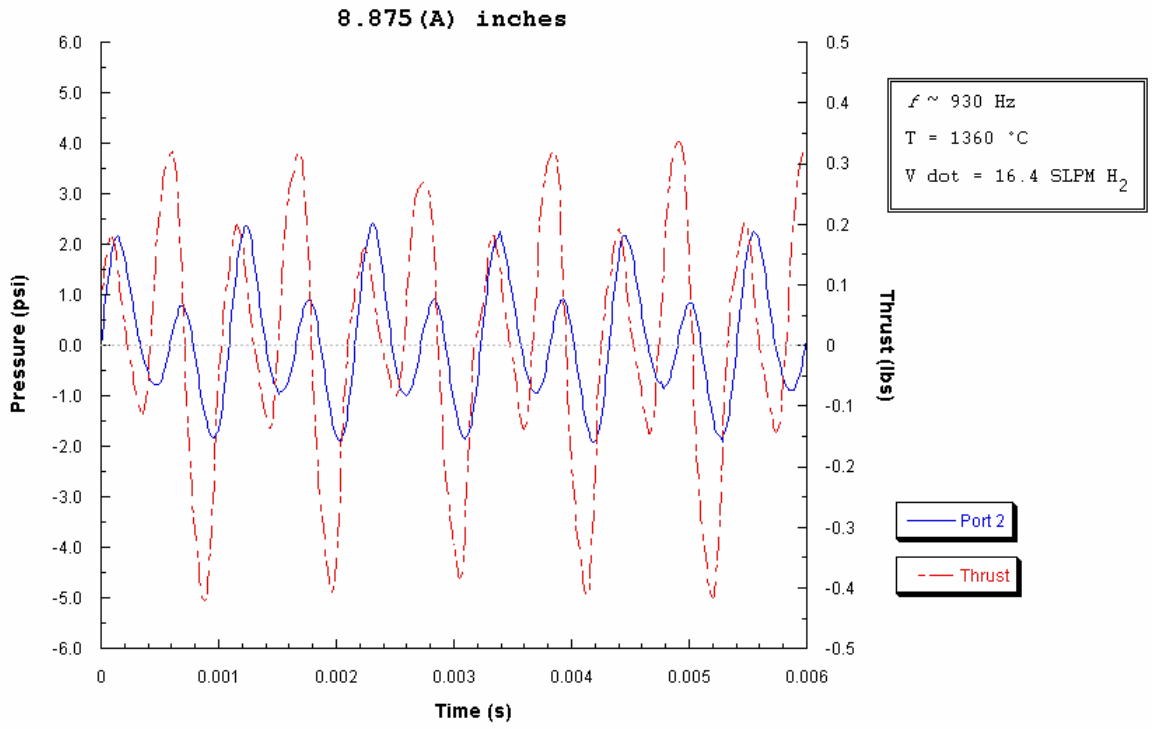
8.875 (A) inches
f ~ 930 Hz
T = 1360 °C
V dot = 16.4 SLPM H2
Pressure (psi)
Thrust (lbs)
Time (s)
Port 2
Thrust

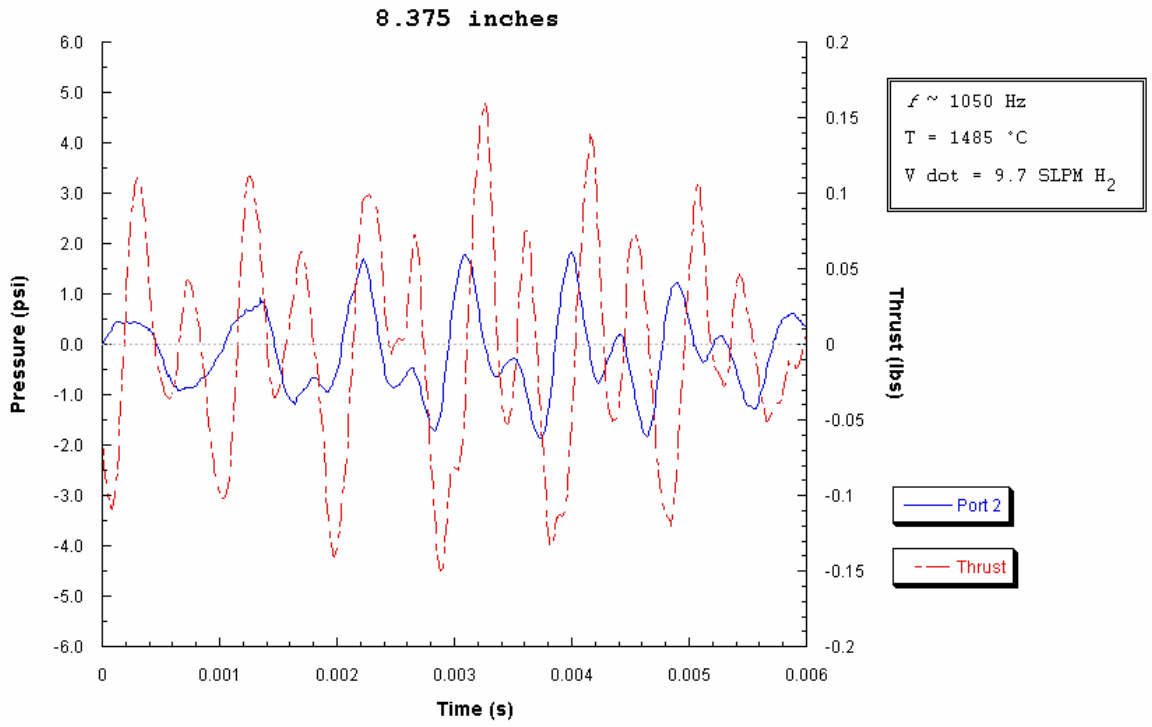
8.375 inches
f ~ 1050 Hz
T = 1485 °C
V dot = 9.7 SLPM H2
Pressure (psi)
Thrust (lbs)
Time (s)
Port 2
Thrust

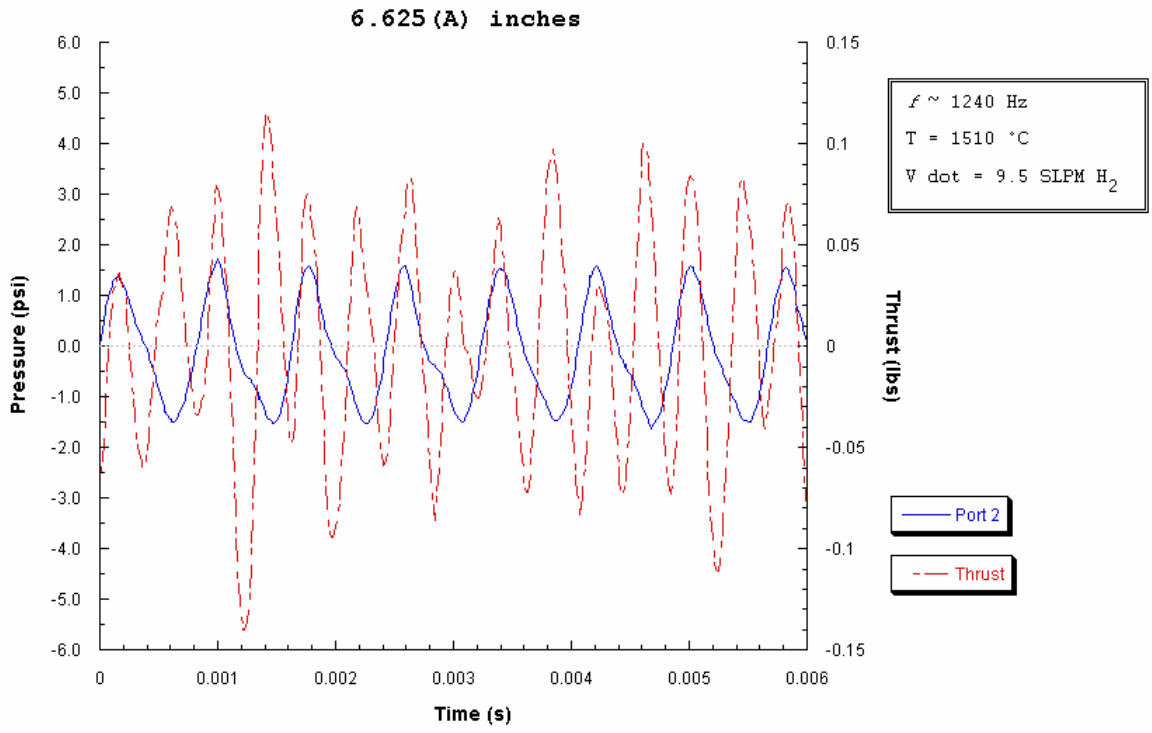
6.625 (A) inches
Pressure (psi)
Thrust (lbs)
Time (s)
f ~ 1240 Hz
T = 1510 °C
V dot = 9.5 SLPM H2
Port 2
Thrust

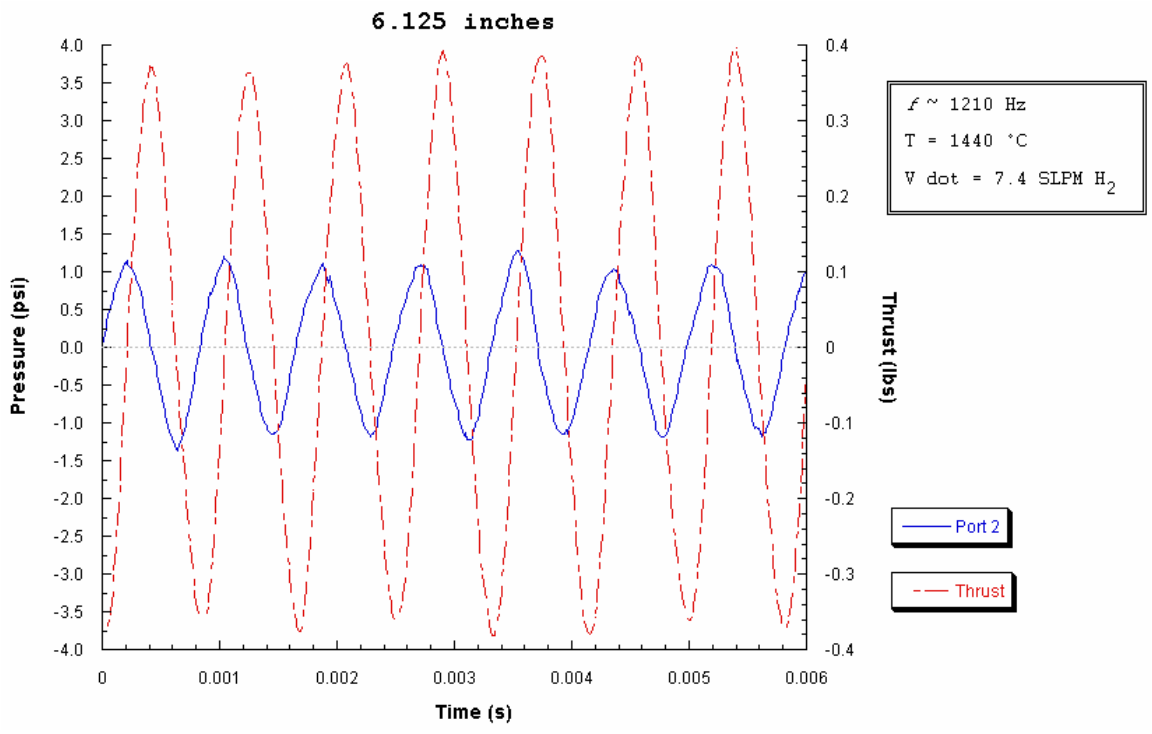
6.125 inches
Pressure (psi)
Thrust (lbs)
Time (s)
f ~ 1210 Hz
T = 1440 °C
V dot = 7.4 SLPM H2
Port 2
Thrust

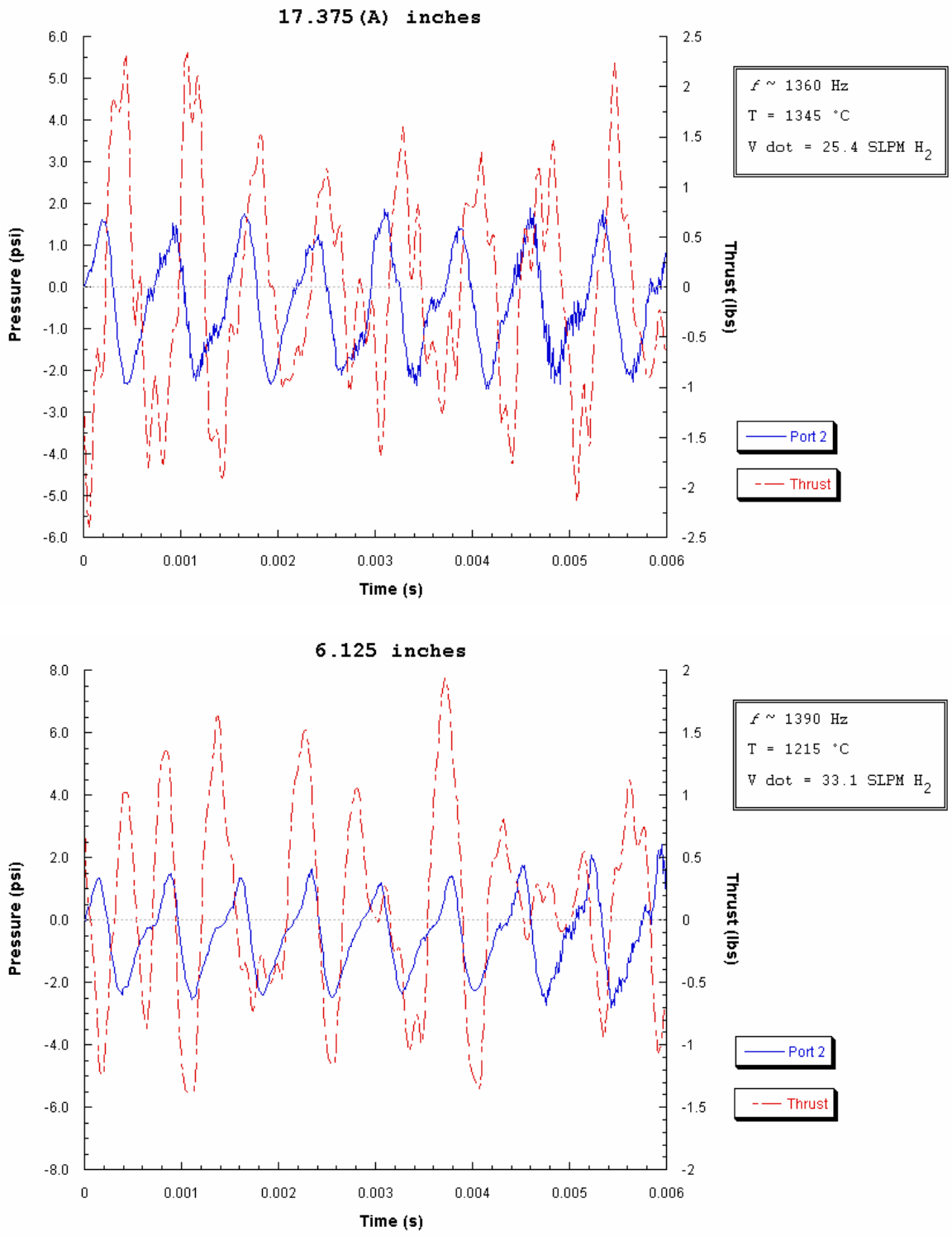

Figure 3.1-19: Maximum $\dot{V}_{H_2}$ at maximum and minimum scalability lengths for an inlet length of 0.5 inches and a 0.086 area ratio.

3.1.3 Case 3

3.1.3.1 2.0-Inch Inlet

Case 3 investigates the scalability characteristics of a 0.040 inlet area to combustion chamber area ratio. As were performed in Cases 1 and 2, tests at this ratio looked at pulsejet performance for inlet lengths of 2.0, 1.5, 1.0, and 0.5 inches at several incremental tail pipe lengths. Figure 3.1-20 displays results for a 2-inch inlet configuration at overall jet lengths ranging from a maximum of 19.0 inches to a minimum of 12.625 inches. To obtain the shortest lengths possible, a diverging nozzle was necessary. In all these cases, nozzle A was employed.

According to Figure 3.1-20, greatest pressure values were obtained at the shortest length configuration, or 12.625 inches with nozzle A. Though, the pulsejet was very difficult to start at this length. All results did not exceed ±4.0 psi pressure and ±1.0 lb thrust. Pressure waveforms remained generally similar in appearance over all length increments. Fuel flow rates would not exceed 7.1 standard liters per minute (SLPM) hydrogen at any increment. Hence, at 12.625 inches, the corresponding plot represents the maximum fuel flow rate for the shortest successful jet length. Even for the full length of 19.0 inches, a maximum fuel flow rate of only 8 SLPM could be achieved, just 1 SLPM greater than conservative flow rate. And, as can be seen by comparison between Figure 3.1-20 and Figure 3.1-21, performance characteristics were not notably affected by the increase.

3.1.3.2 1.5-Inch Inlet

Figure 3.1-22 contains the results of runs performed with an inlet length of 1.5 inches. The shortest successful length was determined to be 10.0 inches, again requiring the nozzle A exit geometry in order to sustain combustion. With just a constant area tail pipe exit geometry, the shortest length achievable was 11.625 inches. At this length, however, the pulsejet was extremely hard to start.

Maximum fuel flow rates did not show any significant increase in absolute thrust nor change in pressure fluctuation range (see Figure 3.1-23). Pressures remained below approximately ±3.0 psi and thrust values did not exceed ±0.5 pounds for all jet lengths observed.

3.1.3.3 1.0-Inch Inlet

Decreasing the inlet length to 1.0 inch allowed further reductions in overall pulsejet length while maintaining resonance. A minimum jet length of 7.25 inches achieved self-sustaining combustion equipped, of course, with the nozzle A extension. At the longest length, 17.938 inches, an atypical higher frequency resonance mode again seemed to be present, leading to the smooth pressure and thrust data found plotted in Figure 3.1-24. The frequency recorded at this length is not in order with the usual progressive increase in operational frequency observed with decrease in jet length. This time, however, the higher frequency mode was repeatable in testing.

At shortest length, maximum fuel flow performance exhibited slightly higher combustion chamber pressures and relatively strong absolute thrust measurements. Also at this length, waveform shape of both pressure and thrust retained their general structure

throughout the tested range of fuel flow rates. This is evident by comparing the maximum flow rate plot (Figure 3.1-25) with that of a conservative flow rate (Figure 3.1-24). Frequency did not change significantly, as well. At full length, a greater fuel flow rate than the conservative rate of 8.0 SLPM H_2 did not result in self-sustaining resonance. Hence, a full length configuration is not found in the fuel flow plots of Figure 3.1-25.

3.1.3.4 0.5-Inch Inlet

Tests performed at the minimum inlet length of 0.5 inch resulted in successful resonance at all jet length increments attempted, including the shortest studied length of 6.25 inches. The most obvious change in pulsejet performance at this inlet configuration is the reduction in pressures seen inside the combustion chamber. Pressure plots of Figure 3.1-26 show chamber pressures more or less staying within ±1.5 psi at all jet length increments. This is in contrast to the 2.0-2.5 psi peak chamber pressures seen at most configurations previously discussed. Absolute thrust values did not exceed 0.3 pound.

Fuel flow rates could not be increased much greater than those flow rates used for conservative runs. Maximum and minimum jet lengths lacking a nozzle extension were utilized in fuel flow rate testing, and results are shown in Figure 3.1-27. At the shortest length of 6.25 inches, the flow rate could not be increased more than 75 percent of that used for normal runs. This figure was limited to only 20 percent for the longest length of 16.875 inches, both significantly low in relation to previous inlet lengths and ratios. In turn, thrust values did not see substantial increases, either. This lack in maximum

performance may be attributed to the limited volume of intake air restricted by the smaller inlet ratio configuration.

Figure 3.1-20:

Pulsejet scalability performance for an inlet length of 2.0 inches and a 0.040 area ratio.

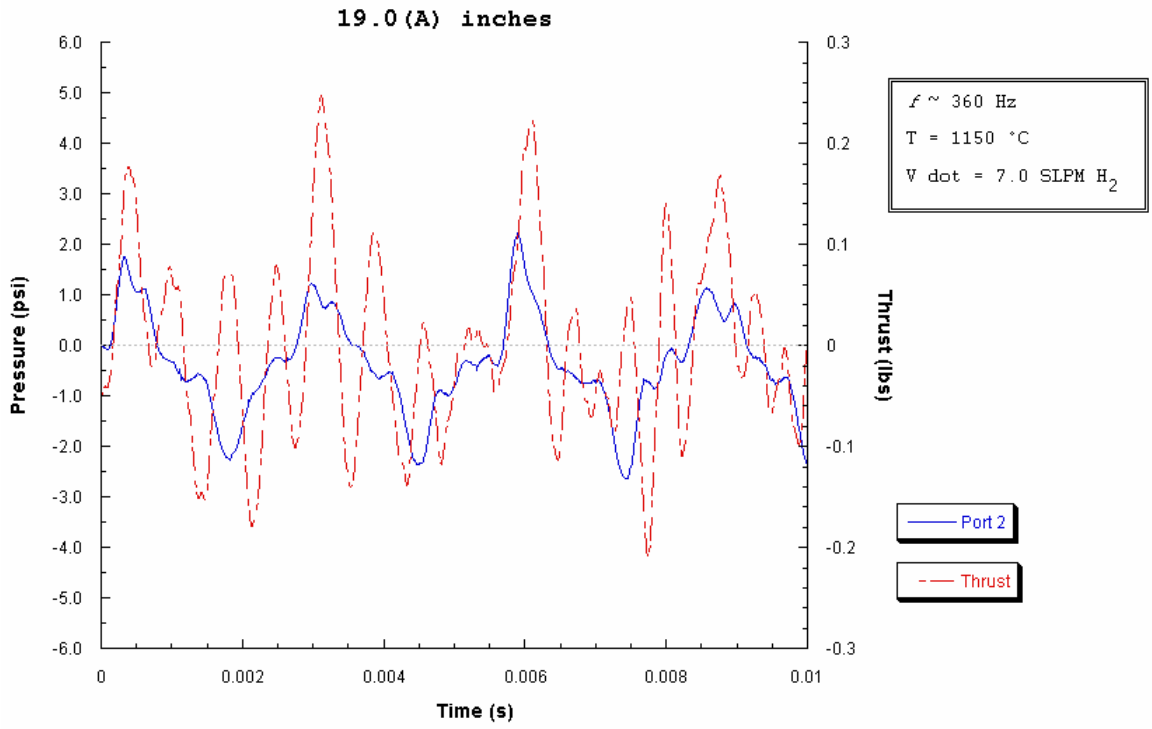
19.0(A) inches
f ~ 360 Hz
T = 1150 °C
V dot = 7.0 SLPM H2
Pressure (psi)
Thrust (lbs)
Time (s)
Port 2
Thrust

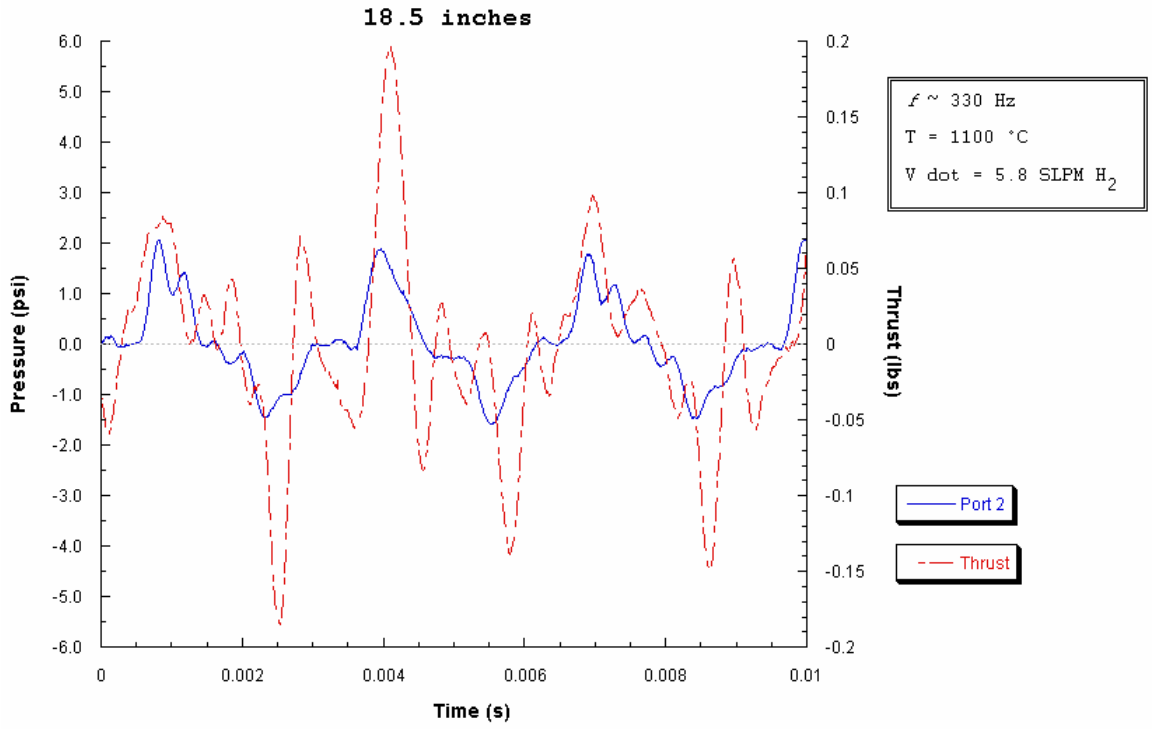
18.5 inches
f ~ 330 Hz
T = 1100 °C
V dot = 5.8 SLPM H2
Pressure (psi)
Thrust (lbs)
Time (s)
Port 2
Thrust

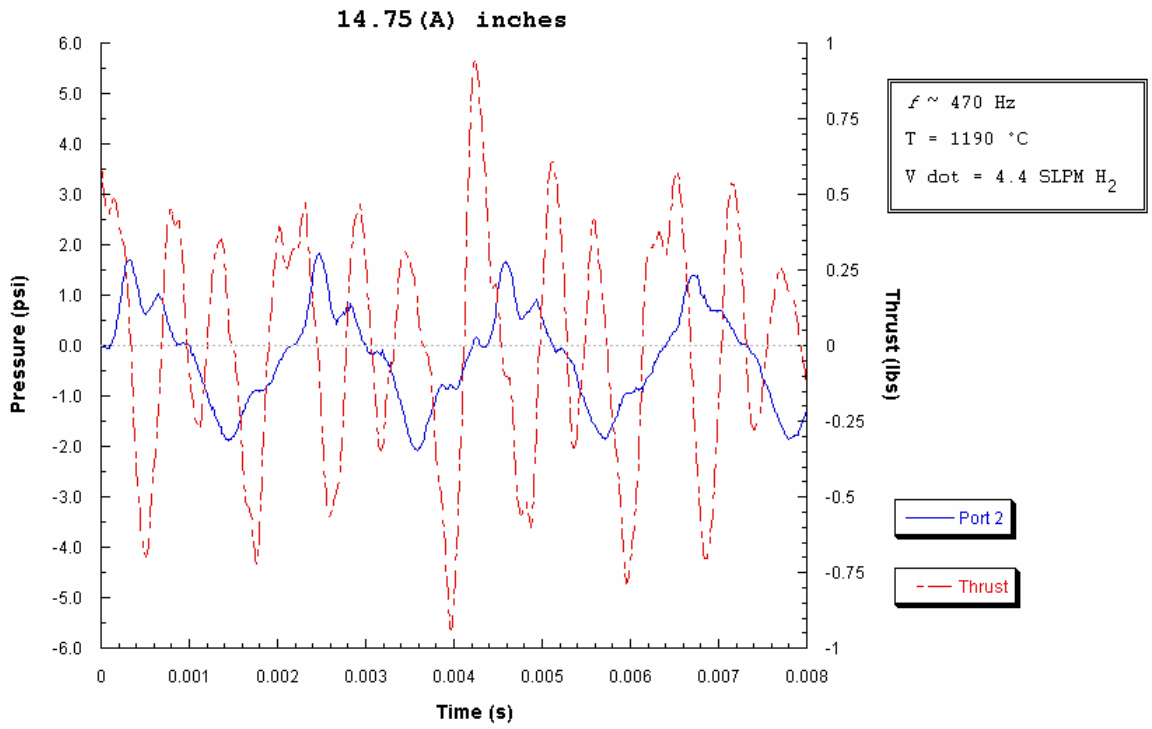
14.75 (A) inches
Pressure (psi)
Thrust (lbs)
Time (s)
f ~ 470 Hz
T = 1190 °C
V dot = 4.4 SLPM H2
Port 2
Thrust

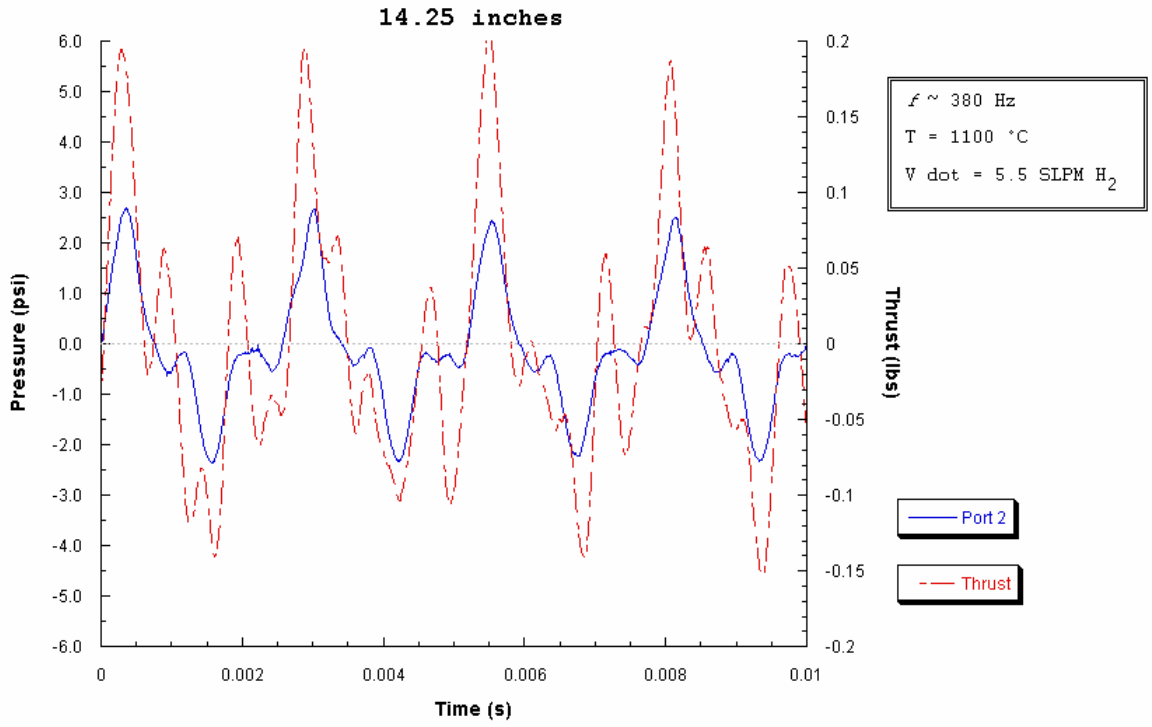
14.25 inches
Pressure (psi)
Thrust (lbs)
Time (s)
f ~ 380 Hz
T = 1100 °C
V dot = 5.5 SLPM H2
Port 2
Thrust

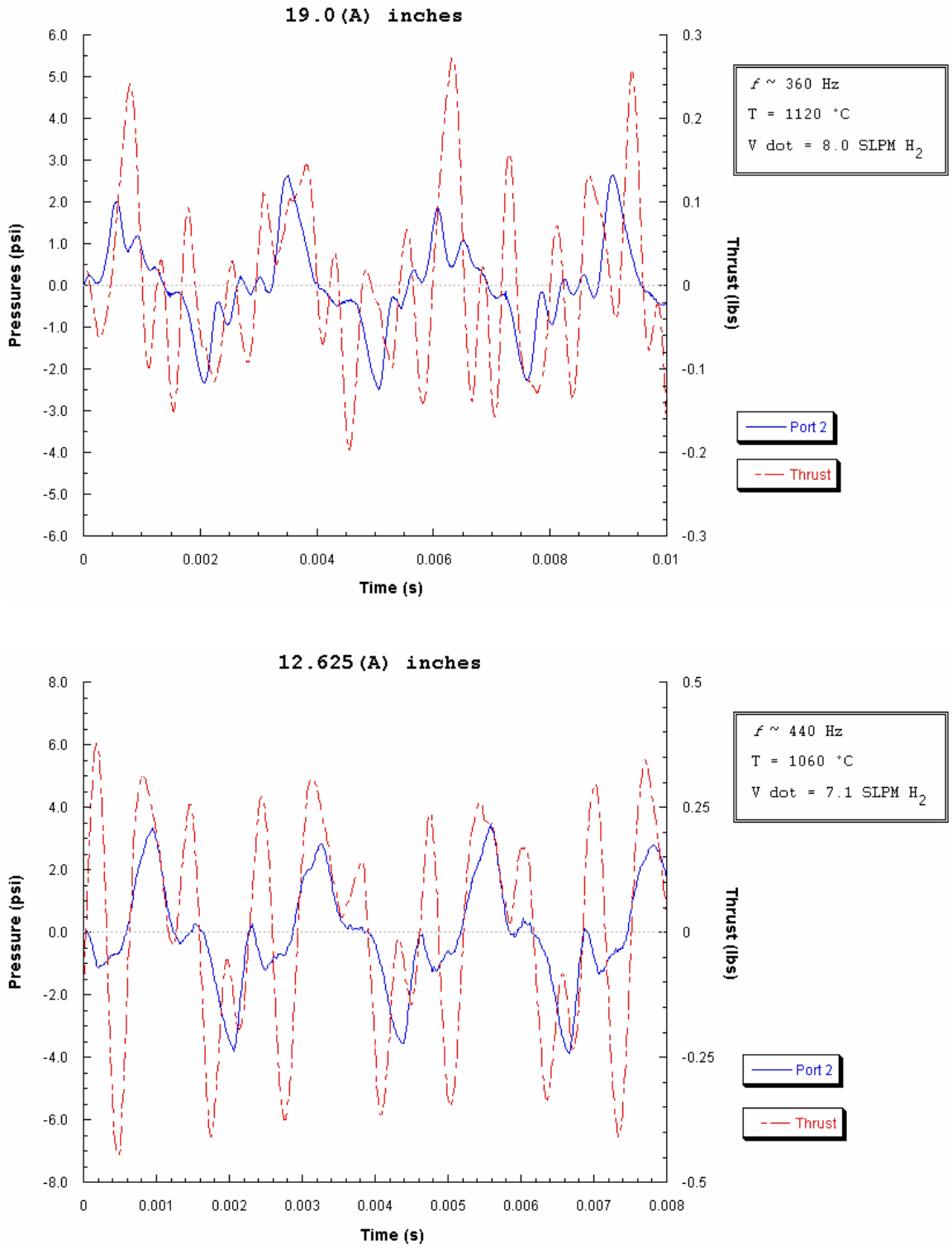

Figure 3.1-21: Maximum $\dot{V}_{H_2}$ at maximum and minimum scalability lengths for an inlet length of 2.0 inches and a 0.040 area ratio.

Figure 3.1-22:

Pulsejet scalability performance for an inlet length of 1.5 inches and a 0.040 area ratio.

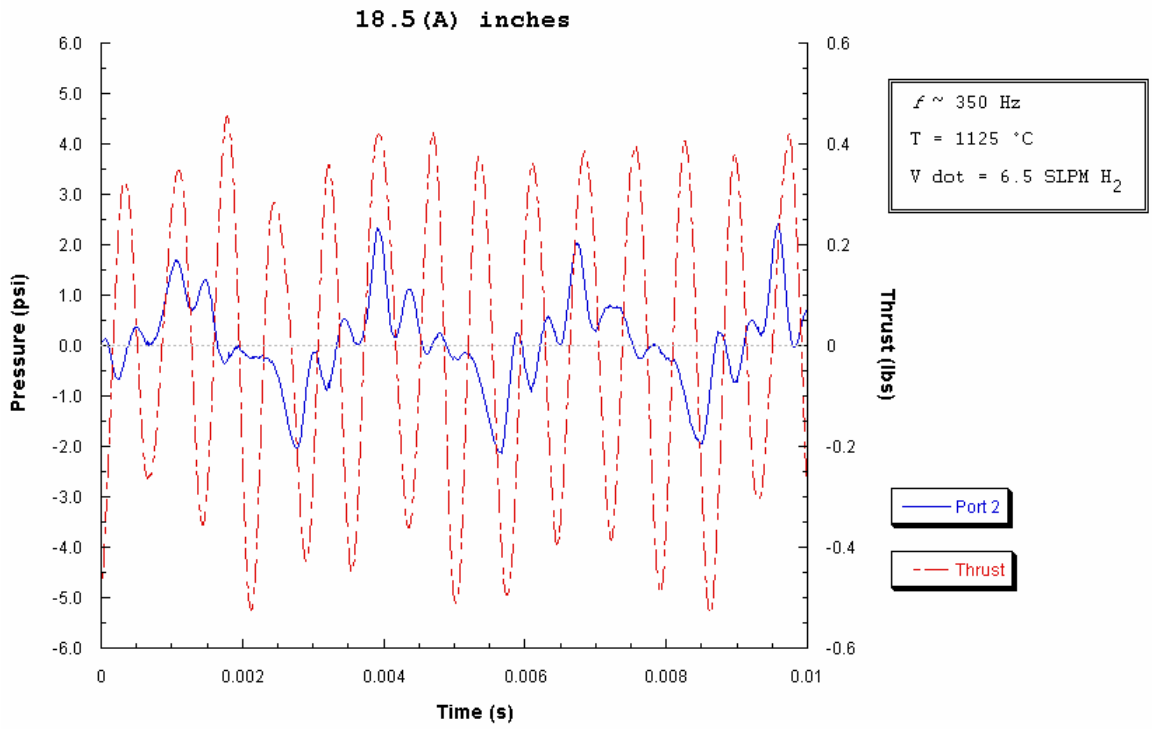
18.5 (A) inches
f ~ 350 Hz
T = 1125 °C
V dot = 6.5 SLPM H2
Pressure (psi)
Thrust (lbs)
Time (s)
Port 2
Thrust

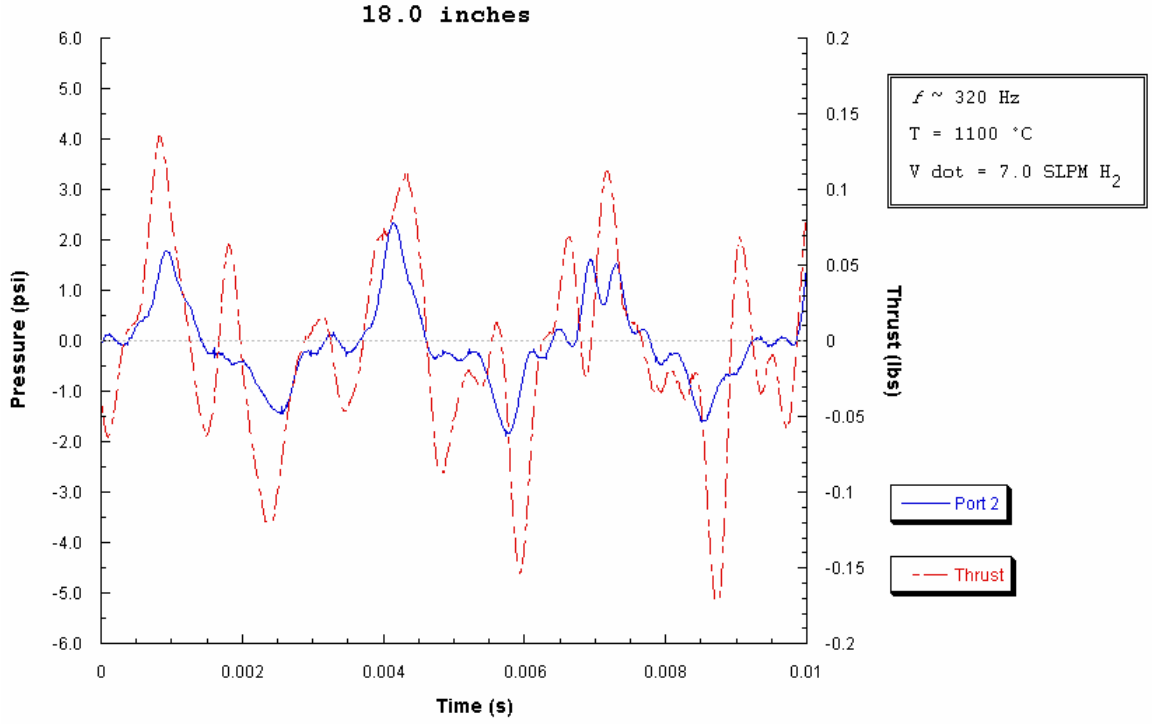
18.0 inches
f ~ 320 Hz
T = 1100 °C
V dot = 7.0 SLPM H2
Pressure (psi)
Thrust (lbs)
Time (s)
Port 2
Thrust

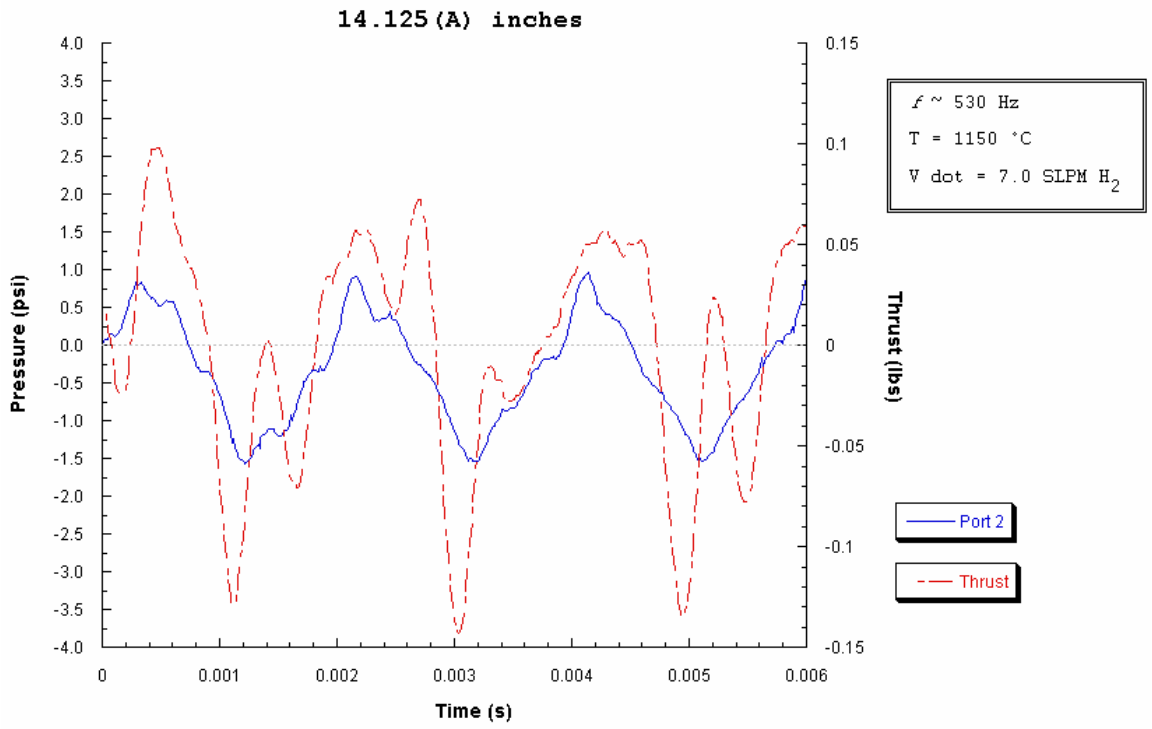
14.125 (A) inches
f ~ 530 Hz
T = 1150 °C
V dot = 7.0 SLPM H2
Pressure (psi)
Thrust (lbs)
Time (s)
Port 2
Thrust

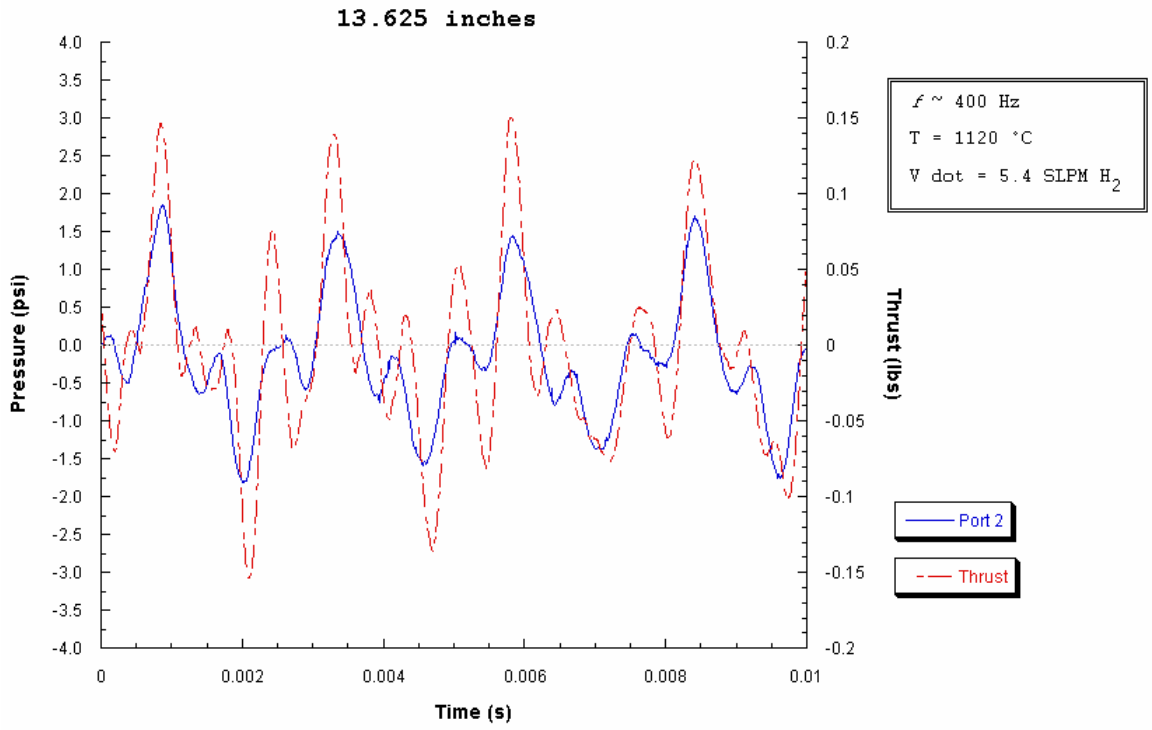
13.625 inches
f ~ 400 Hz
T = 1120 °C
V dot = 5.4 SLPM H2
Pressure (psi)
Thrust (lbs)
Time (s)
Port 2
Thrust

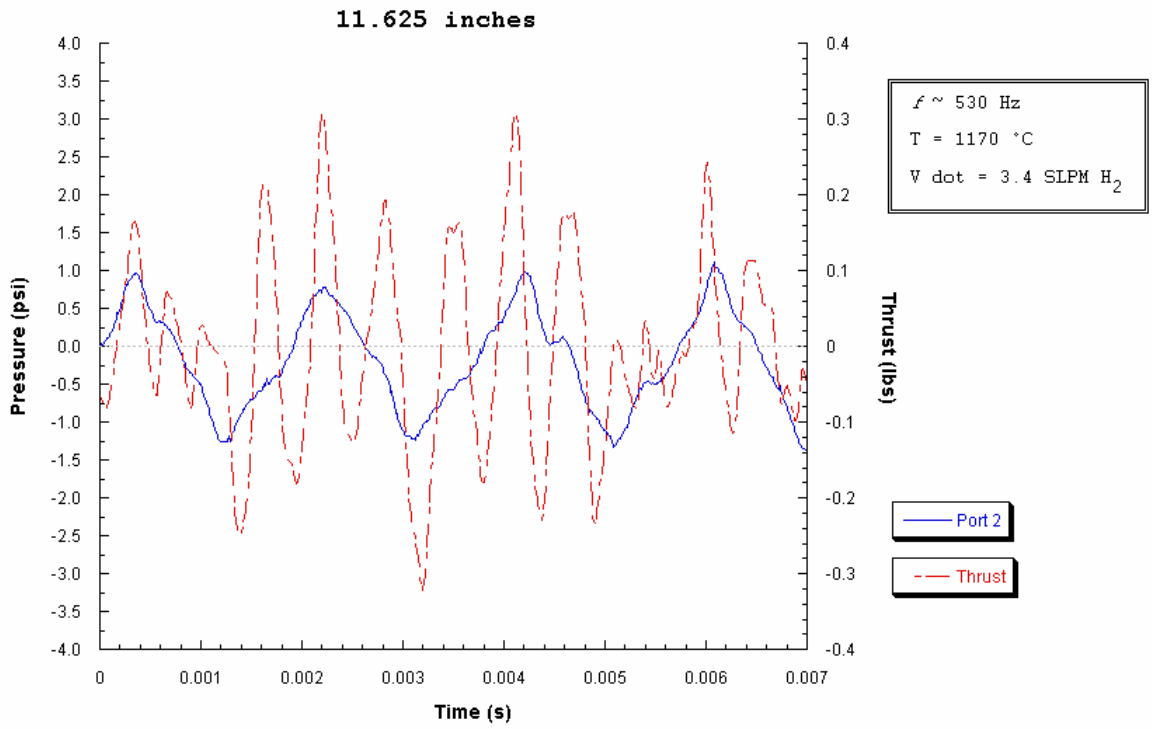
11.625 inches
f ~ 530 Hz
T = 1170 °C
V dot = 3.4 SLPM H2
Pressure (psi)
Thrust (lbs)
Time (s)
Port 2
Thrust

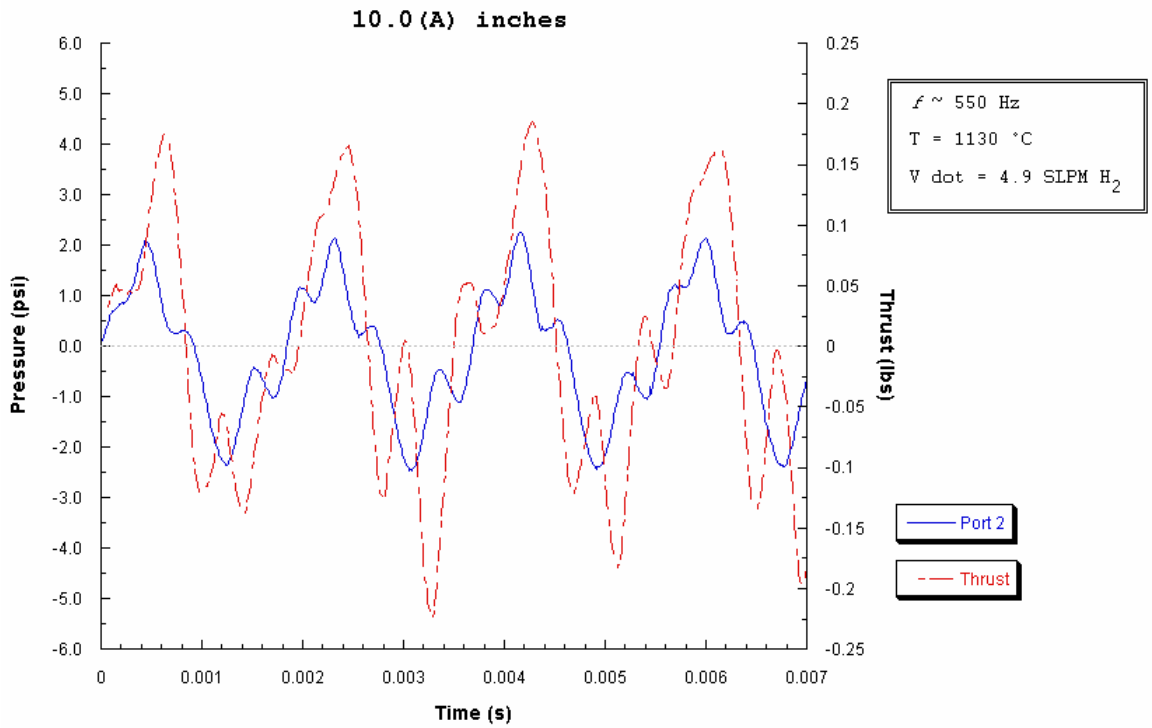
10.0(A) inches
f ~ 550 Hz
T = 1130 °C
V dot = 4.9 SLPM H2
Pressure (psi)
Thrust (lbs)
Time (s)
Port 2
Thrust

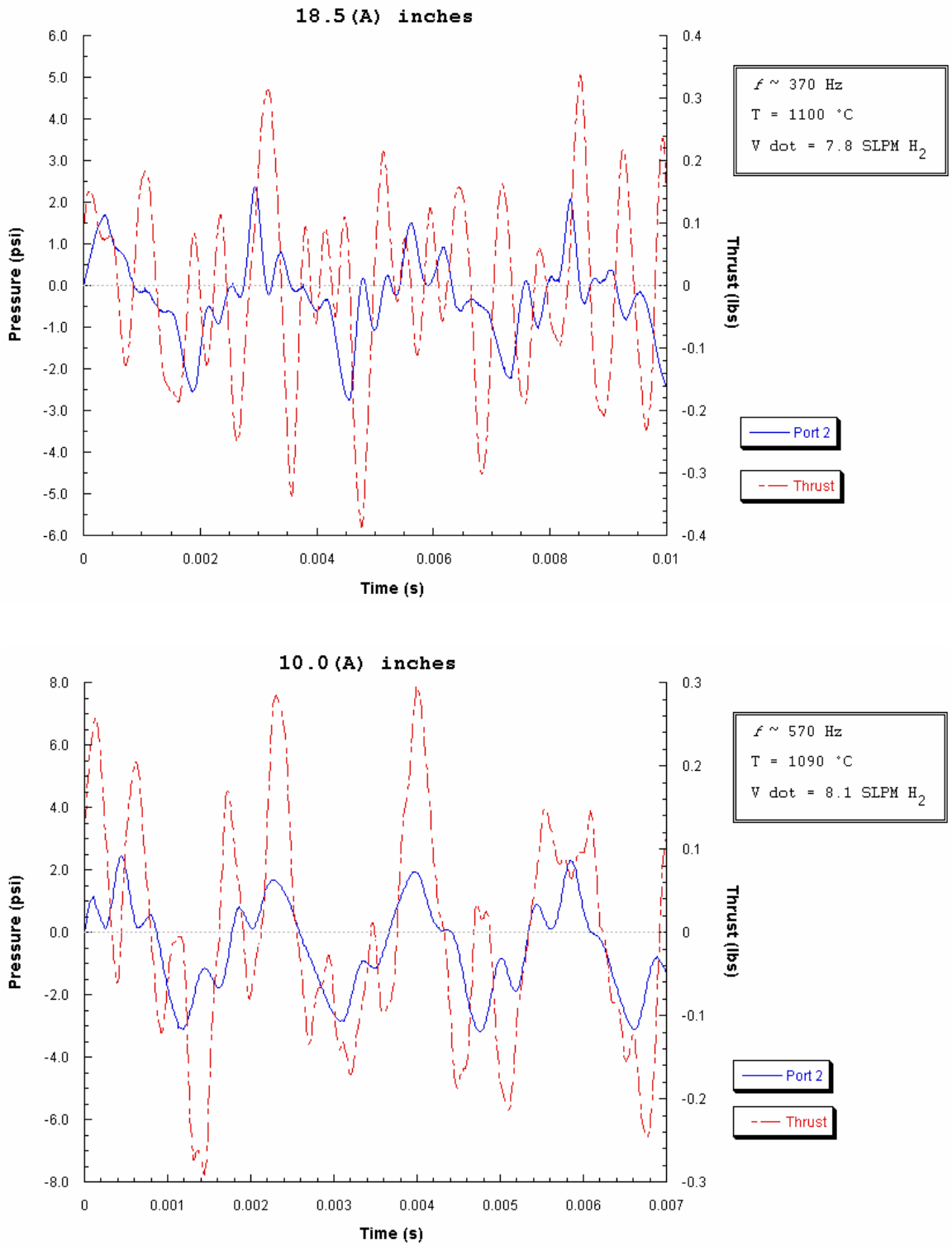

Figure 3.1-23: Maximum $\dot{V}_{H_2}$ at maximum and minimum scalability lengths for an inlet length of 1.5 inches and a 0.040 area ratio.

Figure 3.1-24:

Pulsejet scalability performance for an inlet length of 1.0 inches and a 0.040 area ratio.

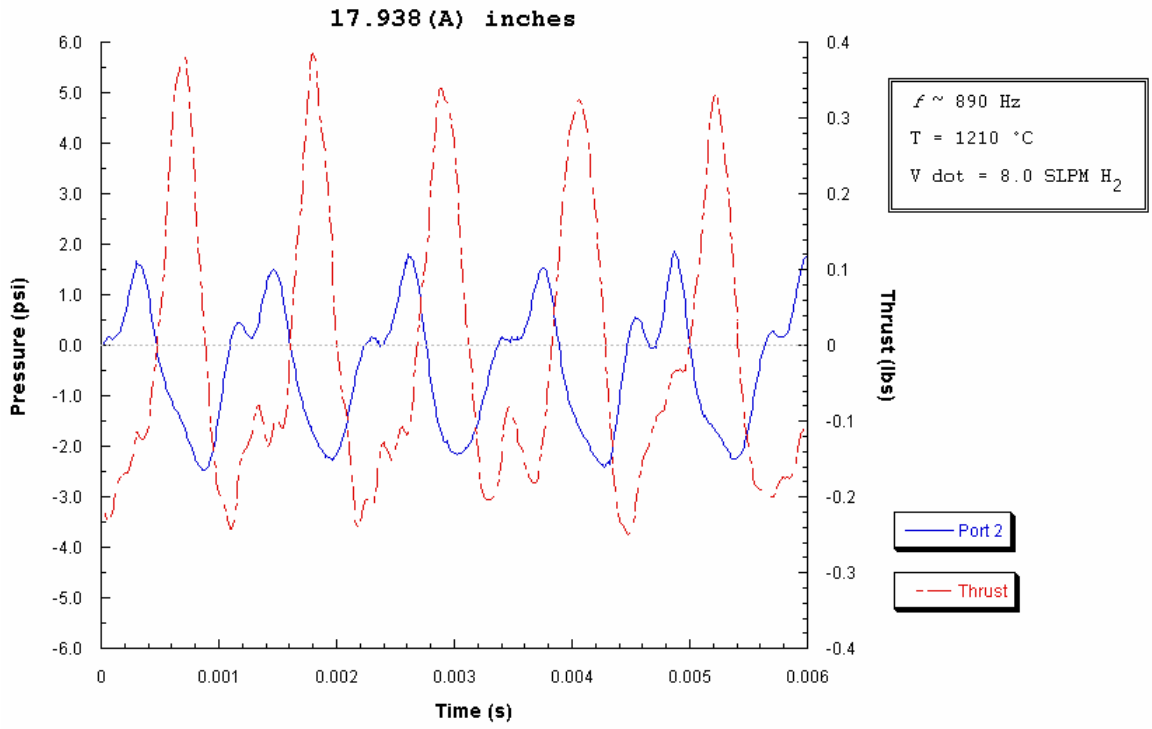
17.938 (A) inches
Pressure (psi)
Thrust (lbs)
Time (s)
f ~ 890 Hz
T = 1210 °C
V dot = 8.0 SLPM H2
Port 2
Thrust

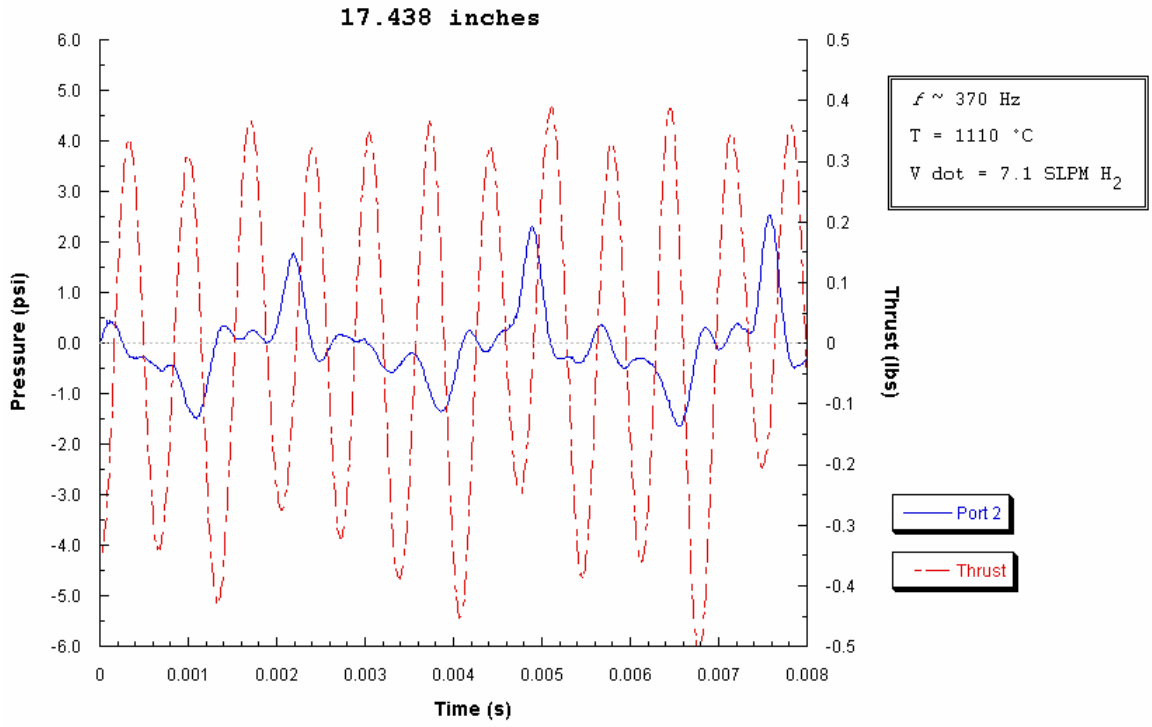
17.438 inches
Pressure (psi)
Thrust (lbs)
Time (s)
f ~ 370 Hz
T = 1110 °C
V dot = 7.1 SLPM H2
Port 2
Thrust

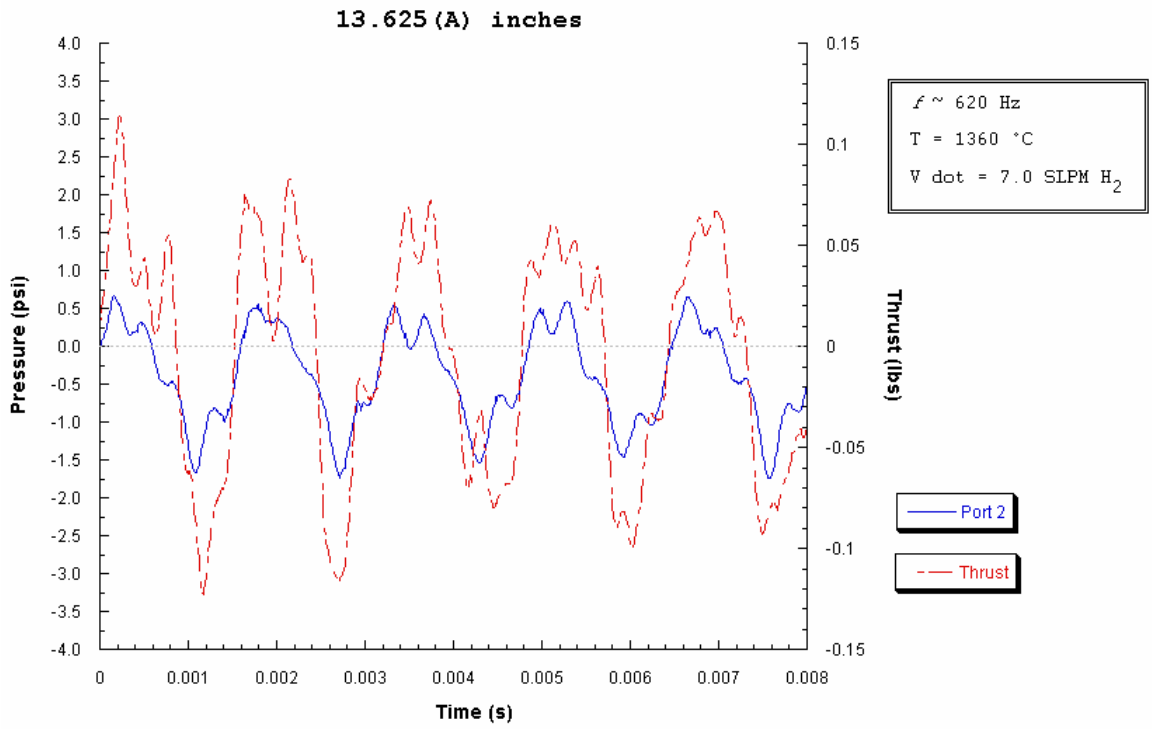
13.625(A) inches
f ~ 620 Hz
T = 1360 °C
V dot = 7.0 SLPM H2
Pressure (psi)
Thrust (lbs)
Time (s)
Port 2
Thrust

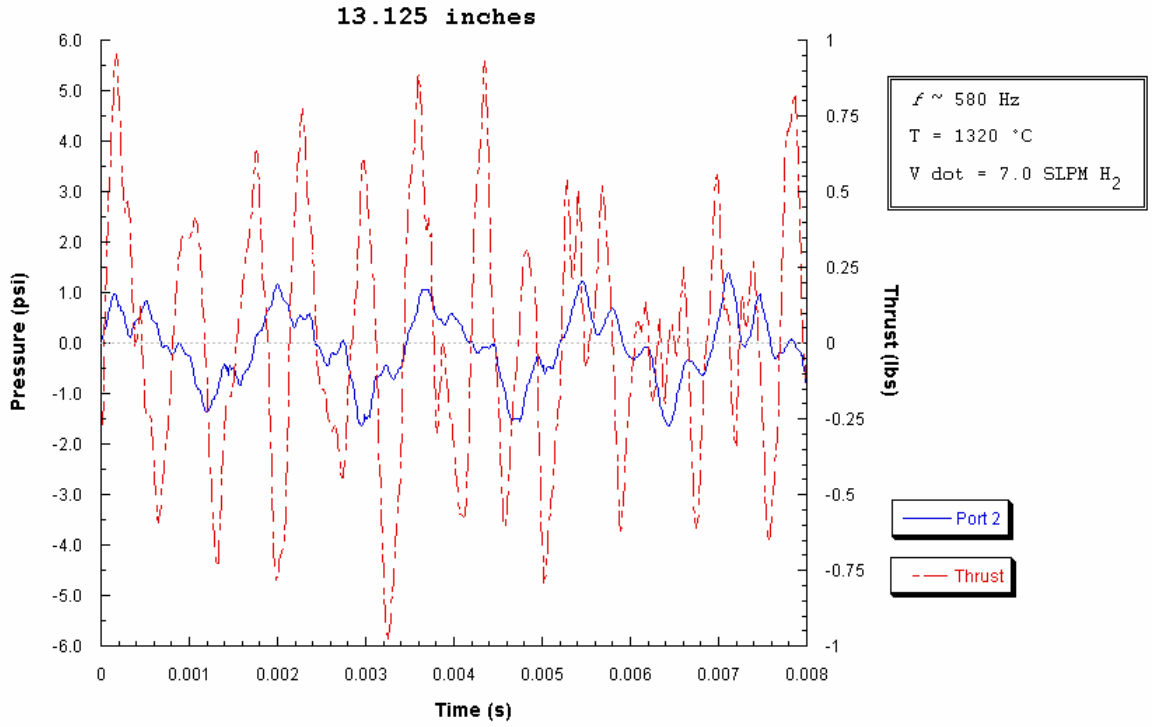
13.125 inches
f ~ 580 Hz
T = 1320 °C
V dot = 7.0 SLPM H2
Pressure (psi)
Thrust (lbs)
Time (s)
Port 2
Thrust

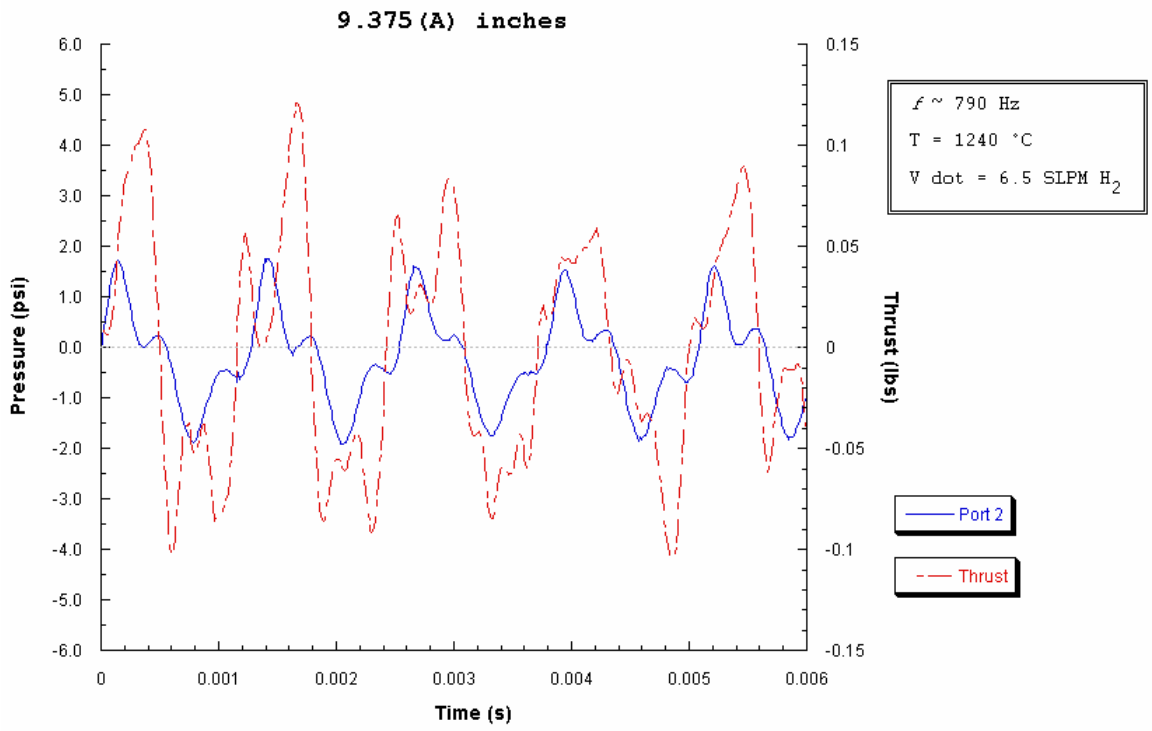
9.375 (A) inches
f ~ 790 Hz
T = 1240 °C
V dot = 6.5 SLPM H2
Pressure (psi)
Thrust (lbs)
Time (s)
Port 2
Thrust

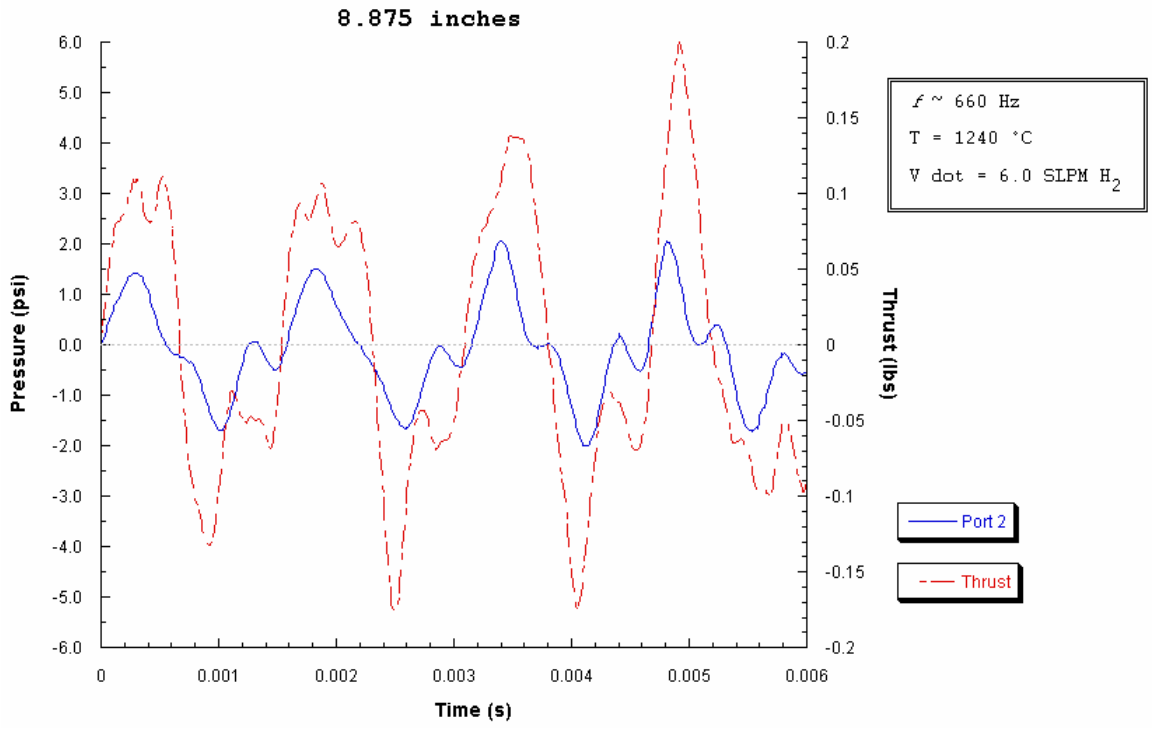
8.875 inches
f ~ 660 Hz
T = 1240 °C
V dot = 6.0 SLPM H2
Pressure (psi)
Thrust (lbs)
Time (s)
Port 2
Thrust

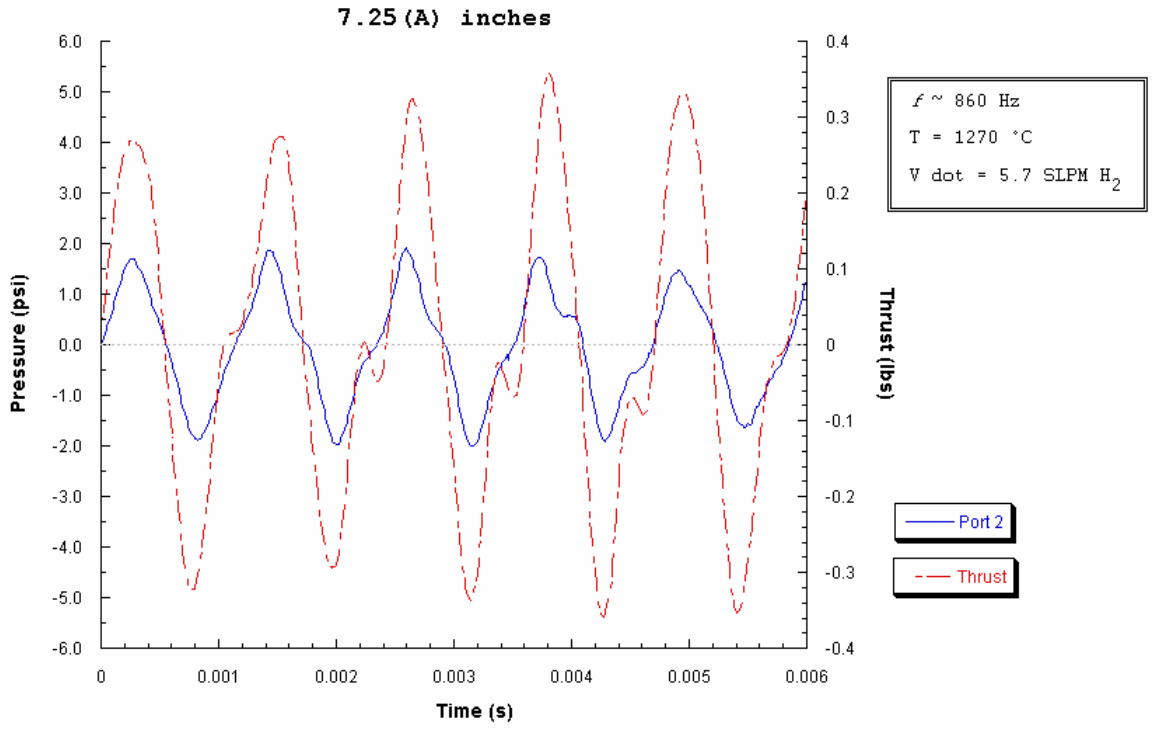
7.25 (A) inches
Pressure (psi)
Thrust (lbs)
Time (s)
6.0
5.0
4.0
3.0
2.0
1.0
0.0
-1.0
-2.0
-3.0
-4.0
-5.0
-6.0
0.4
0.3
0.2
0.1
0
-0.1
-0.2
-0.3
-0.4
0
0.001
0.002
0.003
0.004
0.005
0.006
f ~ 860 Hz
T = 1270 °C
V dot = 5.7 SLPM H2
Port 2
Thrust

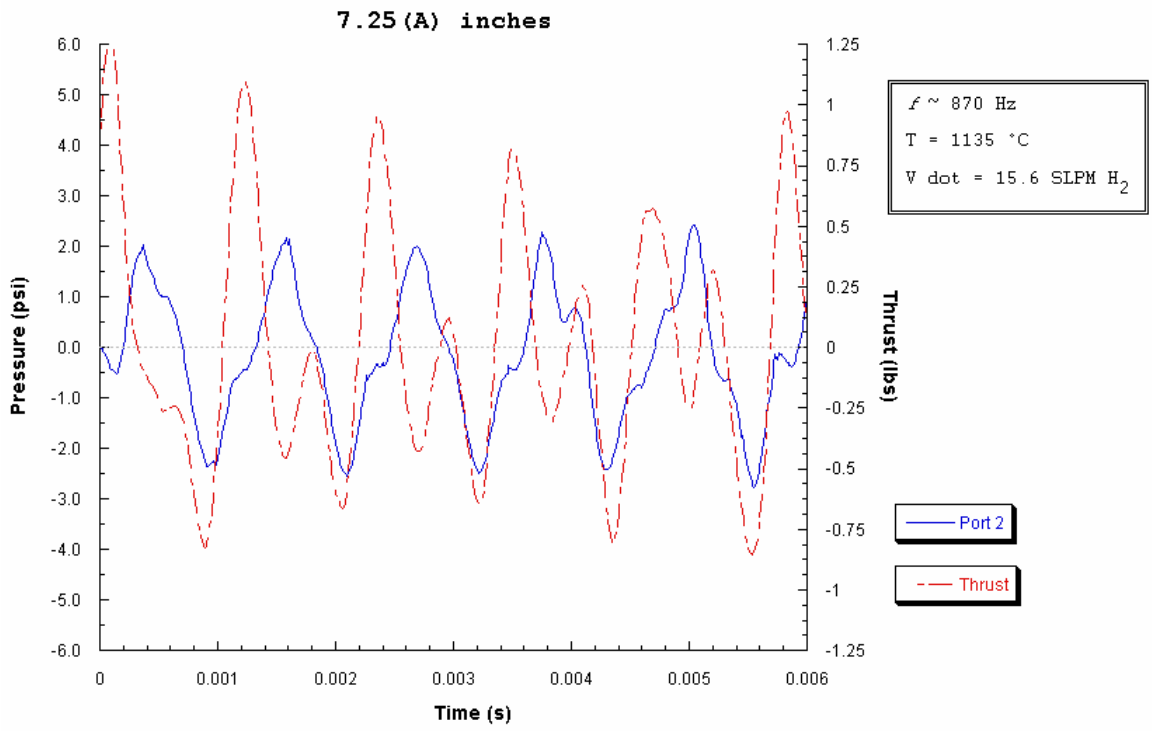

Figure 3.1-25: Maximum $\dot{V}_{H_2}$ at the minimum scalability length for an inlet length of 1.0 inches and a 0.040 area ratio.

Figure 3.1-26:

Pulsejet scalability performance for an inlet length of 0.5 inches and a 0.040 area ratio.

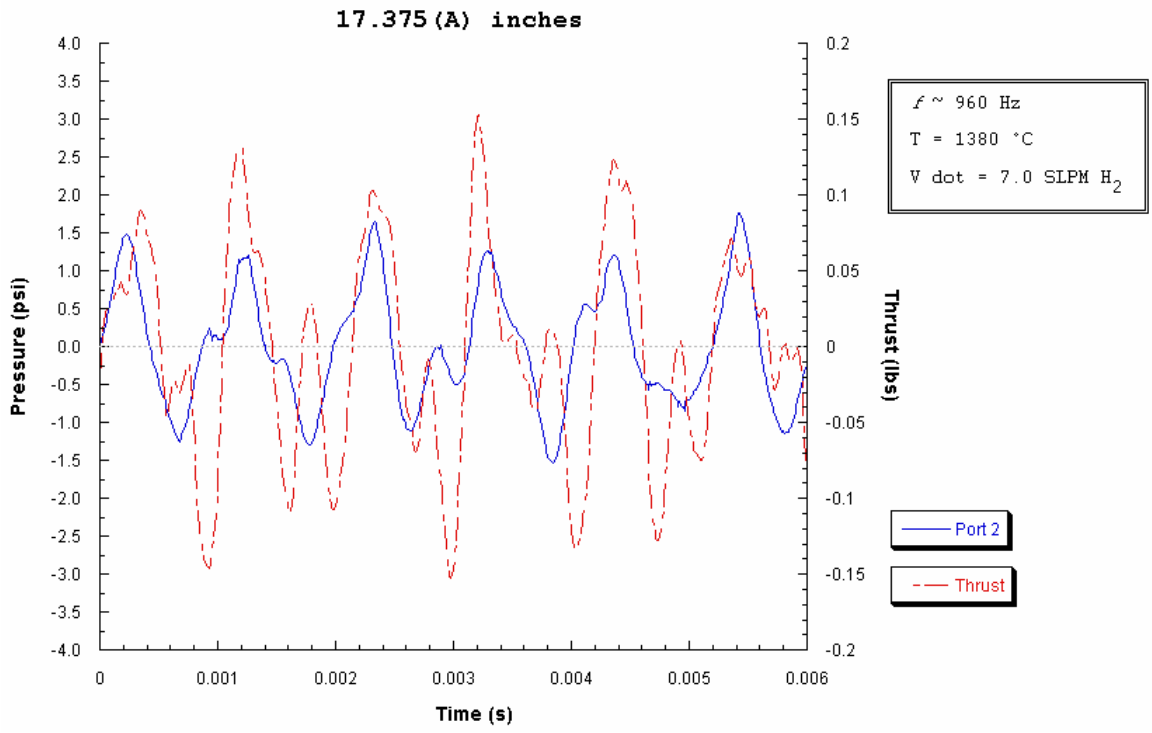
17.375 (A) inches
f ~ 960 Hz
T = 1380 °C
V dot = 7.0 SLPM H2
Pressure (psi)
Thrust (lbs)
Time (s)
Port 2
Thrust

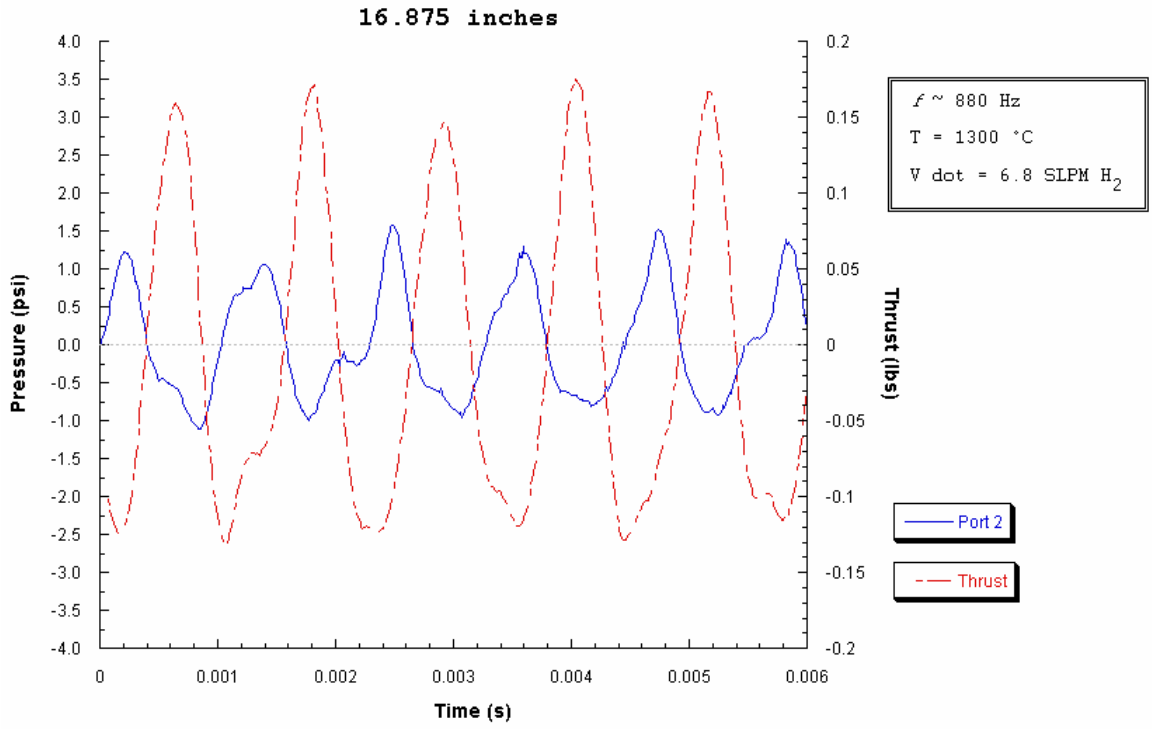
16.875 inches
f ~ 880 Hz
T = 1300 °C
V dot = 6.8 SLPM H2
Pressure (psi)
Thrust (lbs)
Time (s)
Port 2
Thrust

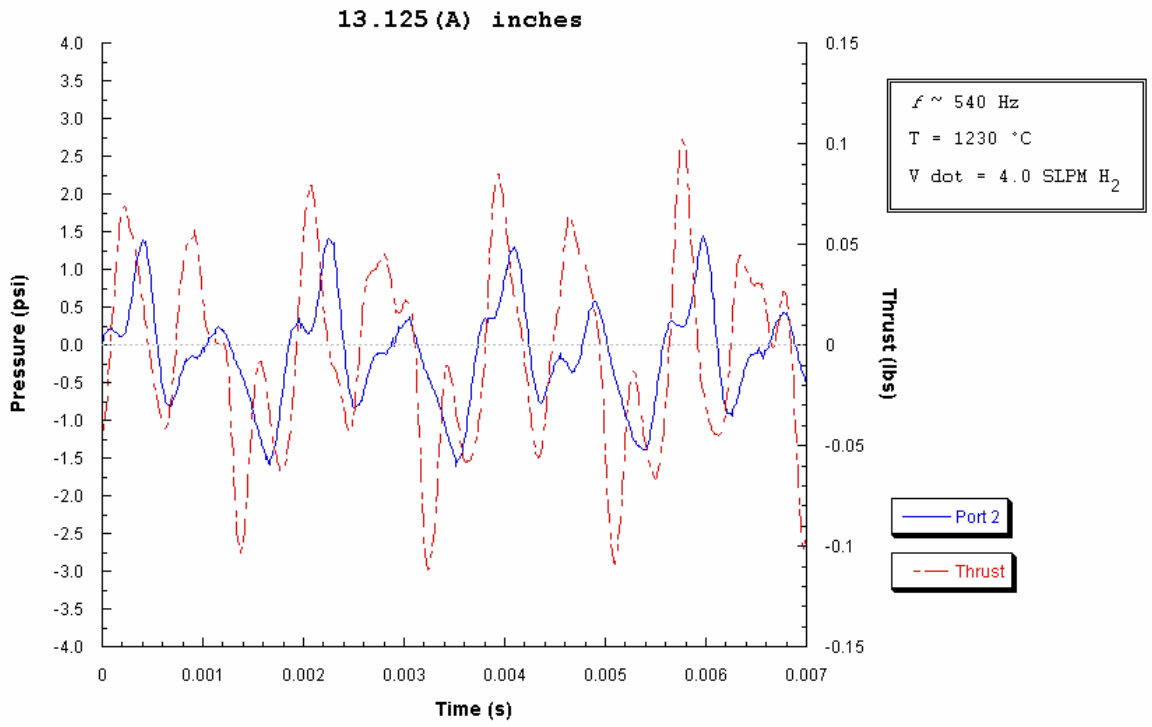
13.125 (A) inches
f ~ 540 Hz
T = 1230 °C
V dot = 4.0 SLPM H2
Pressure (psi)
Thrust (lbs)
Time (s)
Port 2
Thrust

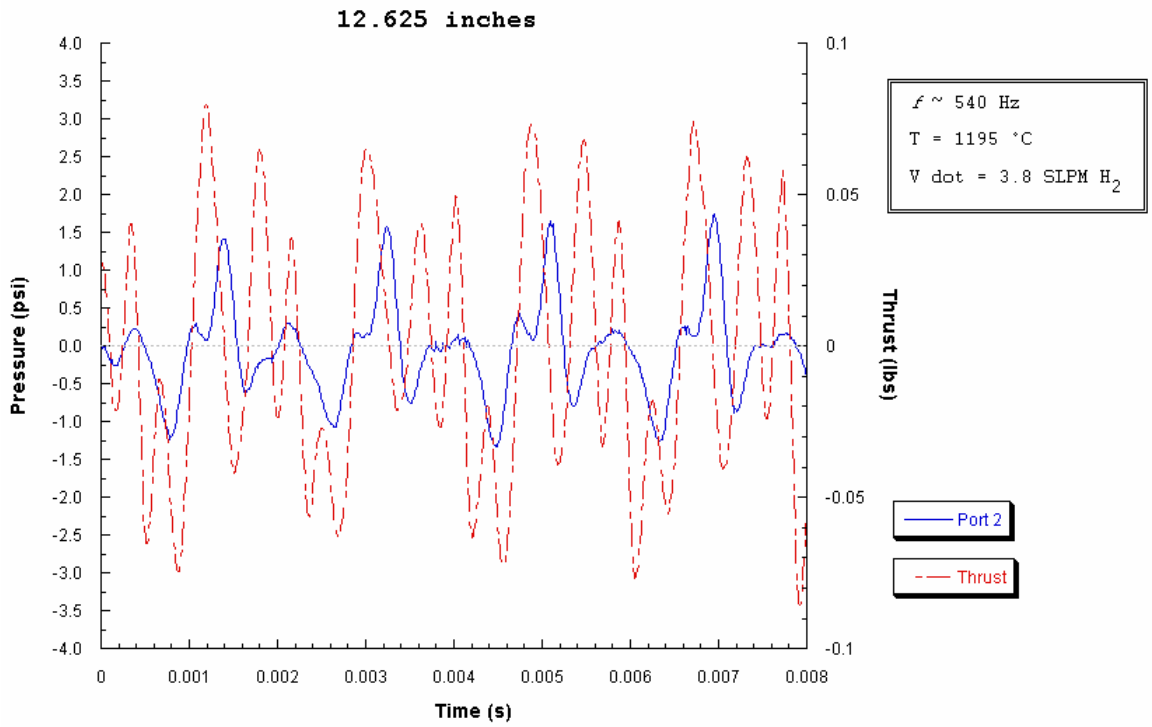
12.625 inches
f ~ 540 Hz
T = 1195 °C
V dot = 3.8 SLPM H2
Pressure (psi)
Thrust (lbs)
Time (s)
Port 2
Thrust

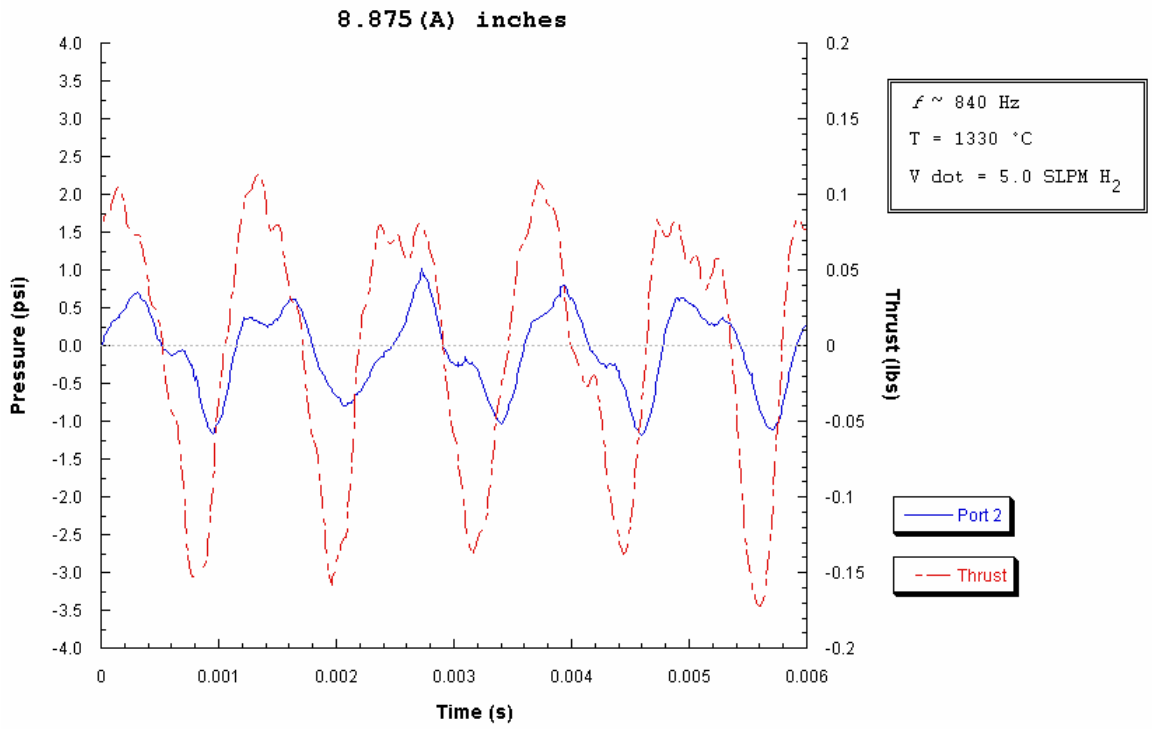
8.875 (A) inches
f ~ 840 Hz
T = 1330 °C
V dot = 5.0 SLPM H2
Pressure (psi)
Thrust (lbs)
Time (s)
Port 2
Thrust

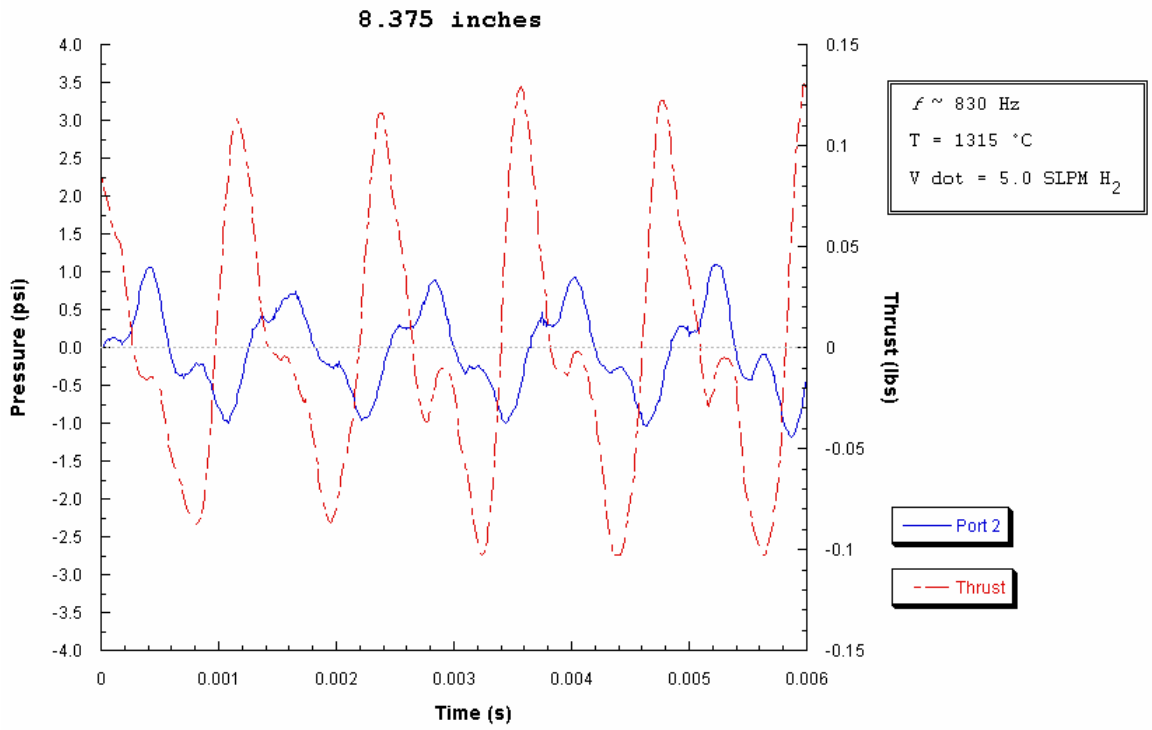
8.375 inches
f ~ 830 Hz
T = 1315 °C
V dot = 5.0 SLPM H2
Pressure (psi)
Thrust (lbs)
Time (s)
Port 2
Thrust

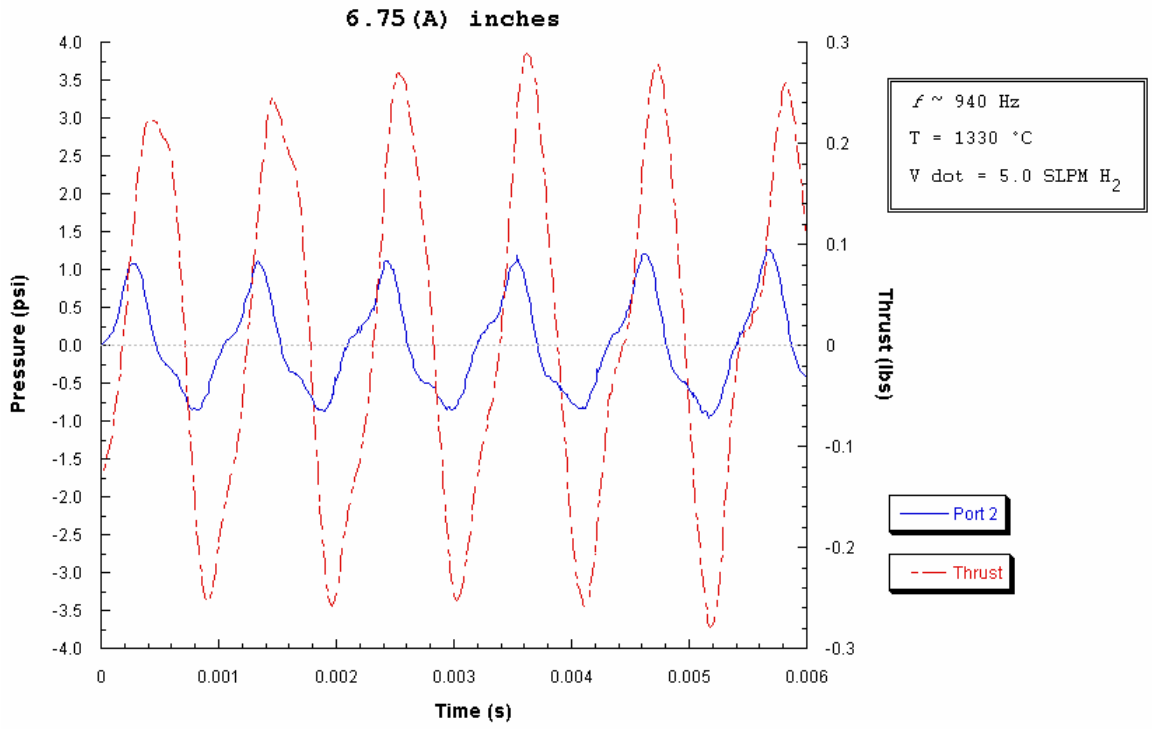
6.75 (A) inches
f ~ 940 Hz
T = 1330 °C
V dot = 5.0 SLPM H2
Pressure (psi)
Thrust (lbs)
Time (s)
Port 2
Thrust

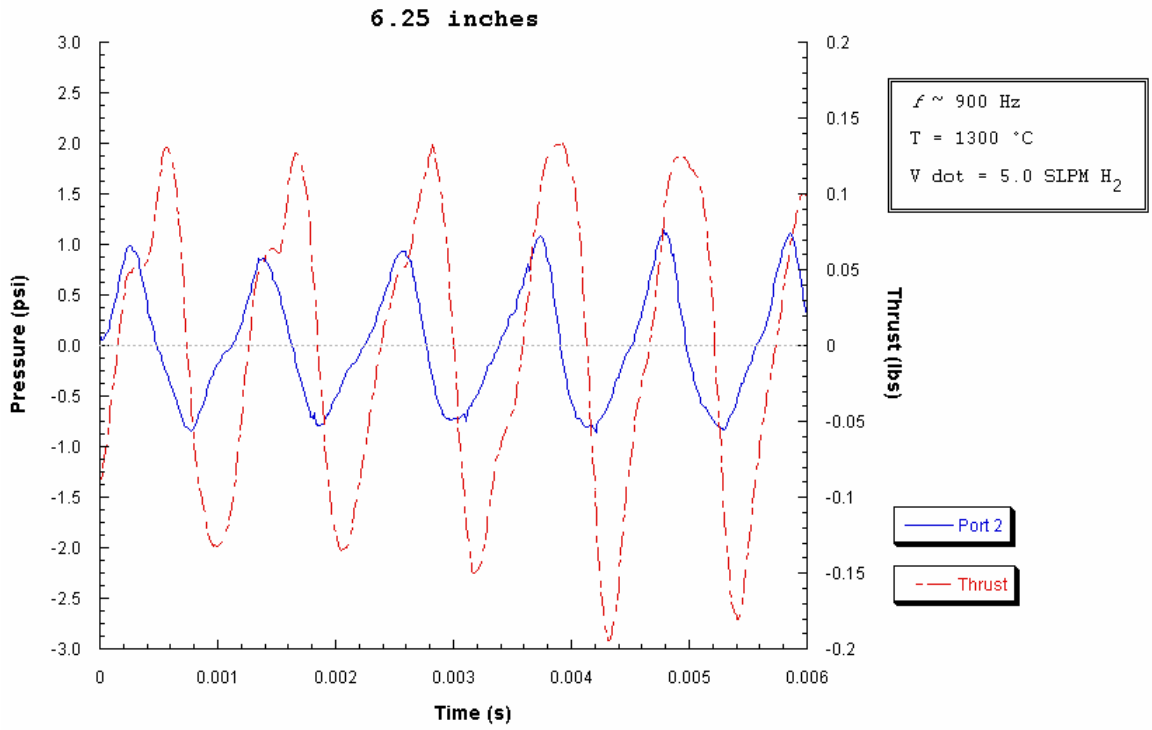
6.25 inches
f ~ 900 Hz
T = 1300 °C
V dot = 5.0 SLPM H2
Pressure (psi)
Thrust (lbs)
Time (s)
Port 2
Thrust

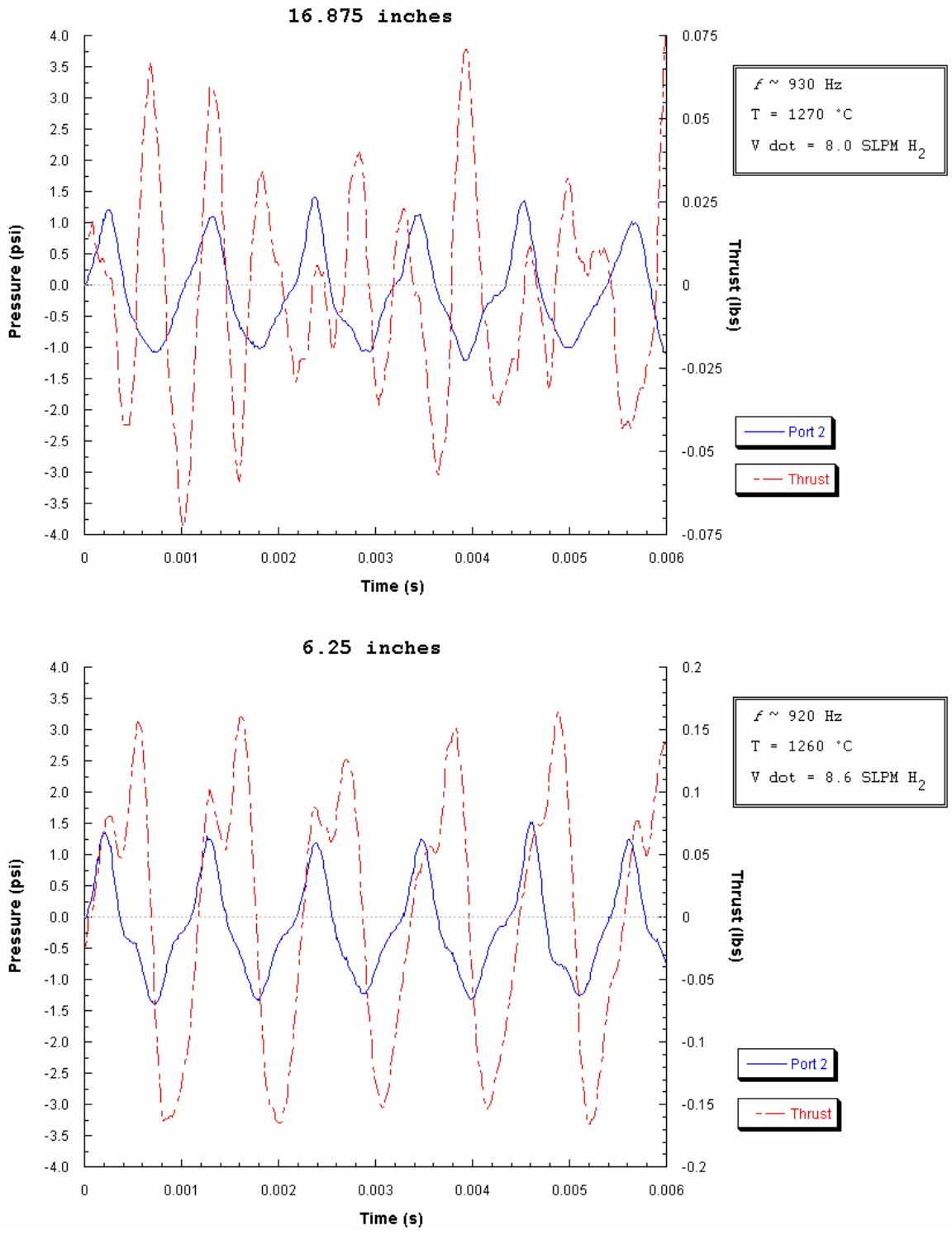

Figure 3.1-27: Maximum $\dot{V}_{H_2}$ at the minimum scalability length for an inlet length of 0.5 inches and a 0.040 area ratio.

3.2 Inlet Orientation Development

Further experimentation was also performed on numerous different valveless inlet orientations to test for operational feasibility. Success was found with a 90 degree-orientated inlet (Figure 2.3-2) at a 0.040 inlet area ratio. For an inlet length of 0.775 inch, self-sustaining resonance at a minimum jet length of 9.938 inches was achieved. Fuel flow was limited to within the range of 11.3 to 15.1 SLPM hydrogen. A maximum overall length of 13.25 inches was attempted for the 90-degree configuration and found successful. At this longer length, the throttle capacity limits ranged from 9.4 to 17.0 SLPM hydrogen.

In addition, tests were performed with an inlet orientated 135 degrees from conventional level, perpendicular with the slope of the transition section as illustrated and described in Chapter 2.3. An inlet area ratio of 0.040 was tested at jet lengths of 19.563, 13.25, 9.938, and 8.875 inches. The inlet was approximately 0.275 inch long. All lengths achieved self-sustained combustion except for the shortest length of 8.875 inches. At 9.938 inches, the pulsejet was difficult to start and was only sustainable for a number of seconds at a fuel flow rate of about 9.4 SLPM hydrogen.

Holes were drilled in the opposing face of the combustion cylinder to create inlets that faced 180 degrees in opposite direction from the conventional valveless position utilized for scalability investigations. As described thoroughly in Chapter 2.1.22.1.2, the inlet holes were drilled in such a way as to intersect the slope of the transition section keeping parallel with the pulsejet's longitudinal axis. To accommodate a shorter inlet, the slope of the transition section was steepened so that the acute interior angle that the

transition surface made with the intersection of the tail pipe was twice that of the '15cm pulsejet.' Thereby, the distance between the surface of the transition slope and the opposing face of the combustion cylinder was shortened.

3.2.1 Reverse Inlet Performance

Initially, two holes, both 0.089 inches in diameter, were drilled axisymmetrically about the longitudinal axis of the pulsejet creating a 0.028 overall area ratio with the combustion chamber. Runs were conditionally successful at both the full length of 15.938 inches and the shortest length of only 7.25 inches, becoming unstable after roughly 30 seconds of continuous operation. The inlet lengths were approximately 0.35 inch long each, and throttle capacity limits stayed within 9.4 and 18.8 SLPM hydrogen.

A third hole was drilled of equal diameter to the previous two, to bring the collective inlet area ratio equal to 0.042. Pressure and temperature were simultaneously recorded for a jet length of 14.75 inches at a location comparable to port 2 of the scalability experiments. The results are plotted in Figure 3.2-1 below. Many similarities can be drawn between the reverse inlet setup and a conventional valveless configuration of similar area ratio, inlet length, and total jet length. If Figure 3.2-1 is compared with the plot for a 12.625-inch jet length in Figure 3.1-26, a likeness in waveform can be seen among the two pressure oscillations. That is, there is both a primary and secondary pressure rise with similar values for the secondary return.

However, the total span of pressures is slightly more extensive in Figure 3.1-26. Absolute peak pressures are almost 75 percent greater in value for conventional design. Furthermore, there appears in Figure 3.1-26 to be a repeated event in the upswing of the

primary pressure rise that is lacking in the opposed facing inlet configuration. The abrupt disruption may be due to a returning refraction wave from the larger and longer inlet of conventional design. Yet, the pressure oscillations of both Figure 3.1-26 and Figure 3.2-1 share a similar frequency and chamber temperature.

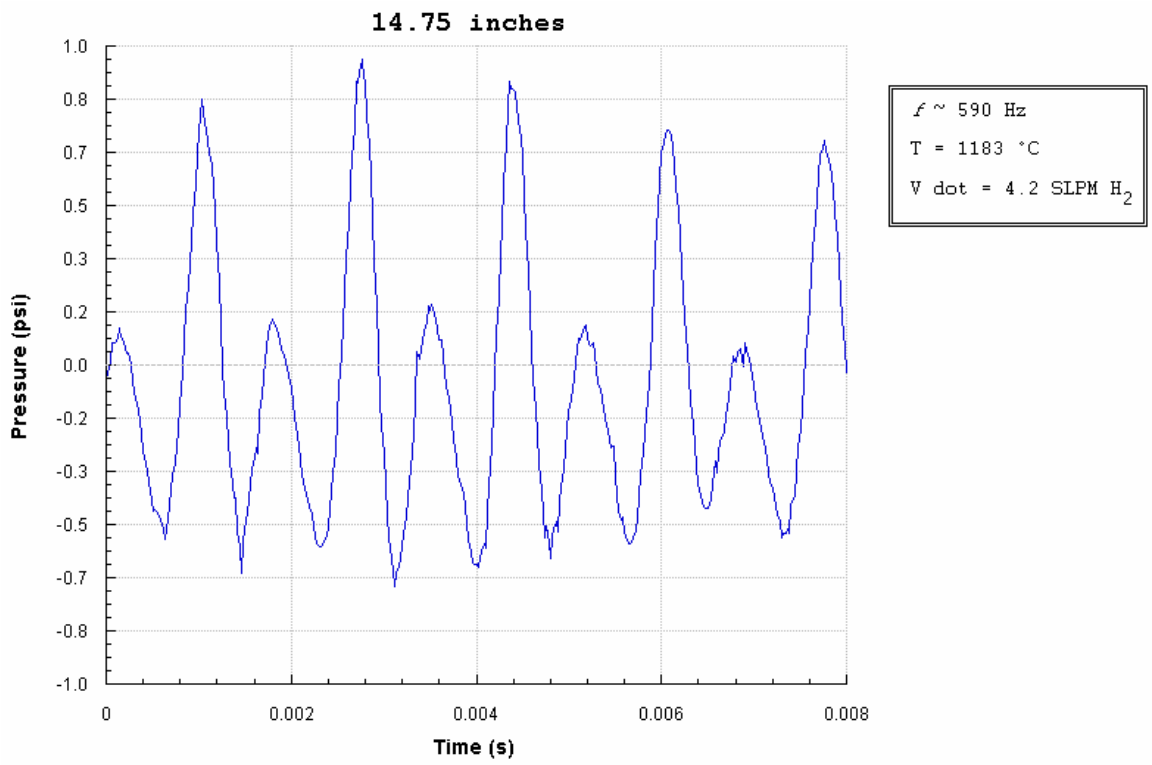

Figure 3.2-1: Pulsejet combustion chamber pressure for an opposed facing 3-inlet configuration with a 0.042 collective area ratio.

4 Characterization of Scalability Response

4.1 Length Investigation

To examine the effective scalability of length determined by this investigation, Table 4.1-1 tabulates the shortest pulsejet lengths, per inlet configuration, that were able to achieve combustion. It appears that an area ratio of 0.086 was most efficient in shortening the overall jet length for the range of inlet lengths tested. This suggests that the length at which a valveless pulsejet chooses to find successful self-sustaining combustion is a function of the chemical processes. Given a certain intake area, the pulsejet appears to operate at shorter lengths with greater success. Inlet area is analogous to the volume of oxidizer (air) ingested with each combustion cycle. Thus, it can be concluded that length may be a function of equivalence ratio of combustion.

Still, Table 4.1-1 attempts to characterize 15 cm class operational lengths. Minimum operating length appears to be a stronger function of inlet length rather than inlet area ratio; suggesting, then, that area ratios may only be utilized to slightly reduce inherent inlet to tail pipe length ratios. In turn, implying that such critical length ratios most likely do exist. Inlet ratios have actually been shown to have a greatest effect on maximum length characteristics (i.e., at longer jet lengths and larger ratios, self-sustaining performance deteriorates). However, it has been discovered that exit geometry can be used to further manipulate the overall operational pulsejet length. This, too, is illustrated by Table 4.1-1.

Inlet Length (in.) \ Inlet Area Ratio	0.13	0.086	0.04
0.5	6.250	6.125	6.250
1.0	8.875	7.125 A	7.250 A
1.5	9.750 B	7.750 A	10.000 A
2.0	12.250 B	12.375 B	12.625 A

Table 4.1-1: Minimum feasible pulsejet lengths for corresponding inlet configurations.
Shaded areas denote the use of an exit nozzle (specified 'A' or 'B').
All measurements in inches.

Inlet length to exit length ratios are plotted in

Figure 4.1-1 against their respective minimal jet lengths in order to investigate trends in behavior. Inlet length, tail pipe length, and minimum jet length are represented by the nomenclature L_i, L_e, and L_{min}, respectively.

Figure 4.1-1 offers a clearer representation of the shortening effects produced by adding a diverging exit geometry to the tail pipe of the pulsejet. It is important to note in Figure 4.1-1 that inlet lengths increase from left to right per data point (by 0.5-inch increments), and an additional inlet length of 2.5 inches was investigated for a ratio of 0.130. Furthermore, the 0.086 case produced two outlying points, both associated with an inlet length of 1.5 inches. These extraneous data points reflect exit lengths that are significantly shorter than the mean length observed in the remainder of area ratios with corresponding inlet lengths of 1.5 inches. However, the extraneous points correspond to

testing configurations that were found unrepeatable immediately following engine shutoff. In this light, they were justifiably excluded from observation in order to extract a discernable trend in the data collected. At greater inlet lengths, a constant length ratio of about .22 is witnessed in Figure 4.1-1 for jets equipped with a nozzle attachment. For those without, somewhat of a linear rise in $\frac{L_i}{L_e}$ is found with increase in inlet length.

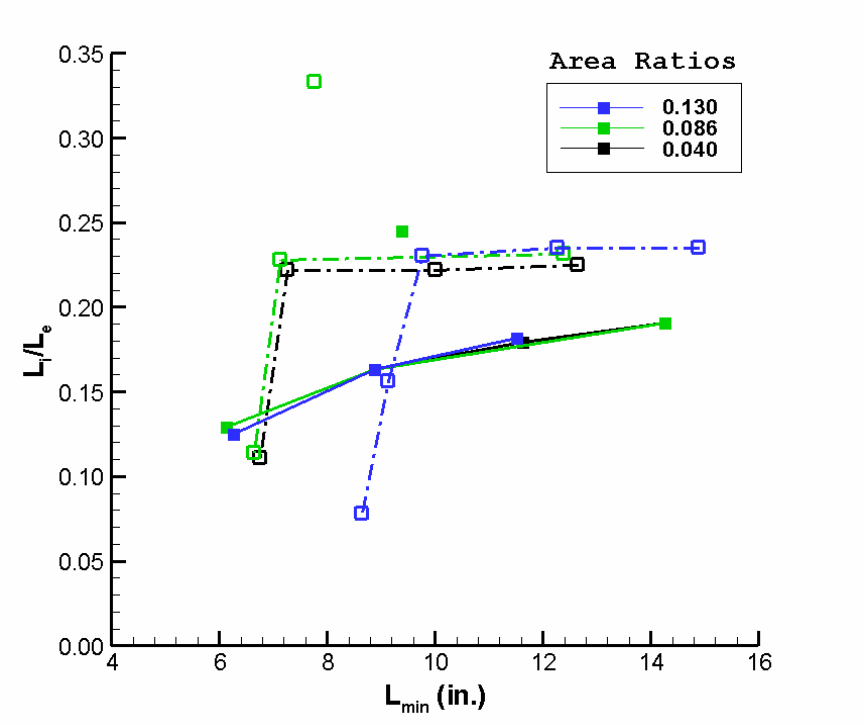

Figure 4.1-1: Inlet to exit length ratios versus corresponding minimum feasible pulsejet lengths.
Solid lines denote a constant area exit geometry; dashed lines denote a diverging nozzle.

4.2 Resonance Investigation

The frequency at which self-sustaining combustion occurs when the pulsejet is running completely independent of a forced air supply is a function of numerous factors. Figure 4.2-1, Figure 4.2-2, and Figure 4.2-3 look at the change in operating frequency as a function of overall jet length, inlet length, inlet area to combustor area ratio, and exit geometry. Hydrogen was used as the fuel source, and fuel flow rates between data points vary but were selected based upon mid-range throttle capacities for each respective length.

For each inlet ratio, plots show an overall increase in frequency with decrease in inlet length, as expected. Frequencies are also generally higher at each length increment for configurations with diverging exit geometries as opposed to configurations with a constant area tail pipe termination. It is interesting to note that at each respective length increment, the pulsejet was a bit longer with a nozzle attachment than without. Yet, somewhat counterintuitive, resonant frequencies remained higher. At each jet length interval, as the inlet ratios were increased the operating frequency increased, as well. That is to say, inlets with larger diameters tended to operate at higher frequencies for a given jet length.

Most inlet ratio and length configurations fit well in a linear trend. This is to be expected, as fundamental acoustic wave theory describes frequency as a linear function of length for constant area pipe geometries. Furthermore, Figure 4.2-1(b), Figure 4.2-2(b), and Figure 4.2-3(b) show a strong similarity in slope between inlet lengths. For those configurations where only two data points were available, no linear fit was applied.

Some points, however, fell significantly outside of the typical trend. In particular, Figure 4.2-3 exhibits a large jump in resonant frequency at greatest jet lengths for several different inlet measurements. This repeatable phenomenon occurred at the shorter inlet lengths for both constant area and diverging exit geometries. As mentioned previously, a higher frequency mode (designated by the symbol '*') seems to have been triggered at those corresponding configurations. Figure 4.2-2(a) shows an unexplained deviation in operating frequency, as well, for an inlet length of 0.5 and a jet length of 13.0 inches. However, this behavior was not repeatable in testing.

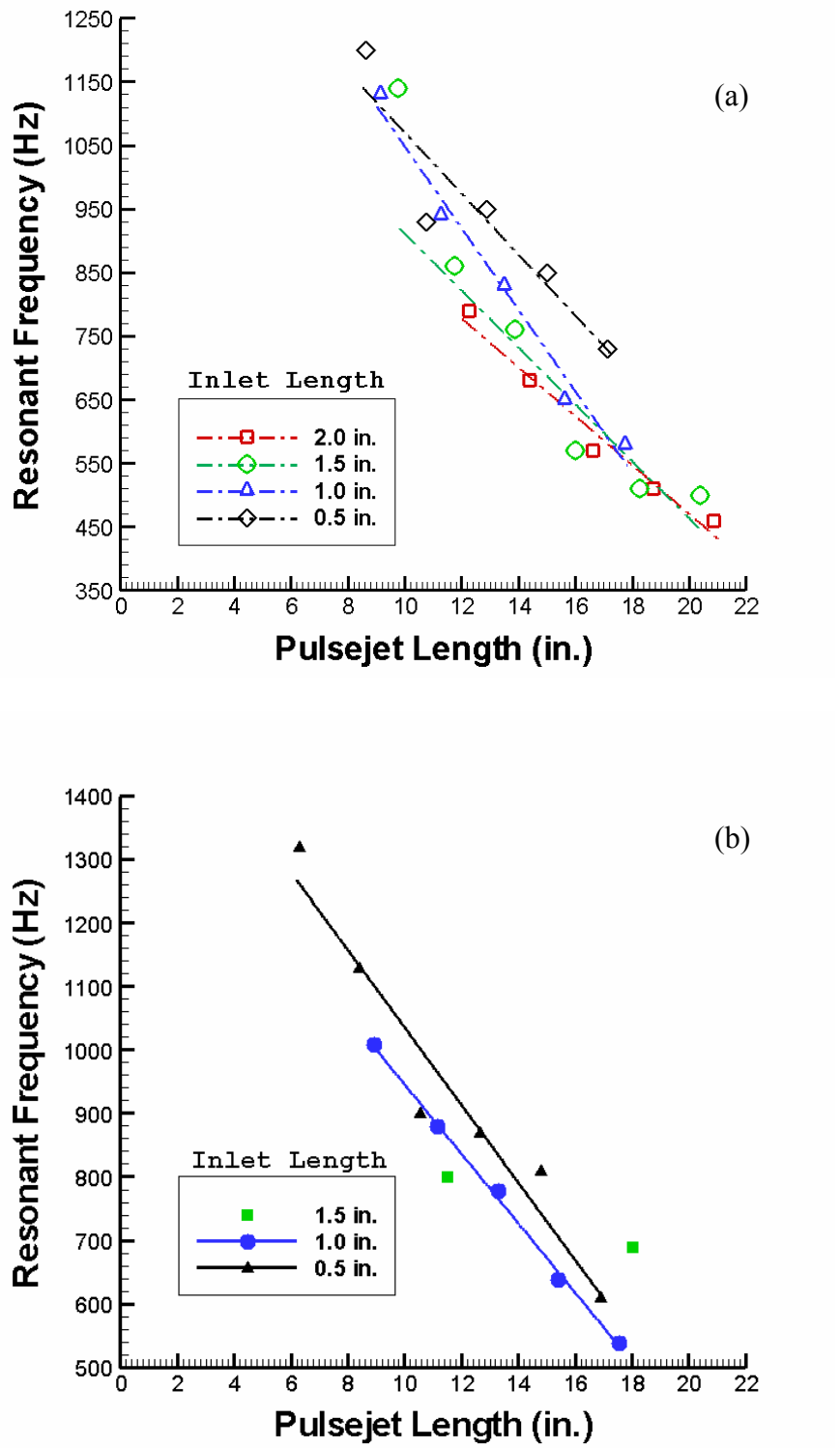

Figure 4.2-1: Frequency versus pulsejet length for a 0.130 inlet area ratio with (a) a diverging exit nozzle and (b) a constant area termination.

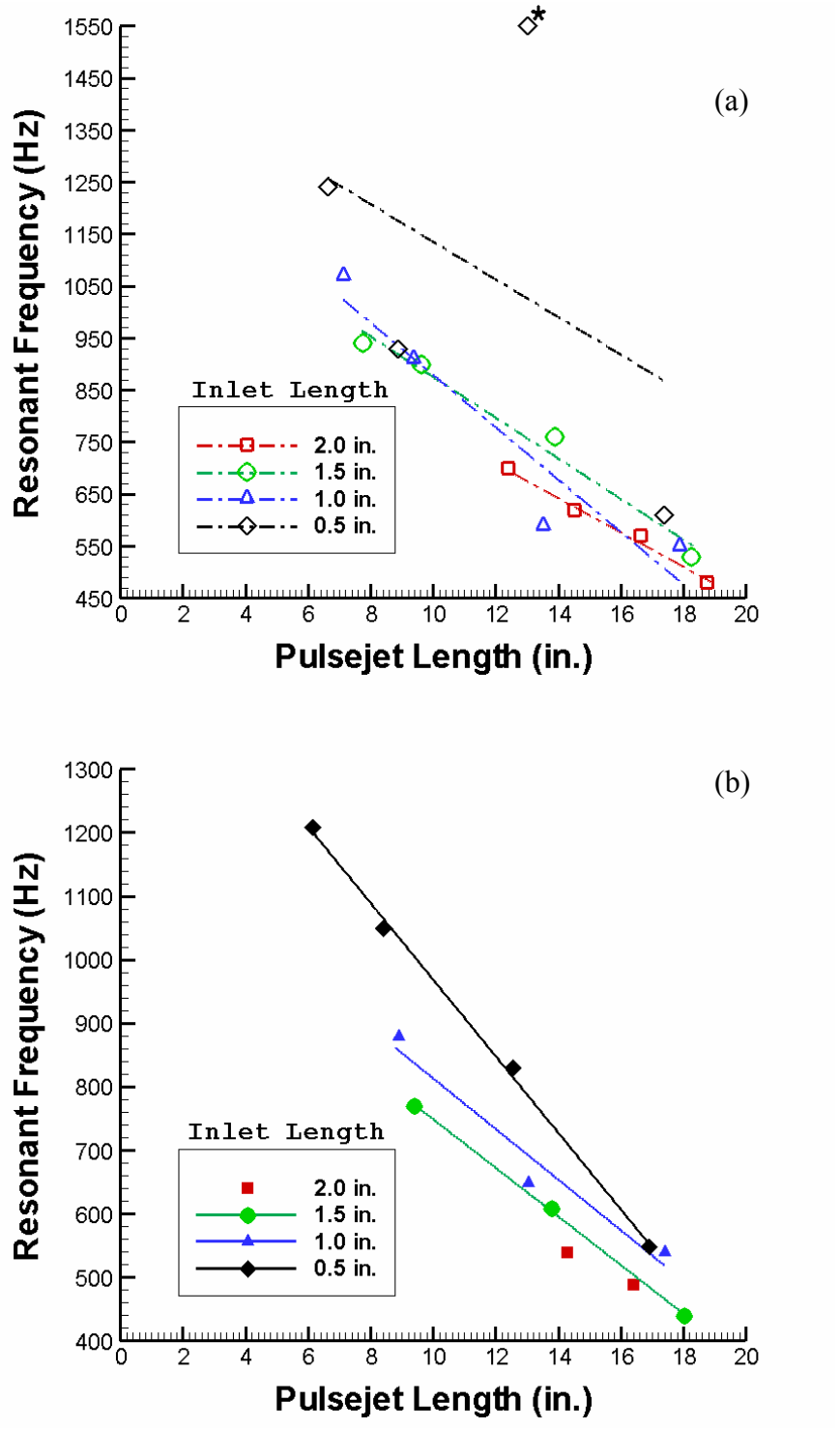

Figure 4.2-2: Frequency versus pulsejet length for a 0.086 inlet area ratio with (a) a diverging exit nozzle and (b) a constant area termination.

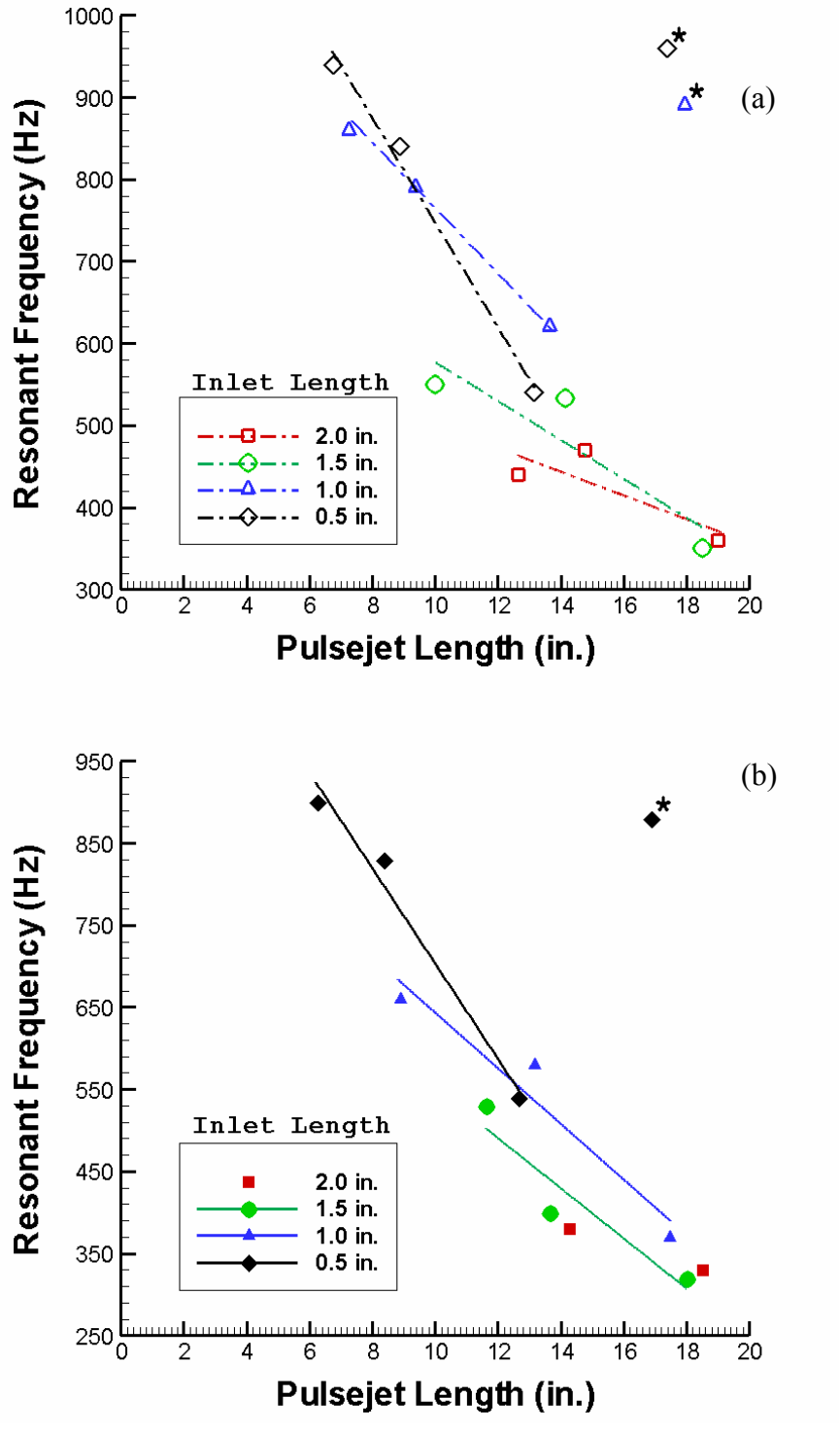

Figure 4.2-3: Frequency versus pulsejet length for a 0.040 inlet area ratio with (a) a diverging exit nozzle and (b) a constant area termination.

4.3 Fuel Flow Investigation

In

Table 4.3-1, the maximum attainable prior to engine choke, or 'rich-out,' fuel flow rates show a dramatic decrease as inlet area is reduced. The same is construed in

Table 4.3-2. However, no distinct trend can be seen with variation in inlet length. This seems to suggest that inlet length did not have a direct effect on intake volume. Thus, boundary layer build up along the walls of the inlet was insignificant at those lengths tested. Flow rate was limited by the volume of air ingested .

Comparison between

Table 4.3-1 and

Table 4.3-2 reveals an increase in rich-out fuel flow limits for decreases in total jet length. This can be explained by the accompanying increase in combustion frequency associated with a decrease in total length. If higher frequencies demand more combustion events per minute, then a higher fuel consumption rate may be related to a decrease in total jet length. Consequently, greater allowable fuel flow rates can be tolerated by the higher consumption rates while maintaining self-sustaining combustion.

Inlet Length (in.)	Inlet Ratio 0.13	0.086	0.04
0.5	45.0	25.4	8.0
1.0	23.6	15.2	8.0
1.5	22.6	20.1	7.8
2.0	22.3	17.5	8.0

Table 4.3-1: Maximum H2 flow rates for a constant tail pipe length of 15.0" and varying inlet configurations.
All measurements in SLPM.

Inlet Length (in.)	Inlet Ratio 0.13	0.086	0.04
0.5	45.0	33.1	8.6
1.0	55.5	38.5	15.6
1.5	51.0	34.7	8.1
2.0	40.0	23.0	7.1

Table 4.3-2: Maximum H2 flow rates for minimum feasible pulsejet lengths and varying inlet configurations.
All measurements in SLPM.

5 Conclusions and Recapitulation

In order to ascertain the scalability limits of the pulsejet engine, it is necessary to first investigate the viability of operation under a multiple of operating configurations for an individual class of engine sizes. Experimentation of the 15 centimeter class pulsejet is a vital stepping stone to bridge the gap between micro-scaled pulsejet engines and the hobby-scaled engines of today's enthusiasts. The research accomplished in this work attempts to classify the physical effects on engine performance subject to changes in jet geometry. To determine characteristics of performance, chamber pressure and temperature, thrust response, and operating frequency were measured and are presented for comparison. This study is unique in that it represents the first technically explored and documented production of an operational valveless pulsejet engine of its size class. The relevant conclusions drawn from this work are as follows:

1. Tail pipe length is a direct function of valveless inlet length.
    a. Self-sustaining combustion at minimum jet lengths was achieved with shortest inlet lengths.
    b. Self-sustaining combustion at longer jet lengths was achieved with shorter inlet lengths and smaller area ratios.
    c. Maximum tail pipe lengths exist for corresponding inlet lengths and area ratios. Results suggest that given a valveless geometric configuration, there exists a critical length over which self-sustaining combustion cannot

be achieved. The critical length tends be quite large as compared to characteristic pulsejet dimensions. This implies that self-sustaining combustion is governed not only by the fluid mechanic codependency between chemical kinetic rates as seen by limitations in length reduction but also by the influence of jet geometry over the characteristic cycle time of the fluid mechanic pressure wave. The correlation between the independent fluid dynamic behaviors within both the inlet and tail pipe may be influencing combustion response. Or, independent cycle times appear to be related to one another.

2. Minimum tail pipe length can be further reduced (from a constant area geometry) by about 16 % on average with the addition of a diverging exit nozzle.
3. No net thrust was measured for the valveless inlet lengths and area ratios examined. However, high time-resolved peak thrust values suggest great potential for alternative configurations, such as rearward facing inlets.
4. Resonant combustion was achieved from 90º, 135º, and 180º inlet orientations with respect to the conventional forward facing valveless design.
5. Preliminary tests indicate that valveless pulsejets with multiple opposed facing inlets present similar behavioral characteristics as those of conventional design. It also may be concluded that the consolidated inlet area ratio of multiple inlets is comparable to that of a single rearward facing inlet, taking into consideration inlet placement and internal direction of inlet flow.

6. The two main parameters determining the success of a pulsejet to resonate are chemical kinetic time versus jet length and inlet area to combustor area ratio.
    a. At shorter lengths, the chemical kinetic reaction rate (combustion time) becomes challenged by the period of fluid mechanic oscillations. This would explain why fuels with lower kinetic rates such as propane did not promote self-sufficient resonance in smaller jet sizes. From previous studies, one can assume combustion is occurring 30% of characteristic cycle time, and 30% of chamber volume is replenished with a fresh charge per cycle.

6 Future Work

While this study presents a very thorough investigation on the geometric design of the 15 centimeter class pulsejet, continued work is needed on the scale effects of fuel injector design. More efficient injector designs could very well decrease chemical kinetic times by increasing mixture enough so to shorten minimum jet lengths at different inlet configurations. Fuel injection may also be the key to unlocking resonance with heavier, more complex fuels. Unfortunately, hydrogen was the only reactant found with a high enough kinetic rate of reaction to support self-sufficient combustion in this study. Hydrocarbon fuels such as propane or even liquid fuels such as ethanol or kerosene may become viable reactants as more efficient injection and/or better mixing characteristics are investigated.

Tail pipe exit geometry was found to influence performance at different pulsejet configurations. In a similar manner, inlet entrance geometry may also prove to favorably affect performance at different lengths and conditions. Combustion chamber volume and shape, as well as, the inclination of the transition section are a few other possibilities to consider when studying the scalable performance of the pulsejet engine.

A positive net thrust was a much desired attribute of the present work. Considering the peak thrust values obtained in the current research with a conventional valveless design, a reverse-inlet configuration shows great promise for achieving notable net thrust. In addition, the mixing characteristics that may promote resonance with heavier fuels have evidently been well investigated by Reynst. If a pulsejet with opposed

facing inlets is viewed as a modified Reynst combustion pot (Reynst, 1961), then lessons learned by the late pulse combustion expert, cleverly employed and coupled with catalytic strategies, may provide a viable avenue for research with hydrocarbon fuels.

An in-depth comparison between results from this study and the performance characteristics of similar pulsejets from other size classes would provide a basis for which to identify scaling trends. Such trends could be used to predict or anticipate necessary direction for further scalability experimentations. In particular, characterizing ratios, such as inlet area ratio and inlet to exit length ratio, identified in the present work warrant further investigation into their credibility as fundamental operational parameters.

A next step in the study of 15 centimeter class pulsejet engines is the production of an operational valved variant. If done so, such an accomplishment would be the first successful development of its kind. Valved pulsejets exhibit higher average thrusts and lower thrust specific fuel consumption than valveless variants (Lockwood, 1963; Logan, 1951; Westberg, 2000). However, the addition of moving valves complicates the scaling process of experimentation.

7 References

Crowe, Robert K., "Pulsating combustion device miniaturization," Master thesis, Univ. of South Carolina, December 1976.

Emmerich, L., "Development of pulse-jet engines for a helicopter rotor system, summary report," *Report No. 163-W-1**, American Helicopter Co., January 1953.

Foa, J. V., *Elements of Flight Propulsion*, John Wiley & Sons, New York, 1960.

Lockwood, R. M., "Pulse reactor lift-propulsion system development program, final report," *Advanced Research Division Report No. 508*, Hiller Aircraft Co., March 1963.

Lockwood, R. M., and W. G. Patterson, "Summary report on investigation of miniature valveless pulsejets," *Advanced Research Division Report No. ARD-307*, U. S. Army Transportation Research Command TRECOM Report 64-20, Hiller Aircraft Co., February 1964.

Logan, J. G., Jr., "Summary report on valveless pulsejet investigation," *Project SQUID Tech. Memo. No. CAL-42*, Cornell Aeronaut. Lab., October 1951.

Logan, J. G., Jr., "Valveless pulse jet investigations, Part I, Test of small scale models," *Project SQUID Tech. Memo. No. CAL-27*, Cornell Aeronaut. Lab., May 1949.

Logan, J. G., Jr., and O. B. Finamore, "Suggested forms for air duct motors utilizing intermittent combustion, Part IV, Intermittent combustion experiments," *Project SQUID Tech. Memo. No. CAL-20*, Cornell Aeronaut. Lab., April 28, 1948.

Ogorelec, Bruno, retrieved February 1, 2005, from Web site: *http://www.pulse-jets.com/valveless/, pulse-jets.com*, October 2002.

Reynst, F. H., "Pulsating firing for steam generators," *Pulsating Combustion*, M. W. Thring, ed., Pergamon Press, New York, 1961.

Rudinger, G., "On the performance analysis of the ducted pulsejet," *Project SQUID Tech. Memo. No. CAL-36*, Cornell Aeronaut. Lab., October 1951.

SNECMA Document, retrieved June 1, 2005, from Web site: *http://www.pulse-jets.com/phpbb2/files/snecma_5_english_992.doc*, pulse-jets.com, May 2005.

SNECMA Document, retrieved June 1, 2005, from Web site: *http://www.pulse-jets.com/phpbb2/files/snecma_1_english_100.doc*, pulse-jets.com, May 2005

Westberg, Fredrik, "Inside the pulsejet engine," a private study, April 2000.

Wilder, J. G., Jr., "An experimental investigation of the effect of inlet ducts on the performance characteristics of a pulse jet," *Project SQUID Tech. Memo. No. CAL-29*, Cornell Aeronaut. Lab., July 1949.

Zinn, B. T., "Pulsating Combustion," *Advanced Combustion Methods*, F. J. Weinberg, ed., Academic Press, Orlando, FL, 1986.